Phase Stabilized Modelocked Lasers: from optical frequency metrology to waveform synthesis of ultrashort pulses

by

Tara Michele Fortier

B.A., Concordia University, Montréal 1998

A thesis submitted to the

Faculty of the Graduate School of the

University of Colorado in partial fulfillment

of the requirements for the degree of

Doctor of Philosophy

Department of Physics

2004

This thesis entitled:
Phase Stabilized Modelocked Lasers: from optical frequency metrology to waveform synthesis of ultrashort pulses
written by Tara Michele Fortier
has been approved for the Department of Physics

Dr. Steven T. Cundiff

Dr. Jun Ye

Date

The final copy of this thesis has been examined by the signatories, and we find that both the content and the form meet acceptable presentation standards of scholarly work in the above mentioned discipline.

Michele Fortier, Tara (Ph.D., Laser Physics)

Phase Stabilized Modelocked Lasers: from optical frequency metrology to waveform synthesis of ultrashort pulses

Thesis directed by Prof. Dr. Steven T. Cundiff

By drawing on the techniques of single-frequency laser stabilization and on improvements of ultrafast lasers, stabilization of Ti:sapphire lasers has led to great advances in both the fields of optical frequency metrology and ultrafast science. This thesis presents the development of the technology and application of modelocked laser stabilization to both domains. Towards the latter I will discuss the use of extremely phase-coherent pulse trains for exploration of quantum interference in semiconductors. As applications to the former, we present synchronization between a Ti:sapphire and Erbium doped fiber laser to produce an absolute comb at 1.5 μm. I also demonstrate an octave spanning Ti:sapphire laser that is a candidate as a transfer oscillator for an all-optical clock.

Dedication

To my grandmother, Martha (Moonbeam) Fortier. In life she has served a strong role model and in death as a continuing source of courage for me.

Acknowledgements

I have had the very good fortune of sauntering into the budding field of stabilization of modelocked lasers. The time that I have spent here and the work that I have been a part of has been nothing short of an eye opening experience for me, very much fuelled by the dynamic energy of the people and the quality of the science at JILA.

My mentor in this adventure has been my advisor Steve Cundiff, whose knowledge in ultrafast lasers and semiconductors has been an invaluable part of my experimental education. The patience and independence that he has allowed me has permitted much of my personal scientific growth, for this I am fully indebted.

Much thanks is also due to my surrogate advisor Jun Ye. Although not an official member of his group, he has always welcomed me into his lab and made me feel like one of his own. Jun's constant personal and scientific support will never be forgotten.

There are a number of people who have directly contributed to the work in this thesis. One person in particular is David Jones who, aside from passing on to me his amazing breadth of experimental knowledge, has also taught me the joys of rock climbing! David has helped me through thick and thin and has been much like a big brother to me during my adventures with physics. The work that is presented in this thesis could now have proceeded as smoothly without his constant support. I have also had the pleasure of working with Pete Roos, who aside from providing much needed fun and laughter, has provided great help in some of my concluding work at JILA. A source of quiet inspiration for me has been John (Jan) Hall. His everlasting enthusiasm

for science and his remarkable electronic designs, without which none of this work could have been done, continue to baffle and amazed me.

Of course, none of the work done here in the last years could have been possible without the amazing skill of the JILA technical staff. In particular I would like to acknowledge Terry Brown and James Fung-A-Fat for their invaluable guidance in electronics and Hans Green for being a friend and phenomenal machinist.

I have also had the opportunity to work with and become friends with some wonderful people. I owe my gratitude to my colleagues and friends for their constant support, especially during the writing of this thesis. Specifically, Martin Griebel has gone above and beyond his duty as a post doc and friend by reading my thesis cover to cover, while at the same time providing amazing editorial help. I would also like to thank my dear friends Emily Gibson, Quentin Diot, Qudsia Quraishi and Paul Haljan for being there during the rough spots.

Much thanks is also due to some of my mentors along the way: Chris Greene and Misha Ivanov for making me appreciate the beauty of theoretical physics, Greg Lopinski for providing guidance during my first true experiences in experimental physics, and Paul Corkum for his past and continuing support in my pursuit of knowledge.

Finally, thank you to my committee members, Steve Cundiff, Jun Ye, Jan Hall, Leo Hollberg, Henry Kapteyn and David Jonas for being kind inquisitioners and thorough readers.

Contents

Chapter

Figures

Figure

Chapter 1

Introduction

Laser stabilization is a powerful technique that is used in many aspects of atomic physics and optical spectroscopy. Possibly more powerful, however, is the application of single frequency laser stabilization techniques to modelocked lasers, which is the work horse for studying ultrashort time scale physical processes. The marriage of the two has brought the techniques and challenges of what were previously two disparate fields into a union that has dramatically impacted both optical frequency metrology as well as ultrafast science.

To most, upon first reflection it isn't immediately obvious that one can use single frequency techniques to stabilize the seemingly complicated optical spectrum of a modelocked laser. This is because modelocked lasers are pulsed lasers, where the laser pulses are formed from millions of optical frequencies. As shown in Fig. 1.1, a modelocked laser periodically emits nearly delta function time duration pulses, separated in time by one cavity round trip, t_{rt}. A natural consequence is that the Fourier spectrum of a train of delta function pulses in time is delta function comb in frequency, with each frequency element separated by $f_{rep} = 1/t_{rt}$. The amazing stability in the periodicity (t_{rt}) of the emitted pulses yields in a very frequency stable comb. What makes it possible to simply characterize the frequencies in the comb is the forced phase coherence between the optical modes of the laser necessary for pulse formation. The strong modelocking condition, in particular for the modelocked Ti:sapphire (Ti:S) laser (Kerr-lens

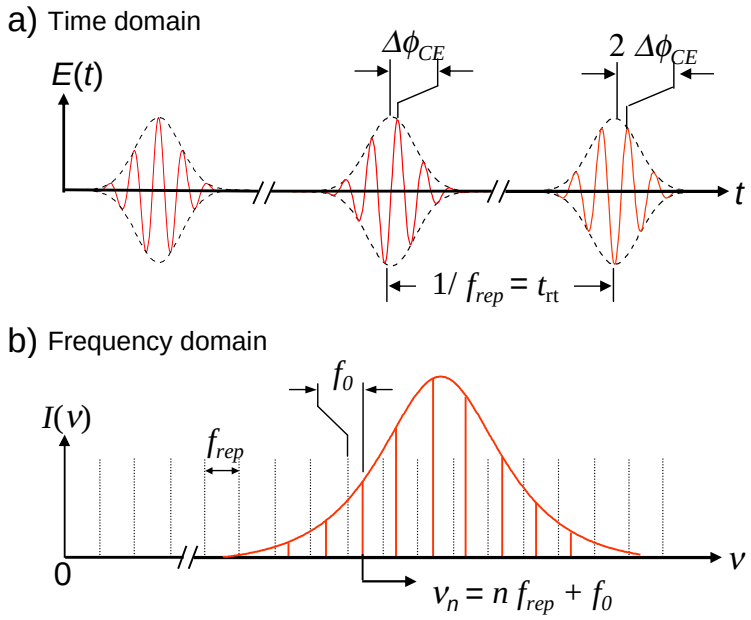

Figure 1.1: The time a) and frequency b) aspect of the modelocked laser. The phase shift between the adjacent pulse in the pulse train, $\Delta\phi_{CE}$ results is proportional to the ratio of the offset frequency, f_0 to the laser repetition rate, f_{rep}, $\Delta\phi_{CE} = 2\pi\frac{f_0}{f_{rep}}$.

modelocking), produces a very intrinsically narrow, and equally spaced comb lines. As a result, each comb element in the modelocked spectrum may be characterized by only two radio frequencies, the laser repetition rate, f_{rep} and an offset frequency, f_0, that is

$$\nu_n = n f_{rep} + f_0, \tag{1.1}$$

where the integer $n \sim 10^6$ takes f_{rep} into the optical frequencies [see Fig. 1.1 b]. For a more detailed discussion of this please consult Chap. 2.

The fact that the seemingly complicated optical spectrum of a modelocked laser may be characterized by only two rf frequencies is an incredible result. The main interest, however, as seen via eqn. 1.1, is that the optical comb spacing provides a direct optical-to-microwave link. The fundamental existence of the repetition rate, which provides 10^5 division from optical to microwave permits absolute stabilization of the laser spectrum using a single optical oscillator and a microwave reference [see Chap. 2].

The"simple" stabilization scheme, described in detail in Chap. 2, has far reaching consequences in precision optical frequency metrology and has all but made obsolete the use of the very technically challenging harmonic frequency chains [60, 15, 14].

1.1 Optical frequency metrology

High precision optical frequency measurements began about 40 years ago with the inception of the first laser. Since then, the development of more stable and spectrally narrow lasers have brought the laser to the forefront of high precision measurement. A laser with a potential dynamic resolution of 10^{17} (for a mHz linewidth centered in the optical) may be used to determine the value of some fundamental constants [75, 68] with unprecedented precision. The high frequency resolution available using stabilized lasers has allowed for experimental investigation into various aspects of fundamental physics [35] such as gravitational wave detection [29], time variation of fundamental constants [60, 15, 14] and quantum electrodynamics [51], to name a few. Aside from providing a means for determination of fundamental physics, the techniques pioneered in precision measurement have also led to advances in optical communications [41] and precision length measurement.

The full potential for the high resolution of the laser remains untapped, however, unless its frequency can be determined absolutely against the current time/frequency standard, the Cs clock, established as the international time standard in 1967. The Cs clock provides our current definition of the second; 1 second equaling 9 192 631 770 atomic cycles between the $F = 4, m_f = 0 \rightarrow F = 3, m_f = 0$ transition in the hyperfine ground state of ^{133}Cs [61].

The challenge in optical frequency metrology is to coherently link optical frequencies (several hundreds of THz) to the Cs microwave standard. The first high precision measurements of optical frequencies were achieved by connecting a high-harmonic of the Cs standard to optical frequencies using a series of single frequency intermediate

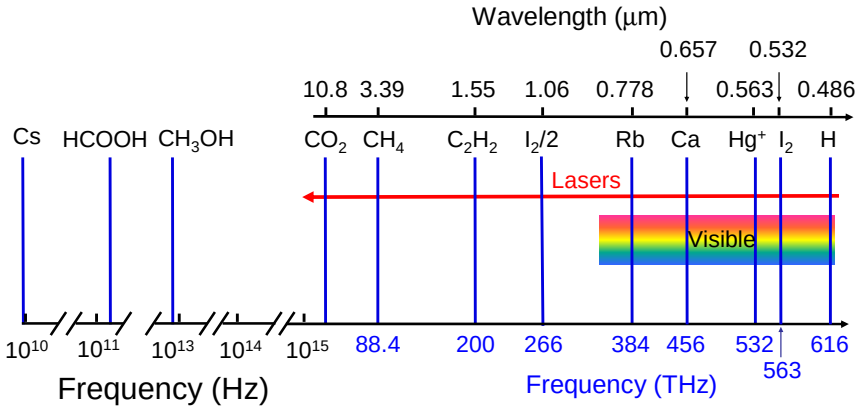

Figure 1.2: A map of the electromagnetic spectrum showing selected measured secondary standards and their corresponding frequencies.

phase-locked oscillators [36, 18, 44]. Aside from being used to provide high precision measurement of optical atomic transitions, these harmonic frequency chains allowed for measurement of secondary optical standards [see Fig. 1.2], which then serve as portable absolute optical frequency references. Using the few available secondary optical standards, several bridging schemes, namely frequency interval dividers [73, 75] and comb generators [21, 50, 42] had to be devised to span the remaining frequency gap between the secondary optical standard and an optical transition of choice.

In the late 1970's the modelocked laser was introduced to optical frequency metrology since its optical spectrum could be used to span several tens to hundreds of THz in the optical [21]. Once one line of the frequency comb [see eqn. 1.1] is referenced to a secondary optical standard, the comb can be used as an optical ruler to measure large optical difference frequencies [76, 65, 64].

With a potential optical bandwidth of 300 nm, modelocked Ti:S lasers set the scene for broadband comb generators. However, this potential was greatly increased in 2000 when it was shown that using microstructured (MS) fiber [62] it was possible to coherently extend the Ti:S comb over the entire visible spectrum. The increased optical bandwidth makes it possible to use nonlinear self-comparison for direct measurement of

the laser offset frequency, without comparison to a secondary standard. The simplified referencing scheme using MS fiber enables absolute stabilization of the optical comb using a single microwave reference [45, 11, 59]. Stabilization of the Ti:S optical comb in this manner results in the production of greater than 10^6 coherently linked CW lines that may be used for high precision absolute optical frequency measurement [40].

1.2 Carrier-envelope phase stabilization

The above stabilization scheme for the Ti:S laser, aside from providing an enormous simplification to optical metrology, also allows for control of the electric field of the laser pulses [74, 45]. As seen in Fig. 1.1 (a), the phase evolution of the laser pulse train is governed by the characteristic frequencies of the comb. This further feature of the phase stabilized Ti:S laser now permits waveform synthesis of ultrashort pulses, in that full characterization can be attained by controlling the laser pulse parameters, the spectral amplitude and phase via pulse shaping and now the phase of the optical carrier. With the current opportunities for generating pulses with temporal durations of ~ 2 optical cycles [17], the strong contrast of the field strength across a phase controlled pulse can be used to influence the outcome of extremely nonlinear processes [58, 6, 3]. The applications of the stabilized modelocked laser to physics in general appear endless. The introduction of the phase stabilized Ti:S laser to ultrafast science heralds a new age of phase-control possibilities from the low to the high field regimes [58, 6, 3] and from atomic to semiconductor [27] systems. The onslaught of absolute optical frequency and phase sensitive measurements, since the first realization of phase stabilization of Ti:S lasers is a testament to the power of the technique.

Naturally, the above brief historical perspective skips much of the painstaking work that has taken us from the development of the first laser, to high precision measurement, to phase control of physical processes. This thesis attempts to fill out a small

slice of the work necessary for the generation of highly phase-stable modelocked lasers for application to both optical frequency metrology and utltrafast science.

Much of the work that I have performed during the course of my graduate carrier has focussed on the development of the techniques necessary for the production of a highly phase stable Ti:S modelocked laser, primarily within the context of the carrier-envelope phase control of the laser pulse train [see Chap. 2]. This has involved development of the laser itself and of the feedback system for stabilization. As in any field of physics, pushing the envelope requires an impeccable tool for exploration of science. This naturally involves the necessary first task, when developing a scientific instrument, of determining its effectiveness. With this consideration in mind I have spent a considerable amount of time on characterization of the laser and stabilization loop. Given, the relative newness of the field, there have been a number of questions concerning the basic stabilization techniques that have required some consideration. One question that arose, when stabilization of Ti:S lasers was first demonstrated, was whether external broadening in MS fiber, given its extreme nonlinear nature, would preserve the optical coherence of the comb. This question is addressed in Chap. 3, which explores the nature of phase noise in MS fiber and determines its effect on the stability of the carrier-envelope phase of the laser pulse train [28]. More generally, Chap. 4 discusses the noise contribution from some of the additional elements comprising the stabilization loop, as well as presenting measurements indicating the stability that has been attained using the stabilized laser system [26]. The present system allows for generation of light pulses with a carrier-envelope phase that is coherent over tens of minutes! That means that, given a laser repetition rate of 100 MHz, we can produce $> 10^{10}$ pulses with nearly identical phase [25]. This ability to produce very highly phase stable pulse trains has opened the possibility for exploration of phase sensitive experiments. To this end, we have exploited the phase stability of the pulse train to investigate quantum interference effects in semiconductors. In particular, using the stabilized output of the laser we

demonstrate directional control of injected photocurrents in GaAs [27]. The details of this experiment are described in Sect. 6.1.

An application of the phase stable Ti:S laser, more toward metrology applications, is to use Ti:S lasers as a reference laser to which other lasers (single frequency or modelocked) may by locked. Specifically, using of the Ti:S laser as a transfer oscillator, for other modelocked lasers can permit coherent extension of the optical comb to the UV or IR, or alternatively for generation of super spectra with the ultimate aim of generating single optical cycle pulses. Here, we have demonstrated synchronization of a modelocked Erbium-doped fiber laser. This experiment, described in Sect. 6.2, aside from exploring the feedback mechanisms with which to control the comb parameters of the fiber laser, also demonstrates an absolute comb at 1.5 μm [63].

One of the ultimate goals for phase control of the Ti:S laser is the possible realization of all-optical clocks [12, 80], which are hoped to one day rival the resolution of the current primary atomic Cs microwave reference. All-optical clocks, using the Ti:S laser as a clockwork to connect the optical and microwave regimes has been previously demonstrated by Ye *et al.* and Diddams *et al.*. Final replacement of atomic Cs by a primary optical standard, however, requires further scientific and technological maturity of the both the optical standard as well its possible transfer oscillator. To this end, Chap. 5 discusses the construction of an octave spanning Ti:S laser that produces the necessary bandwidth for self-referenced stabilization within the laser oscillator alone, without the use of MS fiber [24]. A laser that may be stabilized without MS fiber brings to the fore the possibility of a more reproducible, simpler system with a potential longer term stability than stabilization systems based on MS fiber.

Chapter 2

Phase stabilization of modelocked Ti:sapphire lasers

The work horse for the experiments presented in this thesis is the Kerr-lens modelocked Ti:Sapphire (Ti:S) laser. It is a broadband optical oscillator whose bandwidth may span up to several hundred nm's in the near infrared. The large gain bandwidth of the laser (700 - 1000 nm) makes it ideal for optical frequency metrology and ultrafast phenomena, whereby the former takes advantage of the large coherent bandwidth to span several hundred THz in the the near infrared, and the latter for the formation of femtosecond pulses [4]. The challenge in metrology is overcoming the frequency gap between the optical and microwave regimes. Ti:S lasers, because of the incredible stability in the periodicity of the emitted pulses, result in a discretization of the laser spectrum into a stable comb of equally spaced, coherently related CW frequency components. This comb of frequencies may be used to provide a direct link between microwave and optical frequencies, thus making the modelocked laser a powerful tool in optical metrology. Additionally, absolute stabilization of the laser spectrum allows for deterministic control of the pulse electric field.

This Chapter is intended as an overview toward the concepts of phase stabilization of a modelocked Ti:S laser. The experimental details, optical and electronic, are contained within App. A, which is written more as manual for reconstruction of the experiment.

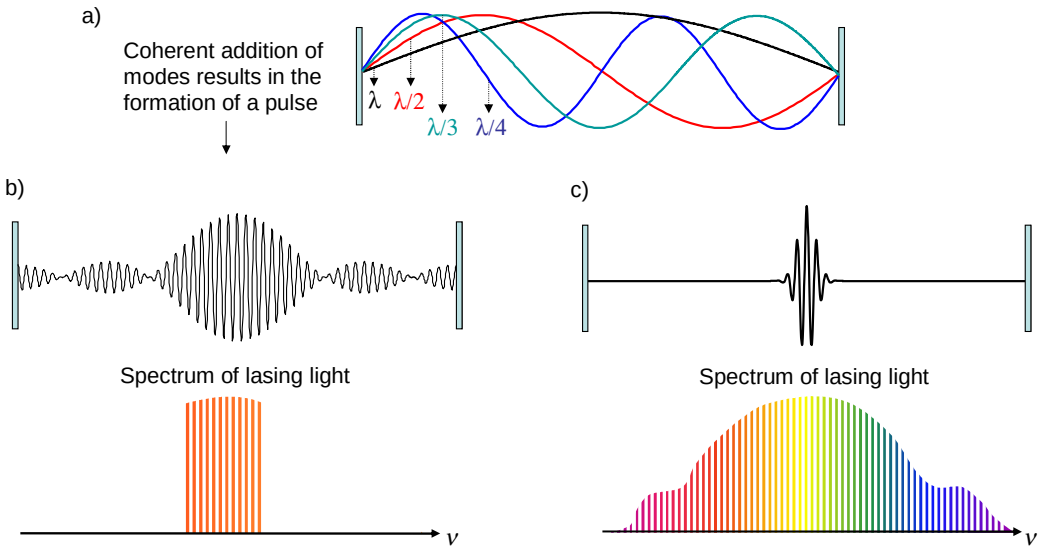

Figure 2.1: Schematic of pulse formation in the Ti:S laser cavity. a) The resonant modes of the cavity represent integer multiples of the fundamental cavity mode, $f_{rep} = c/\lambda$ (optical cavity modes are 10^6 times higher in frequency than those depicted here.) If the field of longitudinal modes are added with the same phase, they result in the formation of a pulse b). c) Neglecting dispersion, the larger the number of coherent modes comprising the light pulse, the shorter the temporal duration and the larger the contrast in field strength across the pulse.

2.1 Time and frequency domain aspects of modelocked lasers

Formation of pulses in the cavity result from the coherent addition of extremely narrow CW wavelengths that satisfy the resonant condition of the cavity [see Fig. 2.1]. This condition forces the optical spectrum to be composed of a comb of equally spaced optical elements, ν_n, that are separated in frequency by,

$$f_{rep} = \frac{c}{\lambda} = \frac{c}{2L}, \tag{2.1}$$

the fundamental resonant mode of the cavity. Here c is the speed of light and $2L$ is the round trip cavity length. The mechanism behind pulse formation in the Ti:S cavity is Kerr-lens modelocking, which is discussed in more detail in Sect. 5.1.3. Just briefly, modelocking, as the term implies, forces a fixed phase relationship between the resonant longitudinal modes of the cavity, ν_n. This coherent addition of the field of the optical

frequencies, ν_n, results in the formation of a train of light pulses,

$$E(z,t) = \sum^{n} E_\nu \; exp[\, i\,\{n\,\omega_n\,t + \phi_{CE}(t)\}]. \tag{2.2}$$

Modelocking of the laser spectrum requires coherence between the longitudinal modes of the cavity, forcing each mode to have a common phase, ϕ_{CE}, defining the phase of optical carrier. Essentially, each light pulse is a carrier-frequency that is modulated by a strong envelope function, $A(z,t)$. Using this representation we can rewrite the above equation in the form,

$$E(z,t) = \sum^{n} A\left(t - \frac{z}{v_g} - n\,t_{rt}\right)\; cos\left[\omega_c\,\left(t\,-\frac{z}{v_p}\right)\right]. \tag{2.3}$$

Here, $\omega_c = N(2\,\pi\,f_{rep})$, where N is a large integer multiplying f_{rep} up to the optical. As shown in Fig. 2.1, the greater the number of coherently added modes comprising the pulse, the narrower the pulse envelope in time, and consequently the stronger the contrast in field strength across the pulse.

Neglecting cavity dispersion, $v_g = v_p$ and consequently $\frac{d\phi_{CE}}{dt} = 0$. For this condition the laser pulse train is a series of identical pulses separated in time by one cavity round trip, $t_{rt} = 1/f_{rep}$. The inclusion of cavity dispersion causes a difference between the group and phase velocities, $v_g = c/n_g$ and $v_p = c/n_p$, of the light pulses in the cavity, where $n_p = n$ and $n_g = n + \omega\frac{dn}{d\omega}$. This results in an intra-cavity time-rate of change in the relative phase between the pulse envelope and the carrier wave,

$$\frac{d\phi_{CE}}{dt} = 2\pi\,\omega_c\left(\frac{1}{v_g} - \frac{1}{v_p}\right)c = 2\pi\,\omega_c(n_g - n_p) = 2\pi\,\omega_c^2\,\frac{dn(\omega_c)}{d\omega}. \tag{2.4}$$

This phase, ϕ_{CE}, common to each optical mode [see eqn. 2.2] results in a rigid spectral shift, f_0, of the entire optical comb [16, 78, 74]. As a result, each optical comb element, ν_n, is expressed as

$$\nu_n = f_0 + n\,f_{rep}, \tag{2.5}$$

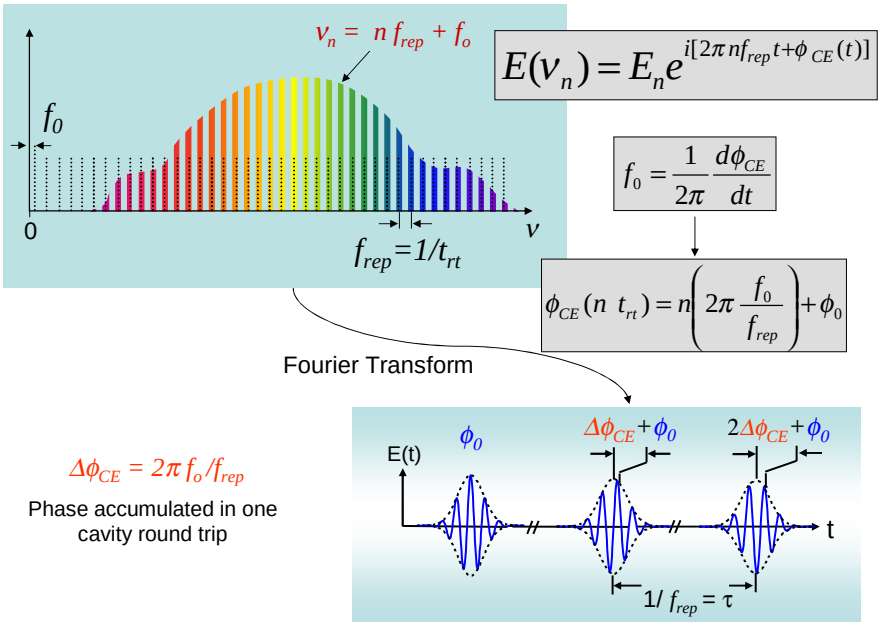

Figure 2.2: Summary of the time and frequency representations of the Ti:S light field. ϕ_0 is a phase offset whose origins and importance are explained in detail in Sect. 4.1.

where,

$$f_0 = \frac{1}{2\pi}\frac{d\phi_{CE}}{dt}. \tag{2.6}$$

To summarize, the modelocked spectrum of a Ti:S laser is a comb of frequencies whose spacing is governed by the laser repetition rate, f_{rep}, and whose absolute position is determined by the laser offset frequency, f_0. Given the fundamental connection between the pulse train and laser spectral components, f_0 and f_{rep} govern the evolution of the phase of the pulse electric field, ϕ_{CE}. Figure 2.2 summarizes this discussion.

Given that both f_{rep} and f_0 are stabilized absolutely the frequency spectrum of the Ti:S laser is an absolute optical comb with approximately 10^6 coherent lines spanning the visible to near IR. As a result the stabilized Ti:S laser is a convenient transfer oscillator to which other laser, single frequency or pulsed, may be synchronized. Additionally, phase stabilization of the laser results in a train of pulses with a phase evolution determined by eqn. 2.6.

Environmental perturbations, however, result in instability in the comb components. Specifically, perturbations within the laser cavity are responsible for fluctuations in f_0 due to pointing and other instabilities. Such instabilities yield a change in the net cavity dispersion and also in amplitude-to-phase conversion in the laser crystal due to extreme nonlinearity resulting from high intra-cavity powers [38, 39]. Once a pulse exits the laser, however, its phase evolution is governed by dispersion outside the cavity. Linear dispersion imparts a common phase shift to the entire pulse train, not a shift in the frequency of the comb. Nonlinear dispersion, in contrast, can result in extra-cavity phase noise due to fluctuations in the intensity of the laser output [see Chap. 3].

Because of these difficulties, the free running Ti:S laser does not serve as a phase-stable source of short pulses, nor does it provide a frequency-stable comb. As a result, active stabilization of the comb parameters is necessary.

2.1.1 Measurement of the laser comb parameters

Measurement of the comb parameters for stabilization is obtained using frequency difference measurement, whose technical maturity and corresponding convenience is the results of many year of development. A huge advantage of the optical comb provided by the modelocked laser is that, given suitable bandwith, the comb parameters may be measured absolutely without the cumbersome use of a secondary optical standard. For instance, the laser repetition rate is directly measurable using a fast photodetector (PD). This is possible because adjacent comb lines in the laser spectrum optically heterodyne yielding an rf spectrum of harmonics of the repetition rate [see Fig. 2.3],

$$|\nu_m - \nu_n| = |(nf_{rep} + f_0) - (mf_{rep} + f_0)| = (m-n)f_{rep}. \tag{2.7}$$

Given a cavity length of ~ 3 m, $f_{rep} = 1/t_{rt}$ is an rf frequency close to 100 MHz, which allows for direct comparison to a microwave standard. Because f_0 is bounded

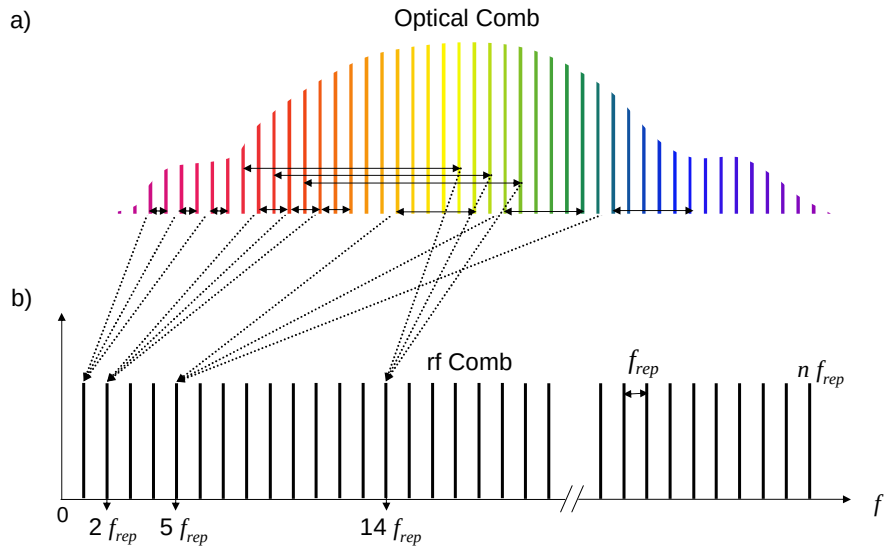

Figure 2.3: Depiction of homodyne detection of f_{rep}. The component in the rf spectrum at f_{rep} results from beating between all the adjacent components in the optical comb. The components at $n\ f_{rep}$ are generated by beating between optical comb components separated in frequency by $n\ f_{rep}$. Since all optical comb components contribute to the beat signal, the generated rf spectrum exhibits a very strong signal-to-noise ratio (SNR) for each rf comb component. The rf signal that results from this interference, in contrast to that shown here, typically exhibits a gain roll off determined by the speed of the photodetector.

in frequency by f_{rep}, it is also an rf frequency. However, because the offset frequency is common to each comb line, the linear optical heterodyne observed when measuring f_{rep} is insensitive to f_0 [see eqn. 2.7]. As a result, f_0 is determined by nonlinear self-comparison, or also possibly via comparison against a secondary optical standard.

2.2 Self-referencing

The major advance in 2000 was measurement of f_0 independent of a secondary optical standard. The measurement scheme was first conceived of in the frequency metrology community and proposed by Telle *et al.* in 1999 [74]. The idea was to use the Ti:S laser spectrum for self-comparison. This is achieved by cross-referencing harmonics of the spectral extremes of the optical comb, $|N(nf_{rep}+f_0)-M(mf_{rep}+f_0)|$ [45]. The

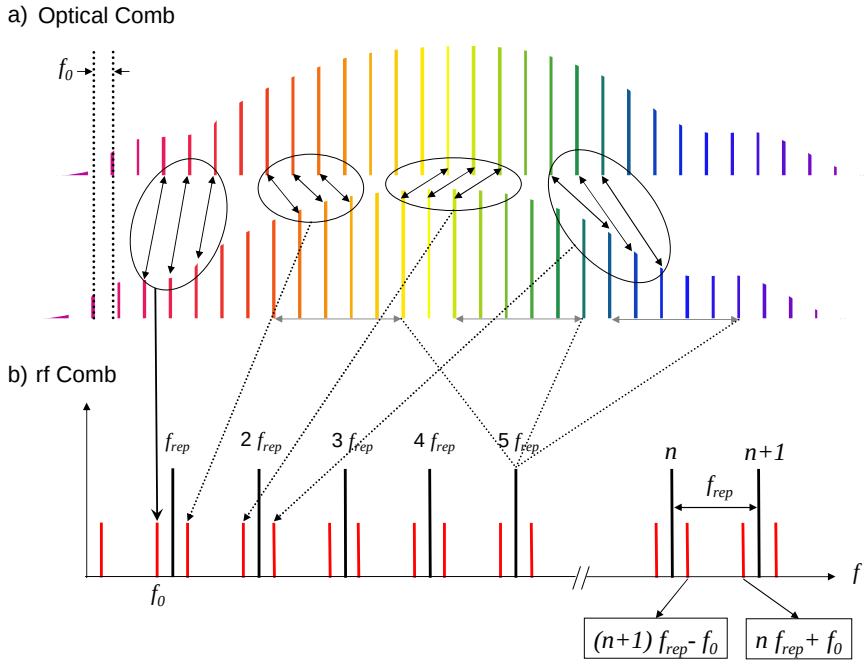

Figure 2.4: a) Depiction of the measurement of the laser offset frequency, f_0. The rf spectrum generated via self-referencing of the laser offset frequency can be thought of as heterodyning two optical combs offset in frequency by f_0. b) There are two components to the rf spectrum, the signal produced by each optical spectrum separately that results in the rf spectrum of harmonics of f_{rep}. The second is the cross-interference of the optical spectra that generate f_0 sidebands on the repetition rate harmonics. The sidebands at the offset frequency are enhanced by the collective addition due interference of the many contributing comb components. The rf signal that results from this interference, in contrast to that shown here, typically exhibits a gain roll off determined by the speed of the measurement device.

harmonics are chosen such that spectral overlap is achieved, that is $Nn = Mm$. If this criteria is satisfied, optical interference of the harmonics results in a beating at the rf difference frequency $(N - M)f_0$ [see Fig. 2.4].

Although the implementation of the self-referencing scheme may appear trivial, the major drawback is the requirement of an extremely large bandwidth. To perform the simplest optical comparison, where $N = 1$ and $M = 2$, the bandwidth requirement is an optical octave (∼500 nm). The typical bandwidth available from a Ti:S laser, however, is on the order of 100 nm. In 2000, microstructure (MS) fiber technology provided a simple solution to the bandwidth problem as it enabled continuum generation using the

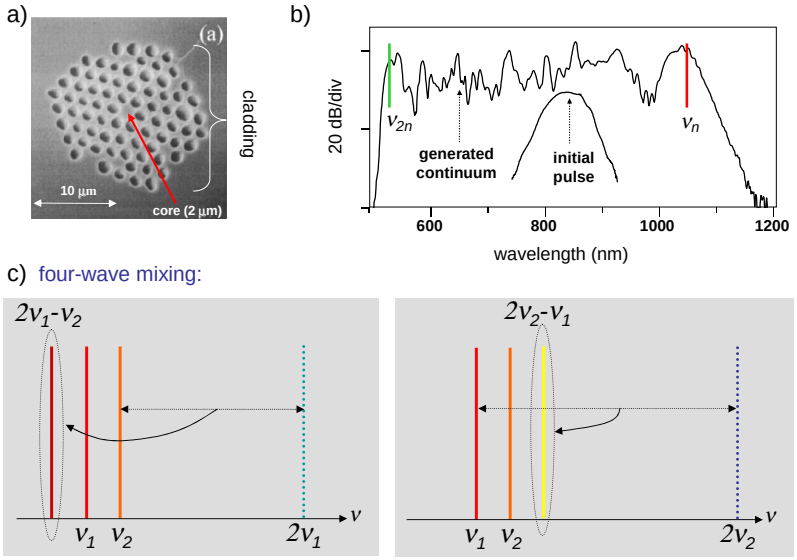

Figure 2.5: a) Cross-section of microstructure fiber developed by Lucent Technologies to work at Ti:S wavelengths. b) The broadening of a Ti:S input pulse to an optical octave with the octave points marked. The ν and 2ν point of the continuum used for self-referencing are marked. c) Schematic depicting the generation of new wavelengths via four-wave mixing of light at ν_1 and ν_2. The dashed line represents the square of the field at frequency ν_i that is optically heterodyned with the field at ν_j to produce light with frequency $2\nu_i - \nu_j$.

pulse energy available directly from the unamplified laser output [62]. More recently, however, ultra-broadband laser have been demonstrated that allow for self-referenced measurement of f_0 using the laser spectrum directly [see Sect. 5.2].

2.2.1 Microstructured fiber

One method used to increase the spectrum of a pulsed laser is external broadening in optical fiber. This technique takes advantage of the high intensity generated and maintained by confining a light pulse within a small mode field diameter defined by the fiber core. Broadening is obtained in optical fiber via the third-order nonlinear process of four-wave mixing, which results in photo-mixing of the incoming light pulse with itself. This process results in the generation new frequencies at $(2nf_{rep} - mf_{rep})$, where m and n define different comb lines of the frequency spectrum.

Continuum generation of modelocked nJ laser pulses from a Ti:S oscillator alone requires a long nonlinear interaction length in optical fiber. The effect of material dispersion on the light pulses launched into standard telecom fiber, however, limits the nonlinear interaction length to only a mm or so. This is because the zero dispersion point for telecom fiber is at $\sim$1.31 μm whereas Ti:S lasers are centered $\sim$ 800 nm. The difficulty posed by dispersion may be overcome by using microstructured (MS) fiber, which is engineered such that the geometrical waveguide dispersion cancels the material dispersion within the Ti:S gain bandwidth.

The cladding of MS fiber is composed of a honeycomb structure of air holes [see Fig. 2.5 a]. By changing the filling fraction of the air-glass cladding and the core size the zero dispersion point of the fiber may be shifted by several hundred nanometers, making MS fiber a convenient method for continuum generation for different modelocked laser sources in the visible and IR [53]. Additionally, the large index step between the core and cladding results in strong confinement of light within the fiber core, and in single mode propagation of light over a bandwidth of at least an optical octave. This is because the large index step causes very weak coupling to higher order modes.

For MS fiber designed to work at Ti:S wavelengths, the high confinement coupled with the zero dispersion point at 780 nm allow for high intensities to be maintained over a much longer interaction length, thereby leading to the incredible broadening observed in Fig. 2.5 b). Broadening in the fiber allows for generation of coherent light from 400 nm to greater than 1300 nm, more than sufficient to perform a self-referenced measurement of the laser offset frequency.

2.3 Experimental setup

Using the continuum generated in MS fiber it is possible to perform a measurement of the laser offset frequency using the self-referencing technique described above. Self-referencing is implemented by using a ν–to–2ν interferometer [see Fig. 2.6 b]. This

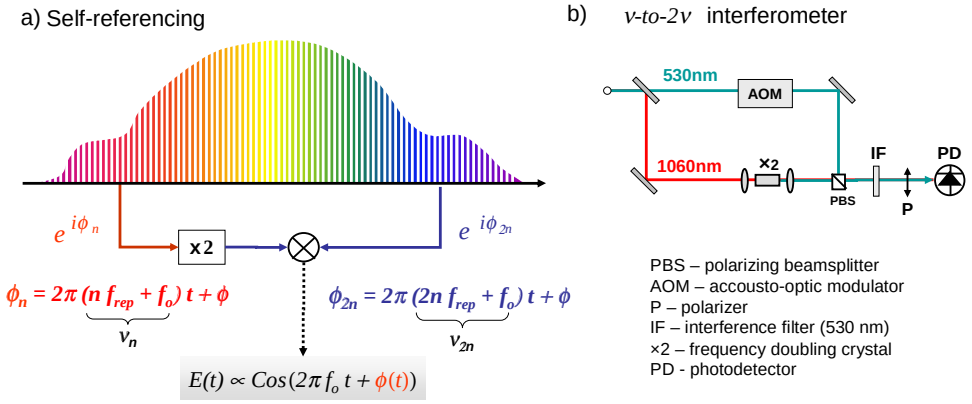

Figure 2.6: a) Depiction of self-referencing. Optical heterodyne between harmonics at the edges of the spectrum results in amplitude modulation of the light at frequency $2\nu_n$ with a modulation frequency, f_0. b) Experimental realization of self-referencing using a ν–to–2ν interferometer. For further experimental details consult Sect. A.5.1.

interferometer performs the simplest $N = 1$, $M = 2$ harmonic comparison [Fig. 2.6] [45], requiring the least number of nonlinear stages but the most optical bandwidth.

The ν–to–2ν interferometer uses a Mach-Zender geometry. Light entering the interferometer is split by a dichroic beamsplitter that reflects the low frequency end of the MS fiber broadened spectrum (for simplicity 1060 nm), and transmits the high frequency end of the spectrum (for simplicity 530 nm.) Light in the 1060 nm arm of the interferometer is then frequency doubled in a nonlinear crystal (for the experiments here either 1 cm LiB_3O_5 (LBO) or 4 mm β Barium Borate (BBO) crystals cut for type I phase matching were used.) Light from the arms of the interferometer are then recombined at a beamsplitter. Measurement of an interference signal requires temporal, polarization, spectral, and spatial overlap between the two beams of the interferometer. The former requires adjustment of the relative path length of the two interferometer arms. The latter is achieved by matching the mode sizes, the wavefront curvature of the beams and by obtaining good spatial and angular overlap between the two beams. Once the beams are recombined, an optical filter (center = 530 nm with 10 nm bandpass) and polarizer are used to satisfy the second and third conditions. Aside from ensuring

spectral overlap, an interference filter or grating selects out only that light contributing to the beat signal. This helps to increase the signal-to-noise ratio (SNR) of the beat signal and makes sure that the photodiode (PD) does not saturate.

The comb-offset frequency is measured as amplitude modulation of the filtered pulse train between the green portion (∼530 nm) and the doubled near IR portion (∼1060 nm) of the spectrum. This modulation is measured using a fast PD and appears as amplitude sidebands on the repetition rate rf spectrum. Once the heterodyne beat signal is measured, it is electronically filtered, amplified and used in a feedback loop for comparison against a known rf reference.

2.4 Phase stabilization of the Ti:sapphire laser

Absolute stabilization of the laser spectrum is obtained by phase locking both f_{rep} and f_0 to synthesized reference frequencies. A phase lock is obtained when the frequency and phase of a slave signal tracks that of a reference signal by the action of a phase locked loop (PLL) [see Fig. 2.7]. For electronic comparison, the PLL uses a mixer that measures the difference frequency between the slave and reference signals. If the two signals have the same frequency, the output of the mixer is a phase comparison that can serve as an error signal to actively correct for errors in the slave signal [see Fig. 2.7]. A loop filter (LF) is used to electronically shape (integrate, filter and amplify) the error signal to match the transfer function of the negative feedback actuator. Negative feedback to the laser acts as a voltage-to-frequency converter that uses the electronic feedback signal to correct for instabilities in frequency/phase.

2.4.1 Stabilization of the laser offset frequency

In the case of the offset frequency, stabilization is actuated by either tilting the laser end mirror after an intra-cavity prism sequence, or via amplitude modulation of the laser pump power [see Fig. 2.7]. The latter is obtained by placing an AOM

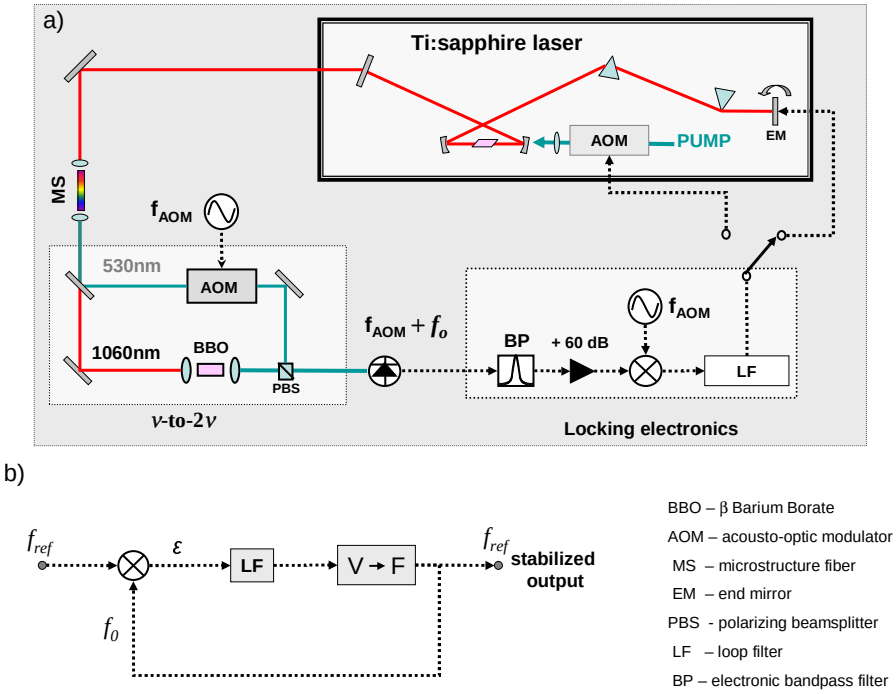

Figure 2.7: Experimental apparatus of a carrier-envelope phase-stabilized fs Ti:S laser. The box in the lower left shows the ν–to–2ν interferometer used to measure f_0. An AOM is included in the ∼530 nm arm of the interferometer to shift the frequency of one arm relative to the other such that f_0 may be set to zero [see Sect. A.5.1.2]. For further details concerning the ν–to–2ν interferometer and the stabilization electronics please consult Sect. A.5.1 and Sect. A.6, respectively. b) Block diagram of a phase locked loop (PLL). An input signal to be phase locked, f_0, is compared against a reference frequency, f_{ref}, using a mixer. The phase difference between the two serves as an error signal that is shaped (gain and filtering) to match the characteristics of the feedback actuator. The shaped voltage signal is then fed back to a voltage-to-frequency converter, here the Ti:S laser, to correct for the phase disparity.

in the path of the laser pump beam [59]. This method takes advantage of nonlinear amplitude-to-phase conversion in the Ti:S crystal to control the carrier-envelope phase (the speed of the feedback of this method is limited by the upper state lifetime of the Ti:S crystal, $\sim 10\ \mu$s.) The former method allows for control of f_0 by adjusting the phase delay between successive longitudinal cavity frequencies. After a compressor prism pair, intra-cavity light is linearly dispersed on the laser end mirror (EM). Tilting of the EM in the horizontal plane results in the addition of a linear time delay vs frequency, which leads to a constant shift in frequency between each pair of comb components. Tilting is

actuated by placing the laser EM on a piezo-electric actuator (PZT), whose speed (< 30 kHz) is determined by the engineering of the mirror + PZT system [see Fig. A.11].

If stabilization of the Ti:S laser is to be used only to produce a CE phase stable train of pulses, it is not necessary to stabilize the frequency comb spacing. Given eqn. 2.6, the accumulated pulse-to-pulse carrier envelope phase between adjacent pulses is linearly related to the ratio of the comb offset frequency to the laser repetition rate, by[1]

$$\Delta\phi_{CE} = \int^{t_{rt}} (2\pi f_0) dt = 2\pi \frac{f_0}{f_{rep}} \tag{2.8}$$

As a result, stabilization of f_0 to a reference signal derived from the laser repetition rate [see Sect. A.6.1.1] is sufficient for producing a phase stable train of pulses, even if f_{rep} is free running. Thus the relative stability of the offset frequency is linked to that of the repetition rate (in this case one establishes stability in the pulse phase, not coherence of the optical comb elements.) This significantly reduces the complexity of the stabilization system since neither the offset frequency, nor the comb spacing need to be referenced absolutely. It is the stability in the ratio between the two which determines the coherence of the pulse train [see Chap. 4].

2.4.2 Stabilization of the laser repetition rate

Stabilization of the comb spacing uses a high harmonic of the laser repetition rate for stabilization. This is necessary given that errors in f_{rep} are multiplied up by 10^6 to reach optical frequencies [see eqn. 2.5]. Because phase noise power on the repetition rate harmonics in the rf spectrum scales as the square of the harmonic number, in principle, the higher the harmonic used for stabilization the better the phase sensitivity obtained.[2] The highest sensitivity measurement of the comb spacing is obtained using an optical

[1] This equation holds only for the simple case that f_0 is a constant. In reality, of course, f_0 is subject to phase noise, whereby $\Delta\phi_{CE}$ picks up a noise term that takes in account noise. This issue is explored in detail in Chap. 4

[2] The quality of the microwave reference source may be poorer, however, at higher frequency.

as opposed to rf reference [see Fig. 5.8] and is the subject of of all-optical clocks [80, 12].

Stabilization of f_{rep} is similar to that used for the offset frequency. The rf spectrum of the repetition rate harmonics are measured on a fast PD. A high harmonic from the rf spectrum is then filtered and amplified such that it may be compared against a synthesized reference frequency. Frequency comparison, which is again obtained using a mixer, results in an error signal that is shaped by a loop filter and used for negative feedback to the laser. Corrections to f_{rep} are controlled by adjusting the laser cavity length by either placing the laser end mirror or output coupler on a PZT.

Instabilities in f_{rep} correlate directly to time changes in optical cavity length that are caused by time changes in the intracavity indices of refraction. Such changes also naturally influences dispersion within the laser cavity thus affecting f_0 [34].

2.4.3 Passive stability of the Ti:sapphire laser

In theory, if the electronics and feedback are infinitely fast, feedback to the laser will take out any intrinsic laser instabilities. Limits to the speed of the PLL, however, make it that passive stability is important for producing a stable laser. As a result of this consideration, the laser used here is engineered to reduce the effects of environmental perturbations to stability [see Fig. 2.8].

The three primary factors affecting phase stability are mechanical vibrations, air pressure changes, and temperature changes. Vibrations are addressed by using low profile and solid mirror mounts throughout the laser cavity, which is not typical practice for ultrafast lasers. Of course, high quality optical tables with vibration isolation legs are required. Enclosing the laser in a rigid box helps to reduce vibrations due to acoustics and also addresses the problem of air pressure changes. Air pressure fluctuations are detrimental because they change the density of the air in the cavity, which in turn changes the effective optical path length. Although this is a small effect, it can easily change the cavity length a wavelength or more, which in turn, changes the comb

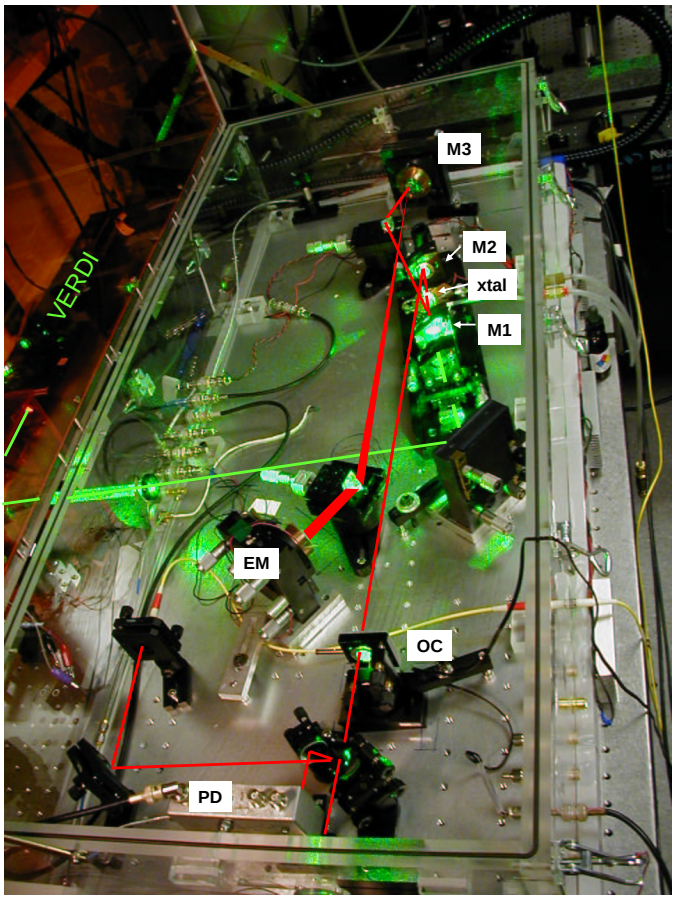

Figure 2.8: The Ti:S laser used in our experiments. Construction details are in the text.

frequencies by f_{rep} or more. Although the long term drift of f_0 and f_{rep} caused by temperature changes can easily be compensated by the feedback loop, due to the limited actuator dynamic range, the duration of locking is limited.

To obtain long term locking, the laser is constructed on a 5 cm thick cast aluminum plate. Typically, the thermal mass of such a plate is sufficient so that active temperature control is not required, although that depends to some extent on the ambient temperature fluctuations. A cavity mirror mounted on a PZT with one wavelength worth of travel, together with thermal stabilization via a gentle water flow through the laser base plate, can usually maintain feedback lock without interruption for many hours. A secondary benefit of the cast plate is a greater immunity to higher frequency

(airborne) vibrations. By carefully isolating the cast plate (typically with rubber stoppers/springs having a resonant frequency of 400 Hz) from the table and arranging the rigid enclosure to entirely span the cast plate, the airborne vibrations are not strongly coupled to the laser. Instead, for the most part, they are directly shorted to the optical table. Additionally, beam tubes are also used to cut down on pointing and pressure instabilities of the pump beam as it is directed to the Ti:S laser. The same general precautions are taken into account in the ν–to–2ν interferometer design.

2.5 The stabilized comb

Once both the comb spacing and the laser offset frequency are stabilized, using the techniques described above, the stabilized Ti:S laser may provide both a source of phase-stable pulses as well as an absolute optical comb in the IR. The stability of the two characteristic frequencies, however, determines the quality of the optical comb and the pulse train.

In metrology, the width of the comb lines and uncertainty in their absolute position present the primary limits on precision and accuracy. Because the accuracy and stability of the comb components of the Ti:S laser are fundamentally limited by the sources to which they are stabilized, much effort must be placed into development of the primary reference [37]. In the microwave regime, the primary standard is the Cs clock transition, although possibilities exist in the optical. Stabilization of the Ti:S frequency comb, for example to neutral atomic Ca [57] and Hg+ [71] or molecular Sr [79], for instance, represent the first generation of optical clocks that in time should rival the current Cs standard (as an application modelocked lasers to all-optical clocks see ref. [12, 80] and also Sect. 5.2.2.)

Phase stabilization of a Ti:S laser for use in waveform synthesis of ultrashort pulses has different requirements from those of optical frequency metrology. In ultrafast experiments that exhibit sensitivity to the electric field of the light pulses, the primary

concern is the carrier-envelope coherence of the laser pulse train, not the stability of the individual comb components. Unlike optical frequency measurement, ultrafast applications are concerned with the relative stability of f_0 to f_{rep} [see eqn. 2.4.1]. The stability in the ratio of f_0 to f_{rep} is paramount to the coherence of the pulse train since instabilities result in accumulated phase error with time [see eqn. 2.4.1]. The accumulation of a π phase error results in loss of coherence of the pulse train and thereby determines the time duration over which a phase sensitive measurement may be performed. This is significantly different from optical frequency metrology, where long time averaging yields an increase in measurement stability of an optical line. Additionally, stabilization of the laser pulse train does not require the use of an absolute reference. In absolute optical frequency measurement, as discussed in the previous paragraph, the reference serves as the primary limit to precision and accuracy. In contrast, carrier-envelope phase stabilization using an rf synthesizer, in practice, is fundamentally limited by the characteristics of the PLL, not the frequency reference.

Chapter 3

Phase noise characterization of microstructured fiber

One of the first concerns plaguing the self-referencing technique was whether external broadening of Ti:S pulses conserved the coherence of the frequency comb. This was an issue considering the extremely nonlinear process that would be necessary. Before the development of MS fiber, it was common to employ broadening of amplified pulses by focusing the pulses into a short piece of glass [48]. The high intensities provided by the amplified pulses allowed for self phase modulation (SPM) of the laser light to produce a continuum of wavelengths. Although a common practice, it was only proven in 2000 by Bellini and Hänsch that this broadening technique preserved the coherence of the laser pulse train [8]. The coherence of the continuum was demonstrated using a quasi double slit experiment where amplified pulses were focused to two points, closely spaced, in a piece of glass. The diverging continuum from both points were then observed to yield interference fringes demonstrating spatial and phase coherence of the continuum. This helped to validate the possible notion of self-referencing, although it was not first demonstrated using this broadening scheme.

In 1999 Lucent Technologies demonstrated extreme spectral broadening of unamplified Ti:S pulses using specially designed microstructured (MS) fiber [62]. The combinations of MS fiber, Jan Hall and the Cundiff group proved a potent combination, whose net result was the first demonstration by Jones and Diddams of self-referenced stabilization of a Ti:S laser [45]. One of the main concerns was whether ref. [45] demon-

strated true coherence of the pulse train. This claim was questioned by the scientific community whose concern was whether the use of MS fiber for broadening resulted in phase noise on the laser pulse train. Clearly, it had been demonstrated by Jones *et al.* that the broadened comb was well behaved enough to produce a clean f_0 beat signal and that the resultant beat was possible to stabilize. Out-of-loop coherence of the resulting pulse train, however, was demonstrated using a cross-correlator that allowed for the generation of a fringe resolved correlation trace between one pulse and a pulse emitted two cavity round trips later. Due to the complexity (length considerations) of the correlator, the coherence measurement was limited to 20 ns, definitely not long enough to claim that the use of MS fiber allowed for long term phase coherence in the laser pulse train [see Chap. 4]. It remained to be demonstrated, as it had been for broadening of amplified pulses in a glass plate, that the continuum generated by MS fiber preserved the coherence of the laser pulse train.

3.1 Amplitude-to-phase noise conversion in microstructured fiber

The concern of using MS fiber for external broadening of Ti:S pulses, was the same as it had been for SPM generated light of amplified pulses in glass. That is because the highly nonlinear process used to broaden the laser spectrum might corrupt the stability of the offset frequency, thereby overwhelming the true value of the CE phase. From the results by Jones *et al.* it could be assumed that this generated noise was not strong enough to make it impossible to stabilize the broadened spectrum. However, even if one could perfectly stabilize the output of the fiber, a problem still remains. When the stabilization loop for the laser is closed, the PLL can only use the laser to compensate for errors in f_0. The stabilization loop, however, contains many possible noise contributions apart from the laser, for instance the ν–to–2ν interferometer [see Sect. 4.3.2], PD's, electronics, and the MS fiber. If any of these components adds noise to the offset frequency, the PLL will write the noise onto the laser output as it corrects

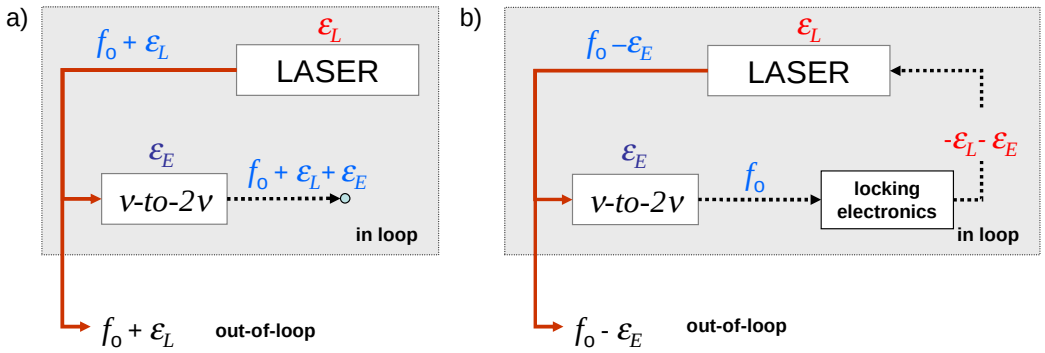

Figure 3.1: a) Schematic of the noise sources within the laser stabilization loop. A ν–to–2ν interferometer measures the laser offset frequency, f_0, plus noise from the laser ϵ_L. Measurement of f_0 adds extracavity noise, ϵ_E, yielding the net sum of the noise on f_0 of $(\epsilon_L + \epsilon_E)$. When the stabilization loop is closed, the locking electronics correct for the error on f_0 via negative feedback to the laser b). The feedback signal suppresses the laser noise completely (given it has an infinite bandwidth) but in the process writes the extracavity noise onto the laser output, $-\epsilon_E$. Subsequent determination of the laser offset frequency using an in-loop interferometer results in perfect cancellation between $-\epsilon_E$ written onto the laser and ϵ_E resulting during measurement.

for the phase error [see Fig. 3.1].

A particular concern with MS fiber is that small amounts of amplitude noise on the input pulses will be converted to phase noise in the fiber. This occurs because of the index of refraction's dependence on intensity, $n(I) = n_0 + n_2 I$, where n_0 is the linear index, n_2 is the nonlinear index and I is the intensity of the light in the fiber core (i.e., including the effective area). Propagation of light with frequency ω over the length of the fiber, l_0, results in phase shift in the carrier-envelope phase,

$$\Delta\phi = \omega\, l_0 \left(\frac{1}{v_g} - \frac{1}{v_p}\right) = \frac{\omega^2\, l_0}{c} \frac{d(n_0 + I\, n_2)}{d\omega}, \tag{3.1}$$

resulting from the group and phase velocity differences, $v_p = c/n_p$ and $v_g = c/n_g$, of the fiber core, where $n_p = n$ and $n_g = n + \omega \frac{dn}{d\omega}$.

Linear dispersion in eqn. 3.1 only adds a constant phase shift to the pulse train, but does not result in added instability to f_0. The nonlinear contribution of the Kerr-effect to the carrier-envelope phase, ϕ_{NL}, results in phase noise. This same process is also responsible for intracavity generation of phase noise in the Ti:S laser crystal due to

fluctuations in laser pump power [59]. The time-dependent shift is directly proportional to the dispersion of n_2 and the change in intensity (ΔI), that is,

$$\phi_{NL} = \frac{\omega^2 \, l_o}{c} \, \frac{dn_2}{d\omega} \, \Delta I = C_{AP} \, \Delta P. \tag{3.2}$$

This equation defines the amplitude-to-phase conversion coefficient for microstructure fiber, C_{AP}, which relates the nonlinear shift in the carrier-envelope phase, ϕ_{NL}, to a change in power, ΔP, on the input beam. This definition for C_{AP} is valid, however, only for a very narrow parameter space, determined by pulse chirp, fiber length, optical frequency.

A ν–to–2ν interferometer is used to measure amplitude-to-phase (AM-to-PM) conversion in MS fiber [Fig. 3.2 a]. This is done by imposing a known amplitude modulation on the laser output, $P(t) = P_o + \Delta P sin(\omega_{mod} \, t)$, before the fiber. The applied amplitude modulation of the laser intensity is converted to nonlinear phase modulation, $\phi_{NL}(t) = C_{AP} \, P(t)$, or in turn, frequency modulation on $f_0(t) = \frac{1}{2\pi} \, \frac{d\phi_{NL}}{dt} = \frac{\omega_{mod}}{2\pi} \, C_{AP} \, \Delta P \, cos(\omega_{mod} \, t)$. As a result, the measured frequency deviation of f_0, Δf, should be directly proportional to the deviation in power, ΔP, that is,

$$\Delta f = f_{mod} \, C_{AP} \, \Delta P. \tag{3.3}$$

The rms frequency deviations of f_0 resulting from AM-to-PM in MS fiber are determined using a frequency-to-voltage (F-to-V) converter. The F-to-V converter measures the FM fluctuations on a high frequency carrier, and converts these to a voltage signal, whose amplitude is directly proportional to frequency deviation [see Sect. A.7.2.2]. Unfortunately, because the F-to-V converter only has a dynamic range of 1 MHz, its use requires stabilization of f_0. The offset frequency, measured in the ν–to–2ν interferometer, is stabilized by tilting the laser end mirror with a net servo bandwidth < 1 kHz. To ensure that the phase noise generated by the fiber is not transferred to the laser, the laser power is amplitude modulated at a modulation frequency, f_{mod}, significantly outside the servo bandwidth (> 10 kHz). This also helps to reduce contamination

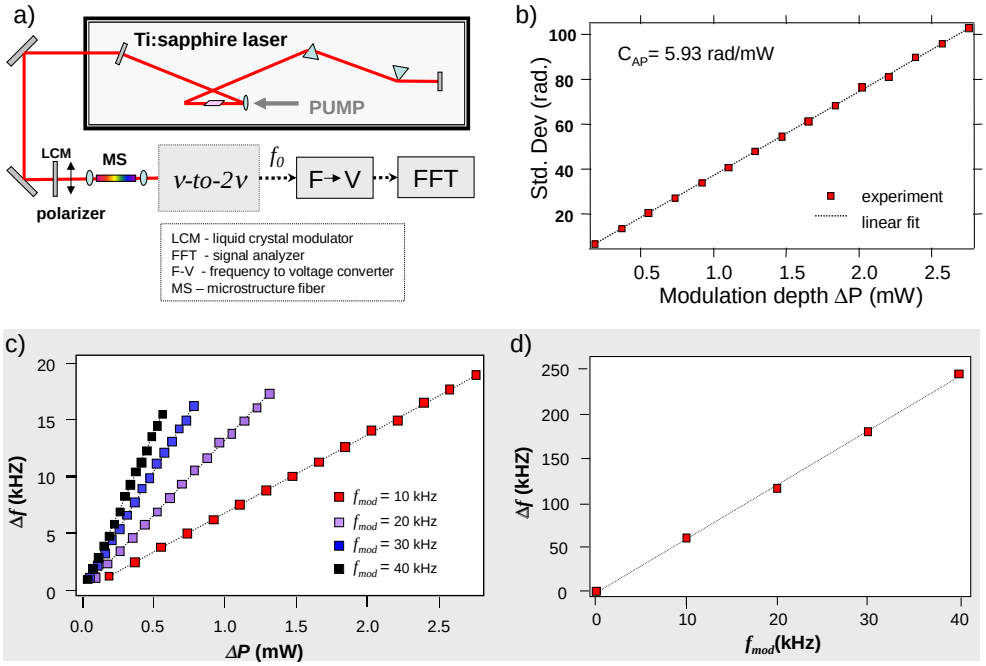

Figure 3.2: a) Experimental setup used to determine the amplitude-to-phase conversion coefficient, C_{AP}, for MS fiber. Amplitude modulation of the laser power into the fiber is obtained using a liquid crystal modulator and a thin polarizer. A frequency-to-voltage converter (F-V) is used to distinguish between amplitude and phase noise on the beat signal and an FFT is used after the F-to-V converter to measured the frequency deviations at ω_{mod}. b) The measured deviations in f_0, Δf, as a function of modulation depth, ΔP performed at a modulation frequency $f_{mod} = 10$ kHz. A linear fit to the experimentally measured deviations results in an amplitude-to-phase conversion coefficient, C_{AP} for a 4.5 cm piece of MS fiber of 5.93 rad/mW at a 100 MHz repetition rate with an average input pulse power of 50 mW for a minimum temporal pulse width of 15 fs at the input to the fiber. c) The observed frequency deviations in f_0 due amplitude-to-phase conversion in MS fiber as a function of different modulation frequencies. d) As expected given eqn. 3.3, the frequency deviation, Δf, is linearly proportional to the modulation frequency, f_{mod}.

of the measurement due to imperfect stabilization of f_0 that results in an increase in broadband noise below 5 kHz. This contamination is further reduced by narrowing the detection bandwidth of the signal analyzer (FFT) that is used to analyze the signal from the F-to-V converter.

By varying the amplitude modulation depth, ΔP_{rms}, and comparing this to the resulting change in frequency deviation, Δf_{rms}, it is possible to determine $C_{AP} = \Delta f_{rms}/(f_{mod}\Delta P_{rms})$ [see Fig. 3.2 b]. The strength of the rms deviation in frequency, Δf_{rms}, is detected at the amplitude modulation frequency, 10 kHz, using a signal analyzer, [FFT in Fig. 3.2 a]. Each data point in Fig. 3.2 b) measures the rms frequency deviation versus amplitude modulation depth. For a refractive index with only first order dependence on intensity, the strength of the phase modulation should increases linearly with power modulation. The experiment was repeated for four different modulation frequencies. By fitting the data obtained from these different modulation frequencies to a straight line we determine an average value of $C_{AP} = 5.93$ rad/mW. This value for C_{AP} was determined using a 4.5 cm piece of fiber with an average coupled power of 50 mW at a 100 MHz repetition rate. The pulses at the input of the fiber were chirp compensated to yield a $\sim$ 15 fs pulse duration. This was confirmed by using an autocorrelator containing the same optical elements. Consequently, this translates to C_{AP} = 593 rad/ nJ. Knowledge of C_{AP} for the fiber then makes it possible to determine the contribution of fiber phase noise to the carrier-envelope phase by measuring the power fluctuations on the laser output [see Sect. 4.3.1 for details].

The validity of this measurement, however, is limited to a very narrow parameter space, but one that is typical for our system. A more thorough examination of MS fiber noise would require systematically studying the affect on C_{AP} due to changes in different parameters such as pulse chirp, coupled power, and fiber length. On the subject of fiber length, we believe that the conversion coefficient, given compressed pulses, may be relatively insensitive to propagation length. This is possible since, for short pulses ($\sim$ 20 fs), most of the broadening appears to occur within the first few mm of fiber. Short pulses incident to the fiber exhibit high enough intensity to allow for broadening of incident $\sim$ 40 nm bandwidth light to an optical octave within 3-4 mm of MS fiber, sufficient for measurement of f_0. The rapid broadening in the fiber results in heavy

chirp of the wavelength components not at 770 nm (zero dispersion point of the fiber) which results in a rapid decrease in intensity within only a few mm's of fiber. Therefore, the amplitude-to-phase conversion coefficient should only exhibit a strong dependence on fiber length within the first few mm's of fiber.

3.1.1 Transfer of fiber noise onto the output of the laser

Next it is interesting to determine whether fiber generated phase noise is transferred onto the laser output as a result of the stabilization process. To gain insight into the transfer of extra-cavity sources of phase noise, a measurement of the noise must be performed independent of the stabilization loop. Such a measurement is often termed out-of-loop, and may be obtained by running two ν–to–2ν interferometers simultaneously, each with its own piece of MS fiber.

To measure the transfer of fiber noise to the laser via the action of the servo loop, sinusoidal amplitude modulation is imposed only on the light into the fiber in the first interferometer [Fig. 3.3 a]. This will result in contamination of f_0 that is then used in a feedback loop for locking the laser. The action of the servo loop is such that the phase error is compensated using the laser as an actuator. The error, then written onto the output of the laser, is measured using an independent ν–to–2ν interferometer [28]. Figure 3.3 a gives a sample set of data, where the sinusoidal deviations in f_0 due to phase modulation from the fiber are measured using a frequency counter. To make sure that the frequency noise from the fiber was transferred to the laser, modulation of the laser power was at 0.1 Hz, well within the servo loop bandwidth.

Aside from demonstrating transfer of phase noise onto the laser output, this out-of-loop measurement may also be used to compare with the previous measurement of C_{AP} in Sect. 3.1. By varying the modulation depth of the laser power coupled into the MS fiber in the first ν–to–2ν interferometer and measuring the rms frequency deviations of f_0 on the second we once again determine $C_{AP} = 2\Delta f_{rms}/(f_{mod}\Delta P_{rms})$ [see Fig. 3.3

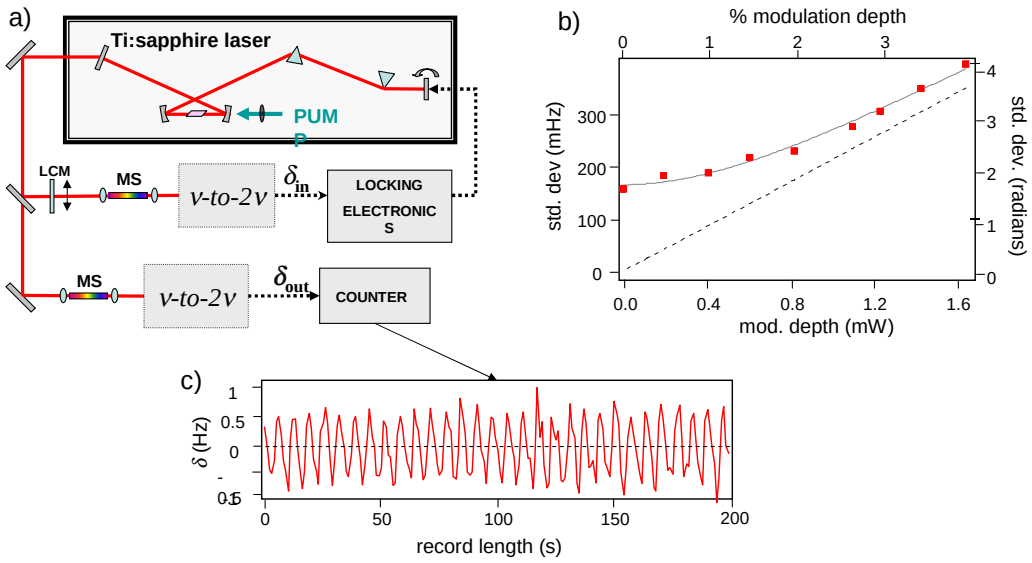

Figure 3.3: a) Experimental setup used to determine whether amplitude-to-phase conversion in MS fiber is transferred onto the laser output by the action of the servo loop. The experiment uses a dual interferometer setup, where AM noise on the laser light to one fiber (with the stabilization loop) induces phase noise on f_0. This noise is transferred by the action of the servo loop onto the output of the laser, whereby the deviations induced in f_0 are measured using a second, independent (out-of-loop) interferometer using a frequency counter. A sample data set is included that shows the sinusoidal deviations in f_0 due to sinusoidal modulation of the laser power into the locking interferometer. This demonstrates the transfer of fiber noise onto the laser by the action of the servo loop. b) The measured deviations in f_0, Δf, as a function of modulation depth, ΔP. A fit to the measured data C_{AP} =6.02 rad/ mW for a 5 cm piece of MS fiber at a 100MHz repetition rate with an average input pulse power of 40 mW.

b].

Each data point in Fig. 3.3 b) is determined from a time record at a 1.0 s gate time over 200 s [see Fig. 3.3 c]. Intrinsic phase noise, η, due to imperfect stabilization of f_0, measured at zero modulation depth, adds in quadrature with those due to AM-to-PM modulation of MS fiber, yielding a total fluctuation given by $\sqrt{\eta^2 + (C_{AP}\,\Delta P)^2}$. Fitting the data to this yields $C_{AP} = 602$ rad/nJ, confirming the result obtained in the previous experiment [$C_{AP} = 593$ rad/nJ, Sect. 3.1].

Side-by-side ν–to–2ν interferometers also yield insight into long-term phase stability and allow verification that accumulated extra-cavity noise does not corrupt this

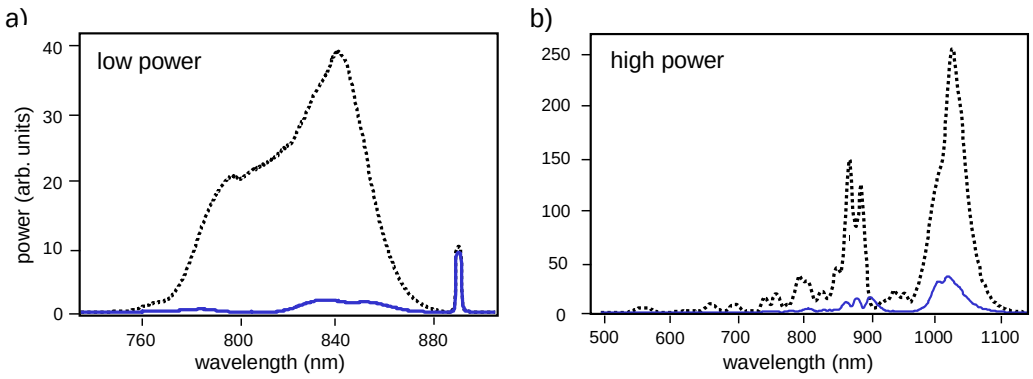

Figure 3.4: Extinction of the primary axis of MS fiber for low (244 μW) a) and high b) intensity light. The dotted (solid) line indicates light launched along the fiber primary axis and analyzed with a polarizer co- (cross) polarized with the input polarization. Imperfect extinction may results from twist in the core along the length of the fiber.

stability. This may be done by analyzing the phase noise spectra of the stabilized offset frequency, determined from each interferometer individually. This measurement determines the noise spectra of the offset frequencies both in- and out-of loop. Ideally, the in-loop measurement is limited by the feedback loop only. Fluctuations in the out-of-loop measurement are due to extra-cavity noise sources as well as residual laser noise not removed by the feedback loop. From eqn. 2.6 it may be seen that an out-of-loop measurement of the total phase noise on f_0 will give insight into the coherence of the carrier-envelope phase, which is the subject of Chap. 4.

3.2 Birefringence and nonlinear polarization rotation in microstructure fiber

The geometry of MS fiber cladding consists of a honeycomb structure of air holes. Asymmetry of the cladding that results during the pulling of the MS fiber, however, can produce a slight transverse birefringence. The effect of the resulting retardance is particularly obvious in these fibers, whereby optimal broadening is obtained along a preferred polarization axis.

Light that is injected along the primary axes of the fiber maintains its input

polarization [see Fig. 3.4]. Light incident to the fiber, with a polarization off of the primary axes, exits with a polarization that is rotated with respect to the input, indicating fiber birefringence. The strength of the linear retardance of the fiber may be easily determined by launching low intensity, broadband laser light from a Ti:S laser into the fiber at 45 degrees to the primary axes [see Fig. 3.5 a]. By analyzing the output using a polarizer, set with its polarization axis either co- or cross-polarized with the input light, one obtains a fringe pattern indicating the strength of polarization rotation due to the fiber birefringence. Figure 3.5 b) shows the fringe pattern in wavelength across the transmitted spectrum. This retardance measurement was performed for a 10 cm long piece of MS fiber, given to us courtesy of Lucent Technologies, with a coupled average power of 0.574 mW at a 100 MHz repetition rate. The Ti:S laser used in the measurement operates at a center wavelength of 800 nm, with 15 fs pulses at the input to the fiber. Analysis of the fringe pattern determines a value of the linear retardance for the fiber to be $\Gamma_\lambda = 2\pi(19914)/\lambda$. At 800 nm the 10 cm fiber yields a net retardance of, $\Gamma_{800} = 49.78\,\pi$.

Increasing the light intensity from the laser, coupled into the fiber, we observe a shift in the fringe pattern, or a nonlinear change in the fiber birefringence, Fig. 3.5 c), and in more detail in Fig. 3.6. For light incident with a polarization that has an unequal distribution of power along the two polarization eigenaxes, a change in field strength will result in a nonlinear differential index between the slow and fast fiber axes, thereby resulting in a nonlinear contribution to the fiber birefringence. This means that amplitude fluctuations on the input beam will be converted to fluctuations in polarization of the broadened output. Nonlinear polarization change in fiber can be understood by considering the full vector model of the propagation of light along two orthogonal polarization axes of the fiber. Propagation in the fiber can be described by the coupled nonlinear Schrödinger equations (CNSE) in the slowly varying envelope

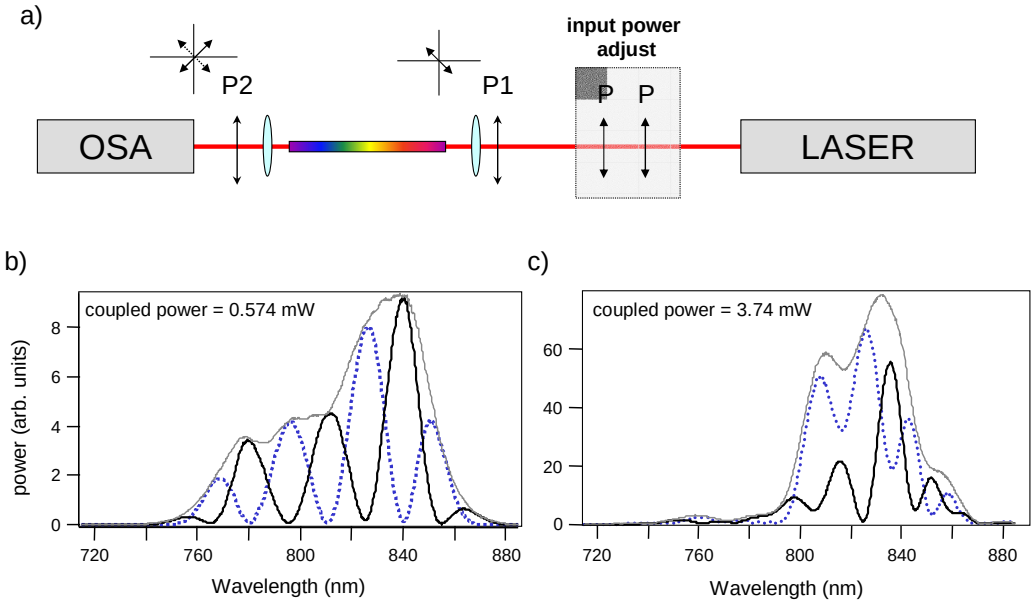

Figure 3.5: a) Experimental schematic to measure the linear and nonlinear birefringence of microstructured (MS) fiber. The two polarizers, P, are used to adjust the input power of the pulses. The pulse duration was measured using interferometric autocorrelation with similar amounts of glass as present for the optical components before the MS fiber. b) and c) show the results of the retardance measurement for MS fiber for low (0.574 mW) and high (3.7 mW) coupled power, respectively. Input light was launched at 45 degrees with respect to the MS fiber principle axis. The dotted (solid) line show the transmitted output analyzed co- (cross-) polarized with the input.

approximation,

$$i\frac{\partial u}{\partial z} + i\frac{\partial u}{\partial t} + \gamma u + \frac{1}{2}\frac{\partial^2 u}{\partial t^2} + (|u|^2 + A|v|^2)u + Bv^2u^* = 0 \tag{3.4}$$

$$i\frac{\partial v}{\partial z} - i\frac{\partial v}{\partial t} - \gamma v + \frac{1}{2}\frac{\partial^2 v}{\partial t^2} + (|v|^2 + A|u|^2)v + Bu^2v^* = 0 \tag{3.5}$$

Here, u and v are the complex envelope components along the slow and fast axes, respectively, 2δ and 2γ are the normalized group and phase velocity differences, z and t are the normalized length and time coordinates, and A and B are coefficients that express the relative strength of the cross phase modulation and coherent energy exchange coefficients, respectively. The direction of energy flow due to coherent energy exchange is determined by the relative phase between the two polarization eigenaxes.

In the case we consider of an input polarization of 45 degrees, only the last term

(the energy exchange term) in eqn. 3.5 yields a nonlinear dependence of the polarization on the light intensity. For the previous two terms in eqn. 3.5, SPM and cross phase modulation, a change in field strength results in an common imparted phase to both the slow and fast axes because the energy is distributed equally between them. This is also the case since χ_3 is nominally the same for both the slow and fast axes, that is $n_{slow} = n_{0_{slow}} + In_2$ and $n_{fast} = n_{0_{fast}} + In_2$, where $n_2 = n_{2_{self}} + n_{2_{cross}}$. Changes in field strength, as induced by the energy exchange term result in transfer of energy between the fast and slow axes, thereby causing a non-zero propagation phase between the two. As a result, the light energy is not equally partitioned between the two axes, yielding a nonlinear change to the fiber birefringence even if light is incident at a 45 degree angle to the slow an fast axes of the fiber.

The issue of nonlinear polarization is problematic for the applications of interest here since it can result in an addition of nonlinear phase noise to the broadened pulse train. This occurs since changes in the pulse intensity at the input to the fiber will result in a time-dependent change in polarization of light at the output of the fiber. Aside from fluctuations in the phase of the broadened output, nonlinear polarization rotation results in amplitude modulation of the beat since it is polarization sensitive.

The effect nonlinear polarization rotation in optical fiber has already been laid out analytically by Winful *et al.* [19]. The analytical result, however, was derived for CW light with a light intensity that is constant as a function of propagation distance. Given the complexity of the propagating spectral components and third order dispersion in the fiber results in a complicated pulse chirp and decrease in pulse intensity that is determined by the interaction between the laser pulse parameters and the characteristics of the MS fiber. Also, because of the complicated interplay between nonlinearity and dispersion, a richer understanding of the effect of nonlinear polarization requires a more complicated simulation of the experiment.

A theoretical study of the above system was conducted by our collaborators

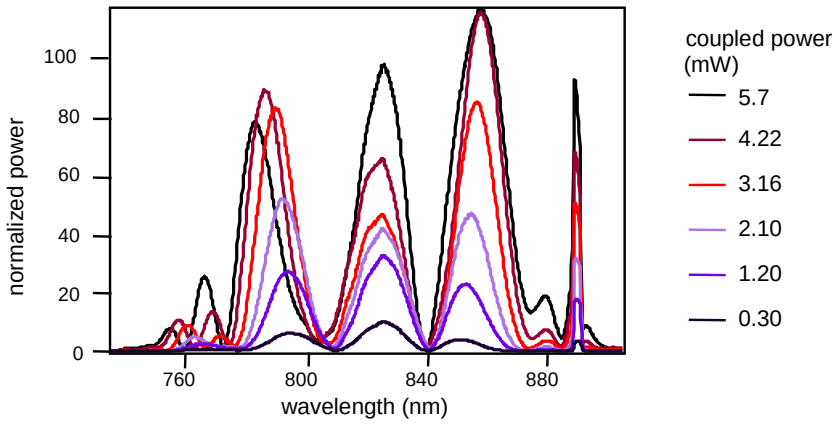

Figure 3.6: More detailed measurement of nonlinear polarization rotation in MS fiber. Light with indicated coupled power is input and analyzed at 45 degrees to the fiber primary axes. As the light power is increased a shift in the fringe pattern is observed.

I. T. Lima Jr., B. S. Marks and C. R. Menyuk at the University of Maryland. To summarize their results, using the nonlinear Schrödinger equation and a split-step algorithm they determined that the factor that allows for an accumulated effect of nonlinear polarization rotation in the fiber are dispersive effects on the propagating light pulse. Without dispersion, the coherence time of the pulses is a fraction of the differential group delay produced by the fiber birefringence. Therefore, without pulse chirp the nonlinear interaction length over which energy transfer between the two polarization axes occurs is limited [23].

Chapter 4

Carrier-envelope phase coherence and the "absolute" phase

Having determined the extent of phase noise generation in MS fiber one starts to question the general stability of the stabilization loop. This is an important question to answer for both metrologists and those interested in exploring phase-sensitive experiments. Phase coherence of the stabilized laser, however, is prerequisite for the latter as discussed in Sect. 2.5.

The first demonstration of the coherence of a stabilized laser pulse train was by Jones *et al.*. The authors demonstrated that by choosing the ratio between f_0 and f_{rep}, one had control over the pulse-to-pulse CE phase of the unbroadened pulse train [see eqn. 2.4.1]. The measurement was performed using an unwieldly cross-correlator [45] that allowed for the generation of a fringe resolved correlation trace between one pulse and a pulse emitted two cavity round trips later. Although, this demonstrated out-of-loop control over $\Delta\phi_{CE}$, it only proved that the process was coherent over 20 ns, the time between pulse i and $i+2$. Phase errors due to instabilities in f_0 result from an integration of the frequency error in time [see Sect. 4.2]. This is the natural consequence of frequency being the time derivative of phase. Integration times of 20 ns (50 MHz) are insignificant when it comes to accumulation of phase error. This is particularly true since the main source of phase error results from mechanical vibrations in the (100 Hz - 10 kHz) range, producing noise that is measurable only at much longer time scales 20 ns. The complexity of the cross-correlation process represents a severe limitation

for extension of measurement time given the huge path length difference between the correlator arms. Consequently, a different method had to be devised to determine the coherence of the laser pulse train.

The importance of a long term coherence time is predicated on the ability to control the"absolute" phase of the laser pulse train. This quantity, to some, represents the "Holy grail" for ultrafast phase-sensitive measurement. The idea behind wanting to measure and control the "absolute" phase is that, given that one is interested in determining the phase dependence of some physical process, one needs to know what the absolute phase is to make the necessary correlation.

4.1 The"absolute" phase

So what is the "absolute" phase? The main interest in the absolute phase lies in the extreme nonlinear optics community, whereby the individual shot-to-shot pulse phase can influence the outcome of a high field experiment. In the frame of the solitary pulse, the "absolute phase" is defined relative to the peak pulse envelope. However, this definition for the pulse phase is in no way absolute in the context of the pulse train. Life also becomes complicated when there is an evolution of the CE phase of the pulse train, $f_0 \neq 0$.

To understand the origin of the absolute phase, let us look for a moment at eqn. 2.6. If we integrate eqn. 2.6 and evaluate it at intervals of t_{rt} we obtain a linear relationship between the carrier-envelope phase of the n^{th} pulse in the train and f_0.

$$\phi_{CE}(n\, t_{rt}) = n\, (2\,\pi \frac{f_0}{f_{rep}}\,) + \phi_0 = n\, \Delta\phi_{CE} + \phi_0(x_0, t_0) \tag{4.1}$$

This is only mathematically valid, however, if f_0 is constant, or noiseless (issues of instabilities in f_0 are considered in Sect. 4.2). Within this limiting case, in the above equation $\Delta\phi_{CE} = 2\,\pi f_0\, t_{rt} = 2\,\pi \frac{f_0}{f_{rep}}$ is the CE phase shift accumulated between adjacent pulses. The one quantity common, however, to each pulse is ϕ_0. This phase

is often defined as the "absolute" phase of the pulse train. Mathematically ϕ_0 is the integration constant determined from the initial conditions of the laser. The question remains, however, which initial condition (x_0 and t_0) do we choose? The fact that ϕ_0 is so dependent on the choice of initial condition indicates how un-"absolute" it is.

What makes the absolute phase so important is the fact that phase stabilization of the Ti:S laser makes it possible to produce a pulse train such that every pulse in the train has exactly the same carrier-envelope phase, ϕ_0. By examining eqn. 4.1, this is accomplished by making $f_0 = 0$, which thus forces $\Delta\phi_{CE}$ to also be zero, leaving us with only ϕ_0. The current interest in the absolute phase is that it is hard to measure (Sect. 6.1), but relatively easy to control (control over the carrier-envelope phase is obtained via stabilization of the offset frequency, given of course, that one can obtain a phase lock). If one could both control and measure the absolute phase, one could boast the ability to determine the phase-dependence of coherent control-type and extreme nonlinear optics experiments [13, 58].

4.2 Measurement of the carrier-envelope phase coherence time and its importance to phase-sensitive measurement

The interest in determining the strength of phase noise generation in MS fiber in Sect. 4.3.1 was to determine its effect on the CE phase of the laser pulse train. The time scale over which pulses emitted from the laser maintain their coherence determines the amount of time one has for performing a phase sensitive experiment. The number of pulses emitted from the laser with this phase (within some standard deviation) is determined by the quality of the stabilization process. Even for a perfectly stabilized laser, extra-cavity sources of noise can contaminate the output of the laser and thus limit the time-scale over which the pulses maintain their coherence [see Fig. 3.1].

In the derivations of the CE phase for the pulse train above, one big assumption was made: that f_0 is constant. This would be the case if f_0 were stabilized perfectly.

More realistically, the limits of the servo system and extra-cavity noise sources cause f_0 to fluctuate about its lock point. To understand the effect this has on the coherence time, we return once again to eqn. 4.1. The time dependence of the fluctuations on f_0 may be written by separating the error in f_0, δf, from the carrier, that is $f_0(t) = f_0 + \delta f(t)$. If we include the time dependence of $f_0(t)$ into eqn. 4.1 we see that fluctuations of f_0 result in phase noise, $\delta\phi$, on ϕ_0,

$$\phi_{CE}(n\ t_{rt}) = n\ \Delta\phi_{CE} + \left(\int^{n\,t_{rt}} 2\pi\ \delta f\ dt + \phi_0\right) = n\ \Delta\phi_{CE} + (\delta\phi + \phi_0) \tag{4.2}$$

From this equation we see that just as f_0 is related to ϕ_{CE}, noise on f_0 is related to noise on ϕ_{CE}. In particular, if $f_0 = 0$, its fluctuations are transferred to fluctuations in ϕ_0 by

$$\delta f = \frac{1}{2\,\pi}\frac{d(\delta\phi)}{dt} \tag{4.3}$$

Therefore, for ultrafast experiments relying on the stability of the CE phase [13, 58], knowledge of f_0's stability is paramount as dephasing of ϕ_0 determines the maximum possible duration of a phase sensitive measurement.

4.2.1 Noise analysis

The stability of the offset frequency is determined via analysis of f_0's lineshape once it is locked. This is a frequency domain analysis of the fluctuations in f_0 about its carrier. If f_0 were a constant, its lineshape would be a delta function in frequency. Frequency deviations on f_0, however, result in the addition of noise sidebands to the perfect carrier. These sidebands, depending upon the detection scheme for f_0 may yield a phase noise spectrum, $S_\phi(f) = \left|\frac{F\{\delta\phi(t)\}}{\sqrt{\Delta f_{RB}}}\right|^2$ (rad^2/Hz) , or a frequency noise spectrum, $S_f(f) = \left|\frac{F\{\delta f(t)\}}{\sqrt{\Delta f_{RB}}}\right|^2$ (Hz^2/Hz) [see Sect. A.7]. These two quantities are called the power spectral density (PSD) of the noise measured with a resolution bandwidth, Δf_{RB}. The connection between the noise PSD in frequency and phase is given by,

$$S_f(f) = f^2\ S_\phi(f). \tag{4.4}$$

Either $S_f(f)$ or $S_\phi(f)$ may be used to determine the linewidth of f_0, $\Delta\nu$, or the coherence time of ϕ_0, τ_{coh}. Both quantities are determined by integration of the PSD, which yields the total accumulated rms error, in phase

$$\Delta\phi_{rms}|_{t_{obs}} = \sqrt{2\int_{-\infty}^{-1/(t_{obs})} S_\phi(f)\ df} = \sqrt{2\int_{-\infty}^{-1/(t_{obs})} \frac{S_f(f)}{f^2}\ df}, \tag{4.5}$$

or in frequency,

$$\Delta f_{rms}|_{t_{obs}} = \sqrt{2\int_{-\infty}^{-1/(t_{obs})} f^2 S_\phi(f)\ df} = \sqrt{2\int_{-\infty}^{-1/(t_{obs})} S_f(f)\ df}. \tag{4.6}$$

What these equations tell us is that over an observation time t_{obs} we can expect an rms error in phase or frequency given by $\Delta\phi_{rms}$ or Δf_{rms}, respectively. For shorter observation times, one would typically expect these deviations to be less than at longer observation times. Additionally, these equations provide a general definition of the carrier-linewidth, $\Delta\nu$, or equivalently, the coherence time, τ_{coh}. In the metrology community it is common practice to define the coherence time of a carrier in terms of the observation time at which $\Delta\phi_{rms}$ accumulates to 1 radian, that is, $\tau_{coh} = \frac{t_{obs}}{(2\pi)} = 1/(\pi\ \Delta\nu)$.

4.2.2 Experimental set up

To obtain a true measurement of the coherence time for the stabilized laser requires performing an out-of-loop measurement. The measurement scheme is the same as that used to determine the transfer of MS fiber noise onto the laser output, and follows the same basic principles [see Sect. 3.1.1]. The measurement is performed using two ν–to–2ν interferometers [see Fig. 4.1] [26]. One interferometer stabilizes the laser, while the second determines the carrier-envelope phase noise.

The carrier-envelope phase coherence time is determined for the stabilized laser system described in Chap. 2. Negative feedback to the laser is obtained with a bandwidth of $\sim$ 18 kHz via tilting the laser end mirror using a piezo-electric actuator (PZT).

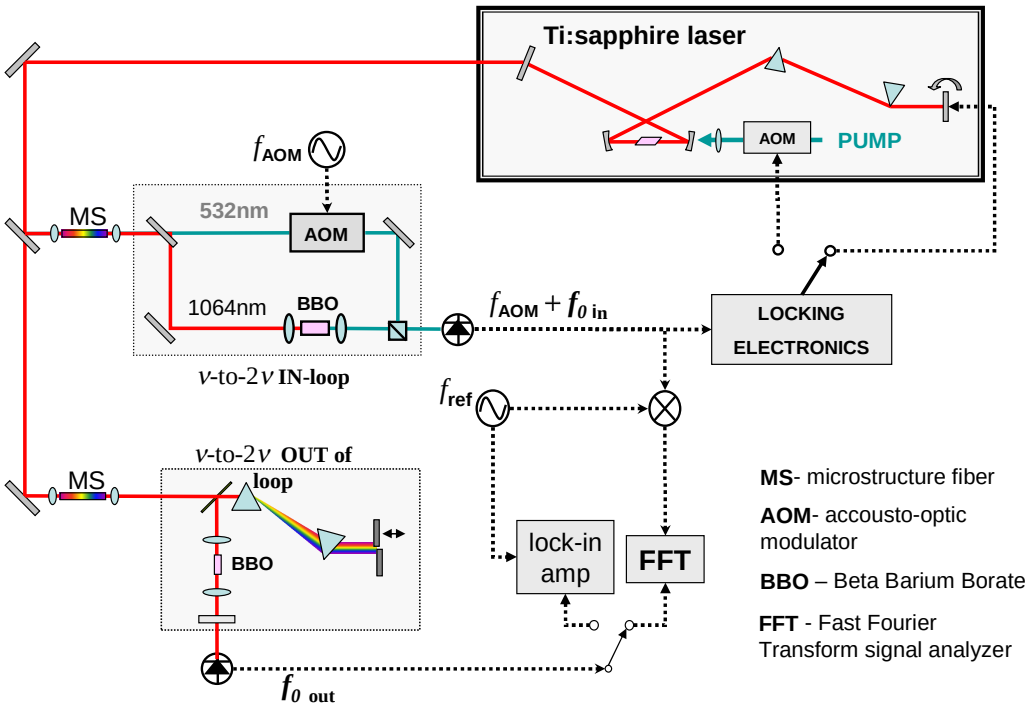

Figure 4.1: Experimental setup showing how the coherence of ϕ_{CE} is measured. One interferometer is used to stabilize the laser while the second ν–to–2ν interferometer determines the phase coherence. The noise of the second interferometer is minimized by making the ν–to–2ν comparison as common mode as possible by using prisms for spectral dispersion [see Sect. A.5.2].

Phase noise produced within the stabilization loop, but external from the laser, is transferred onto the laser output [see Fig. 3.1]. The strength of this transfer is governed by the gain of the PLL as a function of frequency.

The offset frequency measured at the output of the stabilization interferometer gives an in-loop measurement of f_0's phase noise. This noise is only the residual noise not taken out by the PLL, which may be used for monitoring the effectiveness of the feedback loop. The offset frequency, measured at the output of the second interferometer, in contrast, measures the external noise transferred from the stabilization loop as well as the residual noise not taken out by the locking electronics. This out-of-loop noise alone

would present a true measure of the out-of-loop phase noise on f_0. Unfortunately, the second interferometer is also a source of noise. Thus, noise measurement of f_0 using the second interferometer itself results in an overestimation of the total phase noise on the laser.

4.2.2.1 Phase noise or frequency noise?

As mentioned previously, the measurement of a frequency or phase noise spectrum of f_0, depends on the measurement technique. There are two devices that may be used to determine the noise spectrum of a signal. Both act to remove the noise from the carrier, such that noise spectrum begins at DC. Such a baseband measurement allows for generation of high resolution spectrum using a signal analyzer (FFT) [see Fig. 4.1]. A double-balanced mixer may be used to produce a phase noise spectrum of a quiet signal (with phase noise sidebands $<<$ 1 rad) [see Sect. A.7.2.1]. A frequency-to-voltage converter (F-to-V) is used to obtain a frequency noise spectrum of a signal with strong amplitude or phase fluctuations [see Sect. A.7.2.2]. In the noise measurements presented here, noise spectra of the stabilized offset frequency were obtained using a mixer. A frequency spectrum of the noise of the unstabilized f_0 was obtained using a F-to-V converter, and was converted to a phase noise spectrum using eqn. 4.4. Note that in analyzing the single sideband noise spectrum produced using the mixer and F–to–V converter, the factor of two in eqn. 4.6 and eqn. 4.5 is not necessary.

Figure 4.2 presents the results of the coherence measurement. A measurement of the unstabilized offset frequency is used to indicate the available noise suppression. From this, we see a many order magnitude suppression in phase noise at low frequency. The difference between the out–of–loop and in–loop spectra yields the extra-cavity phase noise present within the stabilization loop (e.g., feedback electronics, the ν–to–2ν interferometer, microstructure fiber, etc.) and the differential noise between the two loops. As expected, the out-of-loop noise is significantly higher than the in-loop noise.

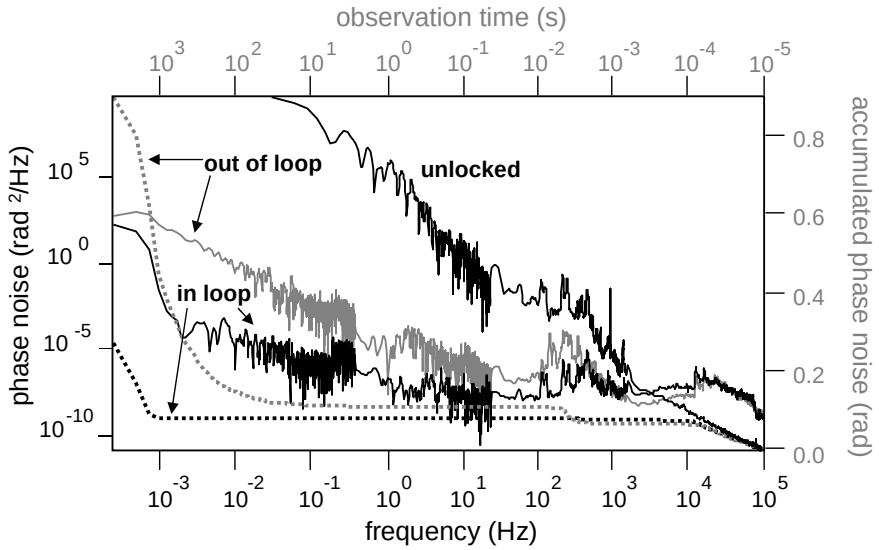

Figure 4.2: Phase power spectral density (left axis), $S_\phi(f)$, for the in-loop, black line, and out-of-loop spectra, grey line, of f_0 versus frequency offset from the carrier. An unlocked spectrum is included to indicate the strength of the phase noise suppression resulting from negative feedback to the laser. The dashed lines show the integrated phase error (right axis) of $S_\phi(f)$ as a function of observation time. Integration of the unlocked spectrum is not present.

Integration of the phase noise PSD out–of–loop (in–loop), in Fig. 4.2 results in an accumulated phase error of 0.8 rad (0.109 rad) over the interval 102 kHz down to 488 mHz (resolution limited). Given that the out-of loop accumulated phase error is less than 1 rad, the lower frequency integration bound determines the coherence time, $\tau_{coh} = 1/(2\pi\ 488\mu\text{Hz}) = 326$ s. This indicates that the phase of the pulses in the pulse train evolve in a coherent manner for > 30 billion pulses.

Comparison between the unlocked and the in-loop phase noise PSD densities indicates a servo bandwidth $\sim$ 20 kHz. The in-loop PSD shows that additional phase noise results from the action of the servo loop at frequencies higher than 20 kHz, and that there is insufficient gain in the acoustic range ($\sim$100 Hz - 5 kHz). This frequency range is also responsible for the majority of the out–of–loop phase noise contribution.

4.3 Characterization of extra-cavity sources of phase noise

4.3.1 MS fiber noise

A major source of out–of–loop noise present in the stabilization loop results from amplitude to phase modulation in MS fiber, where amplitude noise on the laser output [see Fig. 4.4], or amplitude noise resulting from coupling fluctuations [see Fig. 4.3] is converted to phase noise via the fiber nonlinear index of refraction [see Sect. 3.1]. This is detrimental when the direct output of the laser is to be used in an experiment, however it does not affect an experiment that uses the output of the MS fiber.

To measure the contribution of fiber noise that results from power fluctuations due to coupling, we couple a HeNe laser into the fiber and measure the power fluctuations at the fiber output. From this measured noise spectrum we subtract in quadrature the intrinsic power fluctuations due to the HeNe itself. The net result of the fractional power fluctuations due to coupling are shown in Fig. 4.3 as well as the calculated fiber phase noise that would result. The calculated fiber phase noise was determined using the amplitude-to-phase noise coefficient measured in Sect. 3.1 for 40 mW of coupled Ti:s light at a 100 MHz repetition rate.

A shortcoming of the dual interferometer method is that MS fiber is used in both interferometers. As a result, the dual-interferometer may not fully reflect MS generated phase noise resulting from common mode power fluctuations. To estimate the contribution of these fluctuations to the out-of-loop measured phase noise, we measure the laser amplitude fluctuations and use them in conjunction with the amplitude-to-phase conversion factor for MS fiber, $C_{AP} = 5.93$ rad/ mW, as measured on f_0 [see Sect. 3.1]. This measurement is also used to compare the fiber noise induced by the PZT stabilization scheme described above to that obtained via modulation of the laser pump power [26]. Stabilization using the latter method is actuated by placing an AOM in the path of the pump beam for the Ti:S.

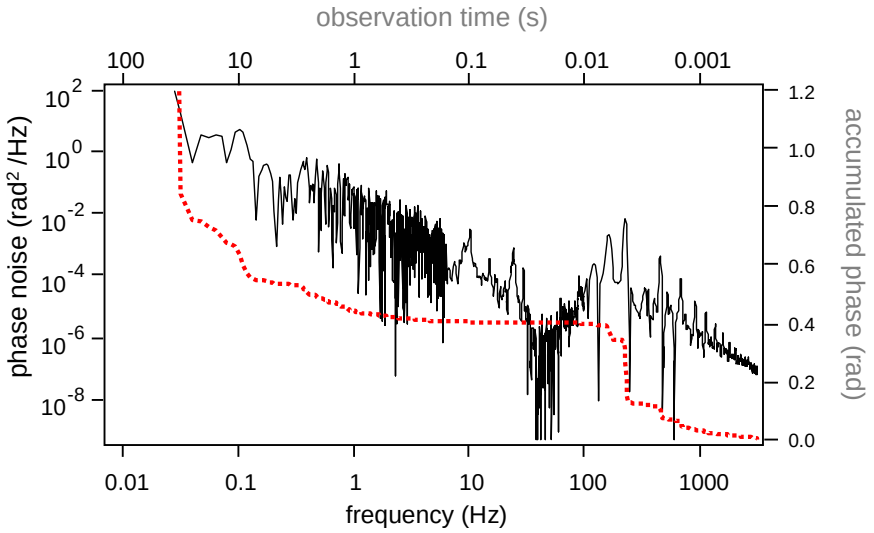

Figure 4.3: Phase power spectral density, $S_\phi(f)$ in rad^2/Hz, of the calculated fiber induced phase noise on f_0 resulting from power fluctuations resulting from fluctuations in the power coupled into MS fiber, for a coupling power of 40 mW. Integration of the noise spectrum yields the accumulated phase error as a function of observation time.

One drawback of modulating the pump power as a means for feedback to the Ti:S oscillator is the possibility of inducing fluctuations on the output power [34]. Figure 4.4 shows the amplitude noise PSD as well as the calculated accumulated fiber phase noise of the PZT versus AOM stabilized systems. A spectrum of the amplitude noise for the unstabilized laser is shown for comparison. As can be seen in Fig. 4.4, the PZT system contributes little additional amplitude noise during stabilization, whereas the opposite is true for the AOM stabilized laser.[1] Integration of the AOM and PZT stabilized noise spectra from 8 Hz to 3.2 kHz yields the rms fractional laser power fluctuation, $(\Delta P/P_0)_{rms}$, to be 0.00473 and 8.34×10^{-5}, respectively. For a coupled laser power of 50 mW at 100 MHz and an amplitude-to-phase conversion coefficient for MS fiber of 593 rad/nJ [28], the amplitude noise would result in 1.40 rad of phase jitter on f_0 for the AOM stabilized system. To connect back to the coherence measurement, the additional fiber noise contributed by the PZT stabilized system to the accumulated out-of-loop

[1] Note that the opposite is true if the dominant source of noise in the laser cavity is due to fluctuations in pump power, as has been shown to be the case for the prismless laser [59].

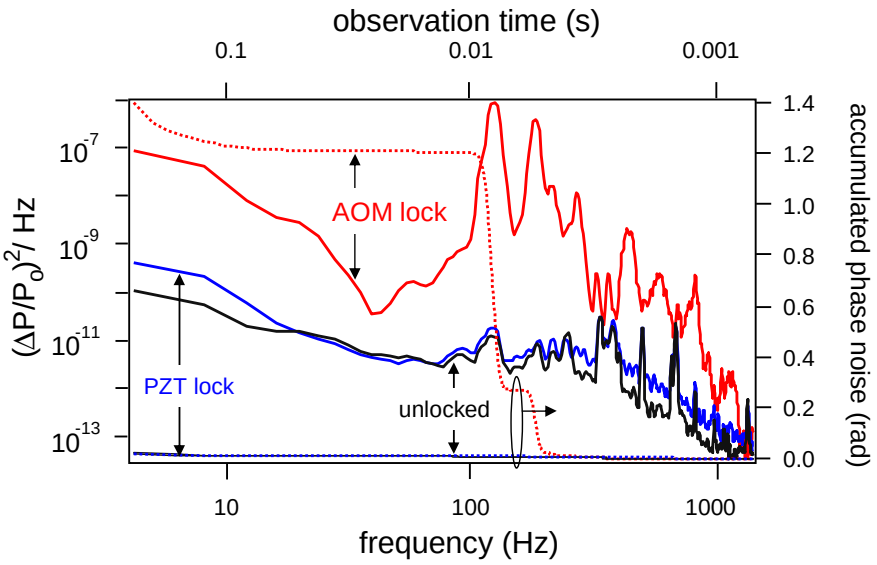

Figure 4.4: Phase noise spectra (left axis) for the unlocked laser, locked by modulating the 532 nm pump power (AOM) and locked using the fast PZT versus frequency. Calculated accumulated phase jitter resulting from amplitude-to-phase conversion in MS fiber (right axis) versus observation time. Both the unlocked and the PZT lock spectra's accumulated phase noise are close to zero.

phase noise presented in Fig. 4.2 is determined to be 0.155 rad rms. Assuming that the out-of loop measurement does not reflect amplitude-to-phase noise conversion in MS due to common mode power fluctuations then the calculated fiber noise brings the total accumulated phase noise (fiber generated noise + out-of-loop phase noise in Fig. 4.2) to 0.955 rad, bringing the observed coherence time determined in Fig. 4.2 dangerously close to 1 rad after $t_{obs} = 125$ ms.

MS fiber contributes more than 50% of the measured out-of-loop phase noise, and dependent on the laser power fluctuations may overwhelm the coherence entirely. Aside from the noise measurements presented here, additional mechanisms in the MS fiber have been demonstrated that result in production of broadband noise, which may limit the stability of the fiber based stabilization scheme in optical frequency measurement [56, 1]. Therefore, elimination of the MS fiber would prove an invaluable step in increasing the simplicity of the phase stabilized Ti:S system [for example see Sect. 5.2].

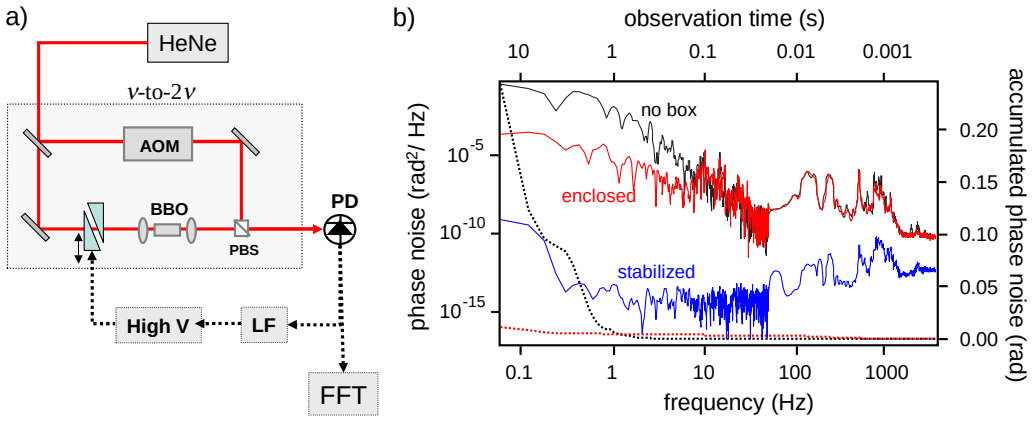

Figure 4.5: a) Schematic for the measurement of the extra-cavity noise caused by interferometer drift. The interferometer is enclosed in a plexiglass box. b) The power spectral density of the phase noise measured using light at 632 nm for three different conditions: interferometer with no box, enclosed in a box and stabilized. Integration of the noise spectrum yields the accumulated phase noise as a function of observation time.

4.3.2 Interferometer noise

Much of the low frequency contributions to noise of the carrier-envelope phase are due to long time scale drift in the ν–to–2ν interferometers. These drifts are particularly villainous because noise at long time scales results in a greater accumulated phase noise than noise at fast time scales. Phase noise in the ν–to–2ν interferometers results from fluctuations in the relative path length between the interferometer arms, $l(t)$.

$$\Delta\phi_{int} = \frac{2\,\pi}{\lambda}\,\Delta l \tag{4.7}$$

Phase noise resulting from path length differences are measured by threading a HeNe laser through the ν–to–2ν interferometer. Changes in relative path length between the arms of the interferometer result in a time-dependent fluctuation in fringe contrast that can be measured using a PD [Fig. 4.5 a]. The resulting fluctuations in voltage measured on the PD are calibrated by determining the voltage equivalent to a π wrap in phase. This calibration, used in tandem with the noise spectrum from the PD is used to determine the phase noise PSD of the interferometer. As described in detail

in Sect. 4.2.1, integration of this noise yields the accumulated phase noise due to the interferometer of 0.3 rad over $t_{obs} = 20$ s [see Fig. 4.5 b].

As seen in Fig. 4.5 b), drift in the interferometer only contributes noise over long time scales, with an accumulated phase noise of 0.24 rad (60 mHz - 3.2 kHz). By enclosing the interferometer, this noise may be cut down by more than an order of magnitude to 0.011 rad. A further two orders of magnitude noise suppression may be obtained via active stabilization of the relative path length (8.5×10^{-5} rad). This is done by placing two glass wedges in one arm of the interferometer, where one wedge is attached to a shearing PZT [see Fig. 4.5 a]. The voltage signal obtained from the PD that measures the fringe contrast is used as an error signal to stabilize the interferometer.

4.3.3 Long-term phase drifts: coherence measurement using a lock-in amplifier

Given a pulse train with a highly stable ϕ_{CE}, an additional method for determining longer term phase drifts may be obtained by looking at the time fluctuations in ϕ_{CE} directly. The only difference in the experiment is that f_0 is measured using a lock-in amplifier instead of an FFT [see Fig. 4.1]. With a dual-phase lock-in, it is possible to directly measure the phase difference between the reference channel and signal channel. This allows for a more visual representation of the phase fluctuations on the pulse train.

To be able to use a standard lock-in, we lock $f_0 \sim 100$ kHz. This reference signal used for stabilization of f_0 is also provided to the reference channel of the lock-in. Figure 4.6 shows a 400 sec time record of the lock-in phase. The standard deviation of the phase fluctuation, at a 1.0 s time constant, is 3.8 deg (0.066 rad) rms, with a maximum deviation of 20.8 deg (0.363 rad) rms. Using a lock-in amplifier, set with a long time constant (1 s), allows for observation of the CE phase noise only within a limited bandwidth at very low frequencies, masking the higher frequency noise. To obtain the long term stability shown in Fig. 4.6 required placing all interferometers in

boxes and enclosing the beams between interferometers in beam tubes. Turbulent air currents can easily result in 2π phase wrap in a matter of seconds.

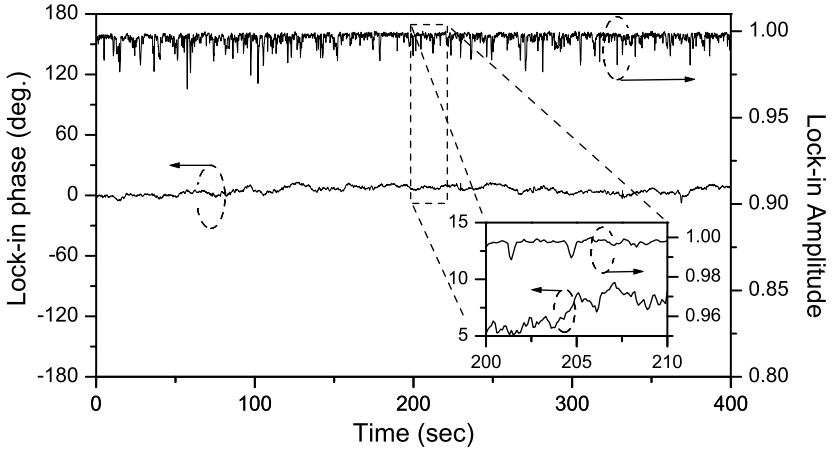

Figure 4.6: Time record of the lock-in phase (lower trace, left axis) and amplitude (upper trace, right axis). The inset shows an enlargement to show that the amplitude and phase fluctuations are uncorrelated.

4.4 "Absolute" phase measurement

In an ideal case, the phase of the f_0 signal, measured using a ν versus 2ν comparison, does not add additional phase offsets to ϕ_0 during measurement. Since a phase-locked loop establishes a fixed phase, it seems that ϕ_{CE} is fully determined by the reference signal to which f_0 is locked, or that a phase sensitive measurement of the f_0 signal gives full knowledge of ϕ_{CE}. One limiting case is $f_0 = 0$ in which case ϕ_{CE} does not evolve pulse–to–pulse and thus is just given by ϕ_0, see eqn. 4.1. However, any ν–to–2ν interferometer is non-ideal and introduces an arbitrary phase shift that prevent this direct connection from being correct. This is illustrated in Fig. 4.7. The phase shifts in the ν–to–2ν interferometer arise from differences in the path length of the two arms and dispersion in any optical elements. (In principle an explicit interferometer is not needed if a chirp free pulse is used, however there is still unavoidable dispersion in the second harmonic crystal.)

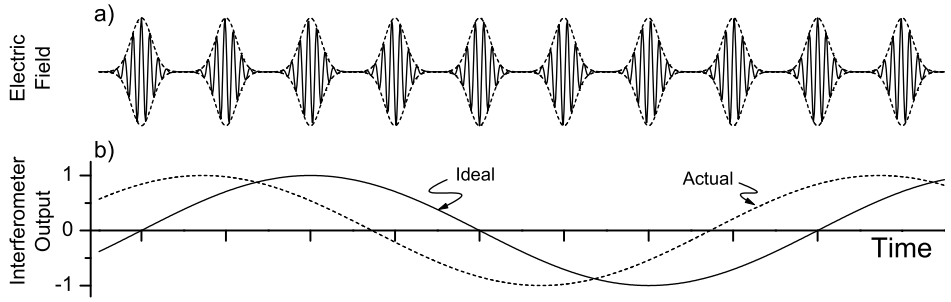

Figure 4.7: Schematic showing relationship between pulse train phase and the phase at the ν–to–2ν interferometer output. a) Pulse train showing pulse-to-pulse change in $\Delta\phi_{CE} = \pi/4$. b) Output of ν–to–2ν interferometer, solid line is the output of an ideal interferometer where zero signal is coincident with the pulse that has $\phi_{CE} = 0$. However, an actual signal from an interferometer has an arbitrary phase shift relative to the ideal signal.

A number of interferometric schemes have been demonstrated that would result in determination of ϕ_0 while minimizing added offsets during measurement. In 2002 there was a demonstration by Mücke *et al.* that by using the 5 fs unamplified output of a broadband (400 nm) Ti:S laser, one could generate both an octave continuum and the necessary second harmonic for nonlinear comparison, all in a 1 μm piece of ZnO [54]. This is wonderful since it eliminates both the need for broadening in MS fiber and the doubling crystal that are necessary in the ν–to–2ν interferometer. More recently, Apolonski *et al.* showed that interaction of unamplified 5 fs pulses with a gold cathode result in a photo-emitted current that observed a dependence on ϕ_0 [3]. Additionally, as will be discussed in Sect. 6.1, using octave spanning, chirp free pulses the injected photocurrent generated in a direct gap semiconductor can be used for solid-state detection of ϕ_0.

Although the above experiments seems very promising for measurement of the "absolute" phase, each of these techniques still suffer phase offsets during measurement. The offsets are particularly bad for measurement of ϕ_0 using semiconductors since it is difficult to determine how far the light penetrates into the material. Even though the estimated phase offset may be small one has to keep in mind the fact that, in the worst

case scenario of using the common ν–to–2ν interferometer, the maximum error that can be measured on ϕ_0 is 2π (even if the actual error is thousands of radians, the detected phase error is always modulo 2π).

Aside from the measurement phase error, there also exist serious problems if one chooses the above methods for"absolute" phase stabilization of the laser. Let us assume first that the system used to determine the absolute phase does not suffer unnecessary phase offsets. On top of the errors that result during measurement (let's not forget the Guoy phase ambiguity), the absolute phase can accrue errors during stabilization or simply by encountering dispersive elements outside the laser cavity. The former results in time changes in ϕ_0 but may be minimized by careful design of the feedback loop (path length stabilization of the interferometers, minimizing MS fiber noise, taking out phase drifts due to temperature changes in BNC cables, etc. [see Sect. 4.2]). Material dispersion outside the cavity only adds a constant phase offset to ϕ_0. The problem with an added offset is if the beam going to the absolute phase measurement and that going to the phase sensitive experiment travel through differing amounts of dispersive material there will exist a phase error between the two pulse trains.

Only the final scientific results that show a direct phase-dependence without ambiguity will really count. For the moment, at best we can maintain the coherence ϕ_0 and shift it in a systematic manner....

Chapter 5

Octave spanning lasers

Aside from the problems posed by fiber induced phase fluctuations [see Sect. 4.3.1], stabilization of the Ti:S laser using MS fiber presents challenges to short pulse experiments because of the large cubic fiber dispersion [62]. Additionally, complexities in the fiber alignment often lead to loss of fiber coupling and degradation in the f_0 signal over time. This is a considerable hindrance in optical metrology since long term averaging is necessary to increase the measurement precision. To overcome these problems requires finding a means for continuum generation that exhibits better stability than is achievable in MS fiber. One possibility is external broadening of laser pulses via SPM in a thin glass plate [8]. This, however, requires very high intensities that may be achieved by amplification of the laser pulses. One other possibility, which is the focus of this chapter, is the generation of continuum directly within the laser cavity.

5.1 The Ti:sapphire laser

5.1.1 Cavity geometry

The Ti:S laser presented here is a standing wave cavity [see Fig. 5.1] bounded by two flat mirrors: the laser end mirror (EM) and the output coupler (OC). The OC is used to couple a portion of the intra-cavity light out of the laser, with a loss determined by the mirror reflectivity. The Ti:S crystal is optically pumped at 532 nm.[1]

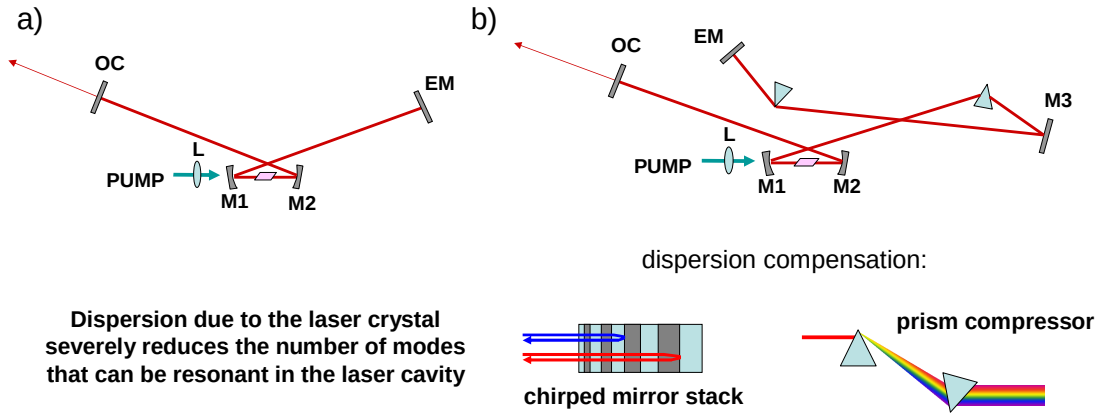

Figure 5.1: a)X-folded Ti:S laser. Intracavity dispersion compensation is used to maximize the lasing bandwidth of the modelocked laser spectrum. b) Kerr-lens modelocked Ti:S laser cavity. Intracavity prisms and chirped mirrors are used to provide negative second order dispersion compensation. A prism compressor results in negative second order dispersion compensation through a combination of light refraction and geometry. Light that is incident on the first prism is refracted such that red light is refracted more strongly than blue. The diverging rays from the first prism are then incident on the second prism in the geometry shown. Light exiting the second prism is horizontally dispersed but not diverging. Because of the orientation of the second prism, red light is forced to travel through more glass than blue thus causing the optical path length of the red light to be greater than that of the blue. Negative disersion in a chirped mirror is obtained, in the simplest case, by a dielectric stack with indicies, n_1 and n_2. By varying the thickness of the layers as shown the half wave condition for reflection of red light occurs deeper in the dielectric stack of the mirror than it does for blue light.

The pump beam is focussed with a 10 cm anti-refection coated lens, L, coupled into the cavity through the first curved mirror, M1. The pump light is focussed to obtain efficient population inversion in the Ti:S crystal. The two curved mirrors (f = 5 cm), M1 and M2 , are used for focusing of the Ti:S laser light into the crystal (x-tal). For optimal single frequency lasing (CW), M1, M2 and L are aligned such that the Ti:S lasing light and the pump beam are spatially overlapped. Stable CW operation of the laser is obtained for $\overline{M1 - xtal} = 5.0$ cm and $\overline{M2 - xtal} = 5.1$ cm for $\overline{OC - xtal} = 0.62$ m and $\overline{EM - xtal} = 1.173$ m.[2]

[1] We use a 6 W Verdi laser from Coherent Lasers. This pump laser is preferable since it is single mode and that it has low amplitude fluctuation.

[2] The stability of the laser for a given geometry is obtained using ABCD matrix cavity stability calculations, which assumes a Gaussian TEM_{00} mode. The optimal mirror positions are determined by the cavity length of each arm since the cavity optics determine the spot size and divergence of the beam

To reduce reflections of the lasing beam from the crystal surfaces, the crystal is cut at Brewster's angle. This makes it such that light in the horizontal, x-direction, and the vertical, y-direction, are refracted differently in the laser crystal. The astigmatism caused by focussing the lasing beam at an angle, θ with respect to the crystal axis [$f_x = f cos(\theta)$ and $f_y = f/cos(\theta)$] may be used to compensate the astigmatism due to the cut of the crystal [49]. The astigmatism is balanced for,

$$\frac{sin^2(\theta)}{cos(\theta)} = \frac{t}{f}\frac{\sqrt{n^4-1}\sqrt{n^2-1}}{n^4}. \tag{5.1}$$

Here n is the index of Sapphire and t is the thickness of the crystal.

5.1.2 Pulsed operation of the Ti:sapphire laser

Pulsed operation of the Ti:S laser is achieved by passive modelocking of the laser spectrum. Just as the term implies, modelocking is achieved by establishing a fixed phase relationship between resonant longitudinal modes in the laser cavity, which results in the formation of a light pulse [see Fig. 2.1].

Formation of the pulse train requires that the longitudinal modes of the cavity be equally spaced in frequency. This is naturally the case for a dispersionless cavity. In reality, however, the bandwidth of the resonant modes is limited by dispersion of the cavity optical elements that yield a wavelength dependence of the index of refraction, $n(\lambda)$. This causes the different wavelengths of light to travel different optical path lengths in the cavity, making the mode spacing uneven in frequency.[3]

in the laser crystal.

[3] Outside the laser cavity, dispersion results in dephasing of the different wavelengths of light, where each wavelength picks up a phase $\phi_\lambda = k(\lambda)\, d = k_0 d\, n(\lambda)$, as they travel the length of the medium, d. This dephasing causes the carrier frequency of the pulse to be chirped (frequency modulated) such that, for normal dispersion, the leading edge of the pulse has a longer wavelength than that of the trailing edge of the pulse. Because $n(\lambda)$ is not linear in frequency, Taylor expansion of ϕ_λ about the center wavelength of the pulse, λ_0 is performed to give the order of the dispersion:

$$\phi_\lambda = \phi_0 + k_0 \left[(\lambda-\lambda_0)\frac{dn}{d\lambda} + (\lambda-\lambda_0)^2\frac{d^2n}{d\lambda^2} + ...\right] \tag{5.2}$$

typically, this equation is expressed in terms of derivatives in ω. Although pulse chirp does not change the frequency components of the pulse it does act to broaden the pulse envelope. This is because the temporal profile of the pulse is determined by the Fourier transform of the spectral components including

The limiting effect of dispersion on the resonant bandwidth of the laser also has strong consequences on the nonlinear processes in the laser cavity that are responsible for pulsed formation. Therefore construction of the modelocked Ti:S laser requires intra-cavity dispersion compensation, which is typically achieved using a prism compressor [22] [see Fig. 5.1]. Alternatively, chirped mirrors (CM) [52, 47] may be used, which in principle can compensate any order dispersion [see Fig. 5.1], limited by the complexity of the coating design. For the laser presented here, dispersion compensation is obtained using a combination of both chirped mirrors and intra-cavity prisms. Because the prism compressor is in one arm of the laser only, the dispersion map of the laser is asymmetric about the crystal center. As a result, nonlinear processes in the crystal primarily occur only on one pass through the crystal, on the return trip from the prism compressor.

5.1.3 Modelocking and the Kerr effect

Pulse formation and the generation of ultra-broadband spectra in a passively modelocked laser is a complicated process, which for the most part is still not fully well understood. The basic idea for the typical Kerr-lens modelocked laser, however, is as follows: if a perturbation is introduced into the laser cavity, this will cause a certain number of longitudinal modes to add coherently, forming a weak pulse. As this pulse travels through the laser crystal it feels the intensity-dependent nonlinear refractive index of the crystal,

$$n(x,t) = n_0 + I(x,t)\overline{n_2}, \tag{5.3}$$

where $\overline{n_2} = 2\,n_2/(\epsilon_0\,c\,n_0)$. Here n_0 is the linear refractive index, $I(x,t)$ is the instantaneous pulse intensity and n_2 is the nonlinear index of refraction and indicates the coupling strength between n and the electric field, $E(x,t)$. Nonlinearity in the laser crystal satisfies two purposes. The first is the generation of new wavelengths by a pro-

their phase. The narrowest temporal profile for a light pulse is that for which each component in the frequency spectrum has the exact same phase, this is termed a transform limited pulse.

cess called self-phase modulation (SPM), which is sensitive to the temporal profile of the laser pulse. The second is self-focussing, which is dependent on the spatial profile of the pulse. For a more thorough discussion of this please consult ref. [43].

5.1.3.1 Self-phase modulation

Let us consider a pulse with a Gaussian intensity profile. The propagation of the pulse in the laser crystal results in a time change in refractive index due to the Kerr-effect, $n(t) = n_0 + \overline{n_2}\, I(x,t)$. The leading edge of the light pulse [see Fig. 5.2 a], with a positive rising intensity results in an increase in refractive index. The time change in $n(t)$ results in a phase modulation, $\frac{d^2\,\phi}{dt^2} = k_0\; n_2\, z\; \frac{\partial I(x,t)}{\partial\, t}$, that results in a red shift of the pulses leading edge. Conversely, the trailing edge of the pulse has a negative slope, causing a decrease in refractive index compared to the center of the pulse. This has the effect of blue shifting the trailing edge of the pulse with respect to the pulse center. The net effect is the generation of new coherent wavelengths with a positive pulse chirp of the central portion of the spectrum. Self-phase modulation is the time-domain equivalent of four-wave mixing.

5.1.3.2 Self-focusing

The transverse effect of the light pulse on the nonlinear index of refraction of the crystal results is the formation of a nonlinear lens with a spatial profile matching that of the light beam, $n(r) = n_0 + \overline{n_2} I(r)$ [see Fig. 5.2 b]. This lens results in self-focussing of the laser beam.[4] This nonlinear effect may be used as a passive saturable absorber for preferential gain of modelocked over CW laser operation, and thus acts as the laser modelocking mechanism. Using the Kerr-Lens effect as a passive saturable absorber requires misalignment of the curved mirrors, M1 or M2, from the optimal CW position. This is done by changing the curved mirror distance with respect to the crystal

[4] For the typical KLM Ti:S oscillator, dispersion eventually reduces the pulse intensity such that self-trapping of the beam does not occur.

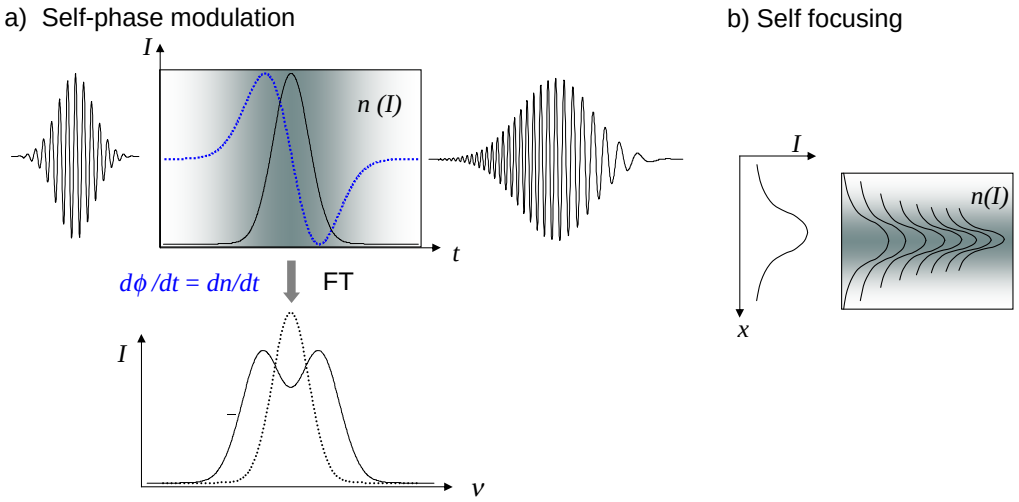

Figure 5.2: Temporal a) and spatial b) effects resulting from the Kerr- nonlinearity. a) Depiction of self-phase modulation, (top) input pulse travels through a nonlinear medium with a Gaussian temporal profile, resulting in a phase profile, $\frac{d\phi}{dt} \propto \frac{\partial n}{\partial t}$. (bottom) shows the incident spectrum of the pulse and the typical double Gaussian final spectrum. b) Depiction of self-focussing.

center. The change in position causes the intracavity beam to no longer be optimally overlapped with the pump in the laser crystal.[5] Perturbation of the laser cavity results in the formation of a weak circulating pulse that is in addition to the CW beam. When the pulse propagates through the laser crystal, the pulse will focus more tightly than the CW beam because it has a higher peak intensity. If the curved mirror position is chosen correctly, Kerr-lensing will cause the pulse to overlap better with the pump than the CW light, thus experiencing a higher gain. Self-phase modulation, due to the higher peak intensity of the pulse, will act to broaden the pulse's existing spectrum. As the pulse then recirculates through the cavity, dispersion picked up in the crystal is compensated by the prism compressor and the chirped mirrors. The new frequency components and chirp compensation yield a shorter duration pulse that results in a further increase the pulse intensity and so on and so forth. Given that dispersion is well

[5] Misalignment of the curved mirror position also results in the production of a slightly asymmetric CW beam. This is because the mirror position determines the condition for asymmetry correction [see Eq. 5.1]. Often, the correct modelocking position may be determined by examining the spatial profile of the CW beam profile.

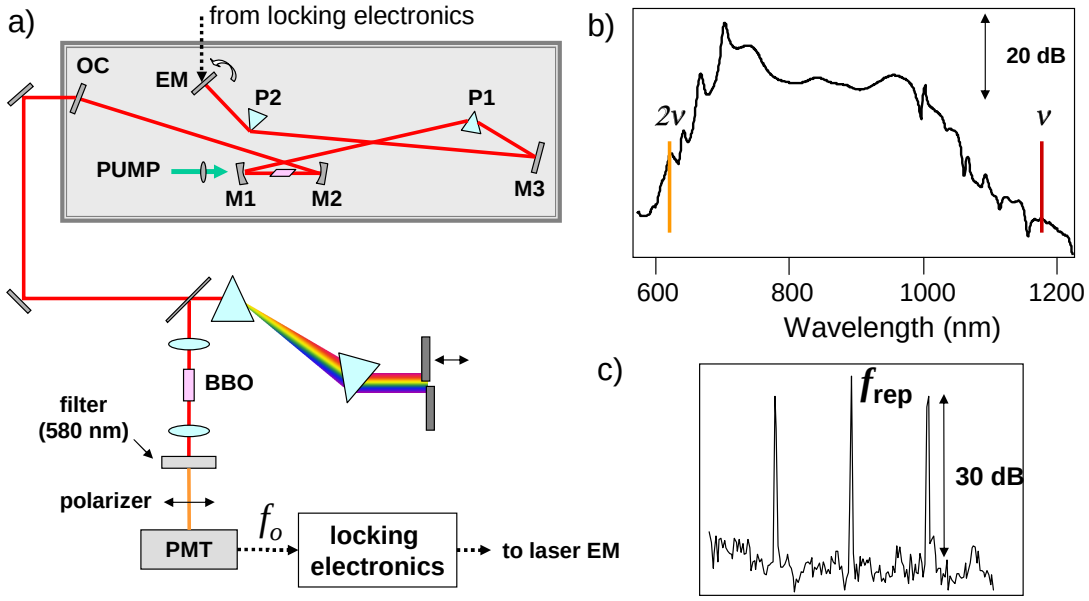

Figure 5.3: a) Experimental schematic of the octave spanning Ti:S laser and the ν–to–2ν interferometer used for measurement of the laser offset frequency. b) the octave-spanning spectrum obtained from the laser that is used for the ν–to–2ν comparison. c) The rf spectrum of the measured beat signal at a 100 kHz resolution bandwidth.

managed and that the proper curved mirror position is found, the laser will result in a stable modelocking of the laser spectrum.

5.2 Characteristics of an octave spanning Ti:sapphire laser

In this section I will describe how the coherent bandwidth of the laser may be extended such that the laser spectrum alone is broad enough to support measurement and stabilization of the laser offset frequency, without external broadening in MS fiber [24].

Ti:S lasers have been previously demonstrated that result in intra-cavity continuum generation [17, 7]. Reference [17] describes a Kerr-Lens modelocked (KLM) Ti:S laser using specially designed double-chirped mirror pairs for broadband dispersion compensation as well as a secondary time and spatial focus in a thin glass plate used for additional intra-cavity spectral broadening. Reference [7] demonstrates a 1 GHz repe-

tition rate ring laser that employs a slightly convex intra-cavity mirror to increase the effect of SPM in the laser crystal. The laser spectrum of ref. [17] was shown to yield a direct ν–to–2ν beat signal and ref. [7] a direct 2ν–to–3ν measurement of f_0.

Given the previous discussion of pulse formation, the less intracavity dispersion, the higher the achievable nonlinearity in the laser crystal, and thus the greater the broadening. As a result, all broadband lasers must, to some extent, minimize the effect of intracavity dispersion. The octave spanning laser that I will describe here is a typical x-folded cavity that uses commercially available negatively chirped mirrors and intracavity CaF_2 prisms for dispersion compensation, Fig. 5.3 a). M1, M2, M3 and EM are all negative chirped mirrors from Layertec^{TM}, with respective part number, 101568(02), 101568(02), 100466 and 101515. The output coupler (OC) is G034-007 from Spectra Physics and the separation between the two CaF_2 prisms is 82 cm.

Before I attempt to explain how the laser works, I will first describe some of its attributes. Figure 5.3 b) shows the spectrum of the laser for a pumping power of 6.5 W. What is remarkable about this laser is the amount of generated modelocked power. Typically, to keep the intracavity powers high, a low transmission output coupler is used for generation of large intracavity bandwidths. The transmission of the output coupler used here is ~ 5 % and results in a modelocked power > 600 mW. A major percentage of the power is simply transmitted by the output coupler since it only reflects over 200 nm bandwidth [see Fig. 5.5].

Because of the extreme breadth of the spectrum as compared to the reflectivity of the OC, the continuum must only be generated on a single pass through the crystal. As a result, light produced outside the bandwidth of the OC is not resonant with, and thus is not forced to obey the spatial conditions of the cavity. For light circulating many times in the cavity, the cavity filters out any spatial aberrations that do not match the permitted cavity spatial modes, thus leaving only beautiful Gaussian profiles. In contrast, light produced on a single pass through the crystal is subject to diffraction

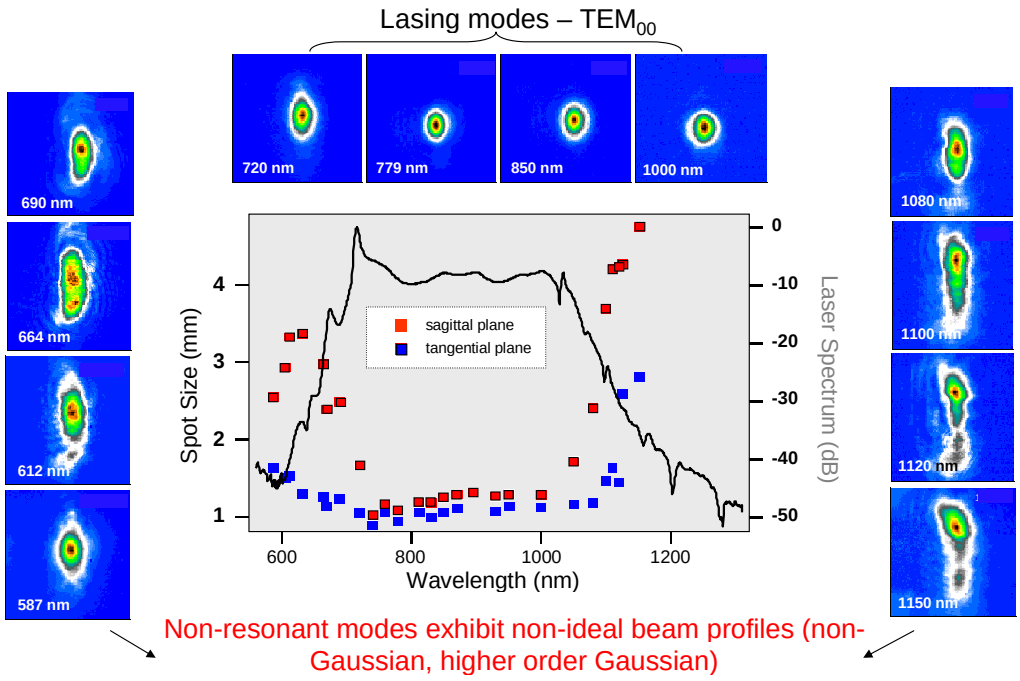

Figure 5.4: The laser beam profile is displayed for selected wavelengths. A 10/90 knife edge fit was used to determine the spot sizes in the sagittal (filled squares) and tangential (empty squares) planes, displayed at the right of the figure. The solid and dashed lines are the respective fits to the expected $1/\lambda$ diffraction limit divergence. Some of the diffraction rings observed for the larger beam modes may result from aperturing of the laser mirrors.

and aperturing of the cavity optics. This results in a significantly different spatial profiles between the resonant and non-resonant spectral modes, as shown in Fig. 5.4. A 90/10 knife edge method was used to perform a second moment measurement of the beam profiles in Fig. 5.4 to yield the beam spot sizes as a function of wavelength [10]. From the spot size, it is seen that the spectral extremes exhibit a significant increase in asymmetry. Additionally, it is also seen, not surprisingly, that these modes also show a significant deviation away from the Gaussian TEM_{00} mode and its corresponding $1/\lambda$ diffraction limit.

The increase in spot size in the wings of the spectrum is understood by examining the beam parameters at the output of the laser, Fig. 5.5. The data in Fig. 5.5 was obtained by performing an M^2 measurement of the laser beam propagation versus

wavelength (given the beam profiles, Gaussian beam propagation theory may no longer hold in the wings of the laser spectrum, and as a result the data in Fig. 5.5 is intended only to indicate a trend in the beam characteristics.) The beam waist measurement [Fig. 5.5 a] shows a sudden decrease of the non-resonant compared to the resonant modes. This is a little surprising but explains the greater divergence in the wings of the laser spectrum that leads to the larger spot sizes observed in Fig. 5.4. Figure 5.5 b) compares the measured beam divergence to that which would result from the propagation of a Gaussian TEM_{00} mode given the respective measured beam waists in Fig. 5.5 a). The ratio of the former to the latter gives the M^2 value as a function of wavelength, indicating the strength of the non TEM_{00} Gaussian beam propagation (non-Gaussian modes and/or higher modes).

The broadband operation of this laser is speculated to result from very good dispersion compensation, but only over the bandwidth of the output coupler (this assumption is supported by the fact that exact choice of broadband chirped mirror doesn't make a huge difference in determining the laser bandwidth). If the dispersion over this bandwidth is close to zero then it is possible to form a very short pulse in the laser crystal. The resultant high intensities would cause the formation of an extremely strong Kerr-lens that, in turn, would result in the production of the continuum. This doesn't seem the least bit surprising and may, in fact, be only part of the story.

Unfortunately, the role of dispersion has not, however, been experimentally confirmed. We did attempt to determine the cavity dispersion by placing a slit after the second intracavity prism sequence for wavelength selection, and measuring any corresponding shifts in frequency of f_{rep} (changes in round trip cavity time) as a function of wavelength. The change in optical cavity length was obtained by measuring a high harmonic ($\sim 10^{th}$) of f_{rep} that resulted from mode beating in the cold cavity[6] . The mea-

[6] The cold cavity refers to a cavity operated CW such that there is no nonlinear effects resulting from pulse propagation.

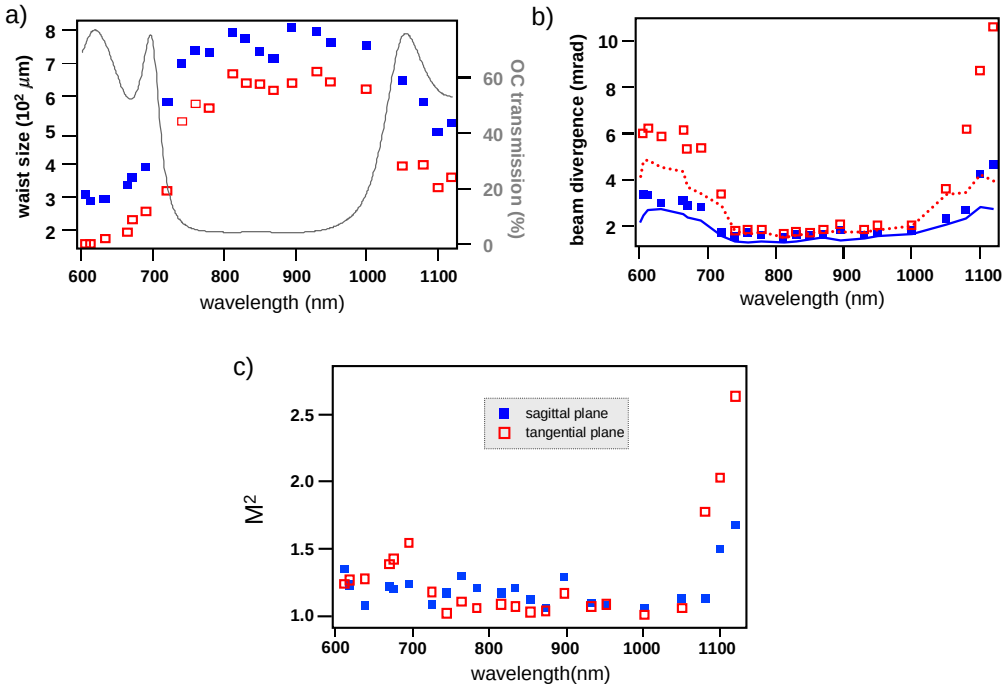

Figure 5.5: a) Measured beam waists and b) measured beam divergence at the laser output coupler of the laser in the sagittal (filled squares) and tangential planes (empty squares) versus wavelength. Also shown in a), the output coupler transmission (right axis) is included to indicate the bandwidth of the resonant versus non-resonant modes. In b) the solid and dotted lines are the calculated TEM_{00} beam divergences from the measured waist sizes shown in a) in the sagittal and tangential planes, respectively. The ratio of the calculated beam divergence to the measured divergence indicates the M^2 value for the mode, which is shown in c).

surement was unsuccessful, however, since ambient temperature drifts caused changes in f_{rep} that overwhelmed those due to dispersion.

The laser is operated in a regime close to that used in non-octave Ti:S lasers. Typically, KLM is obtained by displacing one curved mirror slightly away from the optimum mirror position for CW operation [see Sect. 5.1.1]. In a non-octave spanning Ti:S laser, the displacement of the mirror will result in a slightly elliptical CW beam. Here, however, we take the misalignment a step further, in that the curved mirror furthest from the pump is translated toward the crystal and to the edge of stability for CW operation. Next the bandwidth of the modelocked spectrum is optimized by translating both curved mirrors, in the same direction away from the pump, just until

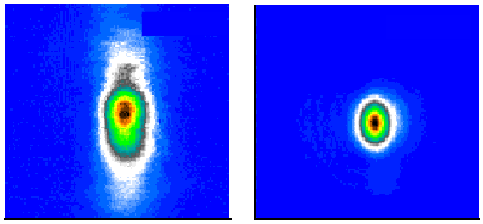

Figure 5.6: Far field beam profiles for CW and modelocked light at 780 nm.

the point where the laser begins Q-switching. The final curved mirror positions with respect to the crystal yield the following results:

1) The misalignment heavily increases the discrimination between modelocked and CW gain. This is also observed in ref. [7]. The discrimination in average power is $\sim$ 100 mW CW as compared to $>$ 600 mW modelocked. This indicates the formation of a very strong Kerr-Lens to correct for the change in overlap with respect to the pump beam.

2) Translating M2 to the edge of CW stability yields a highly asymmetric CW beam (tangential waist/ sagittal waist = 1.56 [see Fig. 5.6]). This occurs because the misalignment of M2 no longer optimally correct for astigmatism due to the Brewster cut of the laser crystal [see Sect. 5.1.1]. Curiously enough, because of the nonlinear correction for the CW asymmetry, the Kerr-lens may in fact be astigmatic. The formation of an asymmetric Kerr-lens may explain the observed beam profile asymmetry in the non-resonant wings of the modelocked spectrum.

3) The mirror positioning gives rise to a much more tightly focused CW beam than the pump beam ($\sim$ ratio of 4:1, calculated using ABCD cavity propagation based on the observed CW asymmetry). This, however, should result in terrible overlap with the pump beam unless either, nonlinearity during modelocking expands the waist, or the focus of the Ti:S light is shifted in the crystal with respect to the pump.

There are a number of questions that remain unanswered as to what accounts for the extremely large bandwidth and the observed mode profiles. In particular it would be interesting to understand the physics behind the observed decrease in waist size of the non-resonant as compared to the resonant modes. As mere speculation, the observed factor of ~ 2 decrease in waist size may be the simple result that, given that SPM is a third order nonlinear process, the non-resonant generated light is produced with a waist that is $\sqrt{3}$ times smaller than the generating resonant modes. This is because, for a Gaussian beam the electric field exhibits a proportionality, $E(r,z) \propto exp\left(-\frac{r^2}{\omega_o^2}\right)$. Light generated by SPM will have an electric field that is proportional to $E(r,z)^2\, E(r,z)^*$, thus being produced with a waist, $\omega_o/\sqrt{3}$. This is only possible if the generated light is not resonant with the cavity, in which case the cavity geometry does not determine the waist size. Perhaps the M^2 data can help to uncover some of the details concerning the nonlinear effects in the Ti:S crystal during continuum generation.

5.2.1 Phase stabilization of an octave spanning laser

Although differing definitions are applied to the term "octave-spanning," perhaps the most appropriate for self-referenced stabilization is the bandwidth necessary to observe a direct ν–to–2ν beat signal. This comparison requires an octave of bandwidth, which for the results presented here, is produced directly by the laser itself. The offset frequency is obtained via optical heterodyne between fundamental light at ∼580 nm and doubled light at ∼1160 nm using a prism ν–to–2ν interferometer [see Fig. 5.3 a]. Because the light intensity in the wings of the spectrum is significantly lower than that obtainable using MS fiber, a photomultiplier tube (PMT), not a photodiode, is used to detect the heterodyne beat signal. For the measurements presented here, the SNR of the offset frequency beat note [Fig. 5.3 c] is 35 dB at 100 kHz resolution BW. This is sufficient for stabilization of f_0 without using a tracking filter [see Sect. A.6.1.2]. This SNR is comparable to that of a beat signal obtained using a spectrum broadened in

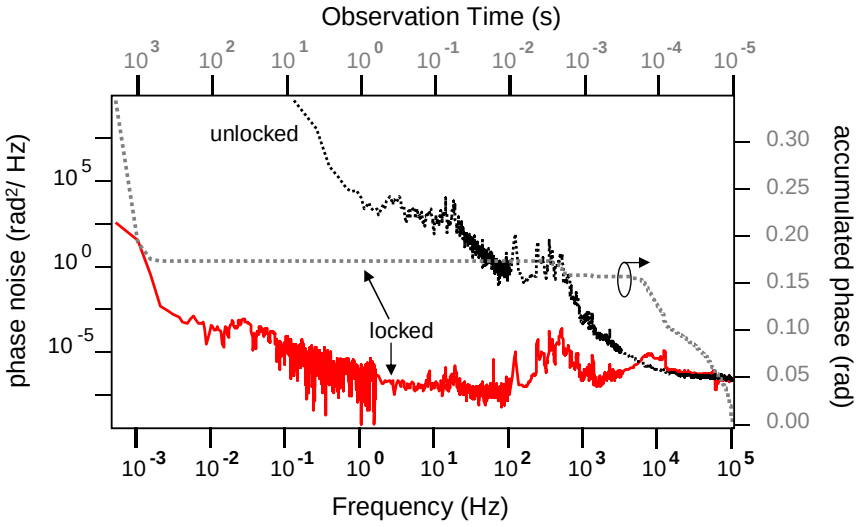

Figure 5.7: Power spectral density versus frequency and the accumulated phase noise versus observation time for the stabilized and unstabilized offset frequency derived from the octave spanning spectrum in Fig. 5.3 b).

MS fiber and using a 100 MHz repetition rate laser.[7] In principle, given that a PMT is a single photon detector, the detector noise should be very low. The SNR of the measurement, we speculate, is limited by light noise from photons not contributing to the beat signal. These photons may either result from insufficient filtering to ensure spectral overlap, or from bad mode matching between the doubled 1160 nm light and fundamental light at 580 nm. By coupling the light, after the doubling crystal, into a single mode fiber, the extra light noise due to mode mismatch should be taken out, thereby increasing the SNR of the beat signal.

Stabilization of f_0 is obtained with an accumulated phase error of 0.18 rad (1.65 mHz - 102kHz), Fig. 5.7 b), following the error analysis discussed in Sect. 4.2. It is important to point out that this is an in-loop measurement of the phase noise, and therefore may not be used alone to characterize the noise on the output of the laser. However, using the octave spectrum produced from the laser directly we altogether eliminate phase noise generated by MS fiber. Also, because the prism based ν–to–2ν

[7] Using higher repetition rate lasers, there is more energy per optical mode. Such systems typically allow for measured beat signals of 45 - 60 dB in a 100 kHz resolution bandwidth.

interferometer used in the measurement of f_0, minimizes non-common mode mirrors, the dominant source of out-of-loop phase noise on the laser should result from the photomultiplier tube and the electronic amplifiers (this is because the noise spectrum of f_0 is measured independent of the stabilization electronics).

5.2.2 Broadband Ti:sapphire oscillators as transfer oscillators for all-optical clocks

The ability to circumvent the use of MS fiber by generating the necessary continuum in the laser oscillator itself, makes broadband Ti:S lasers good candidates as transfer oscillators for all optical clocks. An experiment of interest would be to self-reference the offset frequency of the octave spanning spectrum. Stabilization of the laser repetition rate would then be obtained by comparing of one tooth in the comb to an optical standard. This comparison, used for measurement of the comb spacing, allows for a much increased sensitivity to error in f_{rep} as compared to using a microwave reference. The laser stabilized in this manner would yield f_{rep} as the clock signal [12, 80], which would allow for comparison of the Hydrogen maser [30].

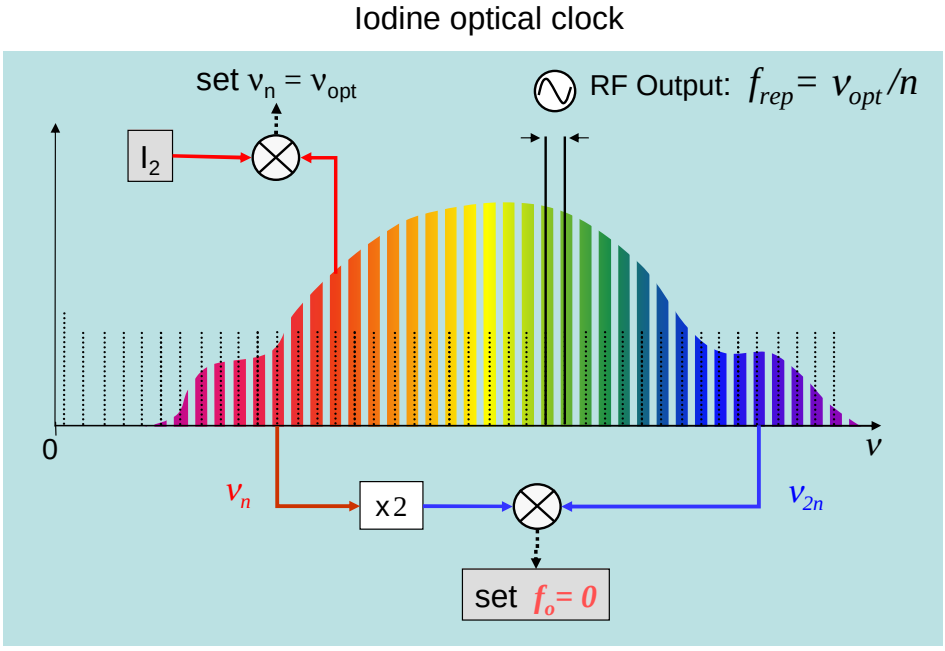

Figure 5.8: Schematic of an all optical clock based on molecular iodine. Stabilization of the offset frequency is obtained via self-referencing. Stabilization of the n^{th} comb element, ν_n to the molecular iodine standard at $\nu_{opt} \sim 1064$ nm would then be used to fix $f_{rep} = \nu_{opt}/n$

Chapter 6

Applications of the stabilized Ti:sapphire laser

A number of possible applications of the stabilized Ti:S laser have been discussed in the introduction of this thesis. Of course, the two primary fields to which such lasers may be applied are optical frequency metrology and ultrafast phenomena. In this chapter I will discuss two experiment that make a small contribution to the huge breadth of possible scientific applications. The first experiment discusses the application of stabilized Ti:S lasers to coherent control-type experiments in semiconductor physics. The second, in contrast, explores the area of optical metrology, whereby synchronization of a Ti:S laser and Erbium-doped fiber laser allow for coherent extension of the stabilized comb to telecommunication wavelengths.

6.1 Quantum interference control in semiconductors: the matter interferometer

Having demonstrated that stabilization of the laser results in a coherent pulse train, one can begin to investigate phase sensitive physical processes. For example, one may begin to consider coherent control-type processes in atomic [2], molecular [69] and semiconductor systems [31]. For example control of highly intense, ultrashort light pulses reveals the phase sensitivity of physical processes in the strong-field regime [58, 6]. A recent illustration of this was presented by Baltuska *et al.* who demonstrated influence over the spectrum of high-harmonic generated light by controlling the phase

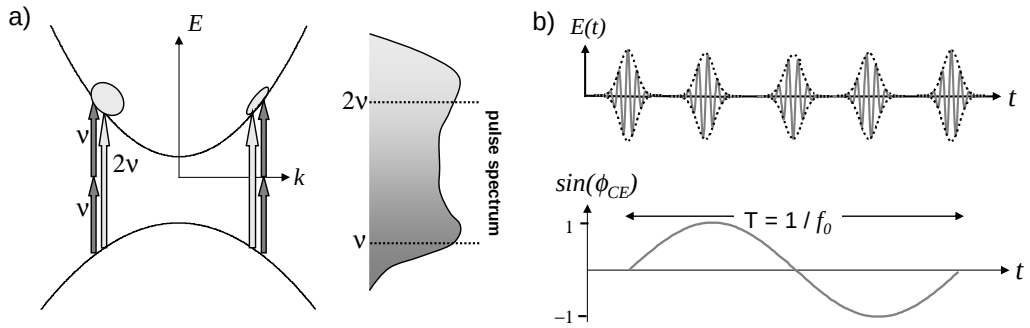

Figure 6.1: a) Schematic depicting the quantum interference of one- and two- photon pathways between the valence and conduction bands in LT-GaAs. Coherent control of the injected photocurrent is obtained using an octave spanning spectrum with a controlled carrier-envelope phase slip. b) The carrier-envelope phase change between pulse to pulse evolves at an defined rate, $T = 1/f_0$.

of the driving field [6]. In the multi-photon regime, the photocurrent generated via interaction of ultrashort pulses and a gold cathode was manipulated by controlling the electric field of the pulse train [3].

Phase-stable modelocked lasers also have strong consequences in the low-field regime given the potential for deterministic control, for example, over the reaction channels in chemical systems and population transfer between quantum states [9]. A convenient medium with which to explore the latter is the semiconductor, whereby the continuum valence and conduction bands circumvent issues of parity that are often common to atomic systems. In this section I will discuss how control over the carrier-envelope phase of the laser pulse train from a Ti:S laser may be used to determine the direction of injected photocurrents in low temperature grown GaAs (LT-GaAs). I will also discuss the potential for this technique as a means for solid state detection of the carrier-envelope phase of a modelocked laser.

A simple experiment for exploring quantum interference in a semiconductor relies on interfering one- and two- photon pathways between the continuum levels of the conduction and valence bands [77]. In the presence of a two-colour light field with

frequencies ν and 2ν, there is quantum intereference between one- and two-photon transitions. The carrier population excited to conduction band states of a given crystal momentum $\hbar\mathbf{k}$ can be modulated by the phase parameter

$$\Delta\phi = 2\phi_\nu - \phi_{2\nu}, \tag{6.1}$$

where $\phi_{\nu\,(2\nu)}$ is the phase of the $\nu(2\nu)$ field. Such a modulation occurs at any point in momentum space that energy conservation allows, although the modulation at different points are not necessarily in phase. In fact, to a good approximation in GaAs, transitions at **k** and -**k** are completely out of phase. To understand this let us examine the semi-classical interaction of light with vector potential **A**, interacting with an electron. The Hamiltonian for matter-field interaction takes the form

$$\mathbf{H_{int}} = \frac{1}{2m}(\mathbf{p} + e\mathbf{A})(p + e\mathbf{A}), \tag{6.2}$$

where e is the electron charge and $\mathbf{p} = \frac{\hbar}{i}\nabla$ is the momentum operator. Because **A** and **p** do not commute we obtain

$$\mathbf{H_{int}} = \frac{e}{2m}(\mathbf{p}\cdot\mathbf{A} + \mathbf{A}\cdot\mathbf{p}) = \frac{e\hbar}{i\,m}\mathbf{A}\cdot\nabla \tag{6.3}$$

The vector field has the form $\mathbf{A}(\nu) = A_\nu\, cos(\omega\, t + \mathbf{k}\, y)$ for a plane wave travelling in the $\hat{z}$ direction with corresponding electric field $\mathbf{E} = A_\nu\,\hat{z}\ sin(2\,\pi\nu\, t + \mathbf{k}\, y)$. The transition rate from the valence band (ground state) to a state with a momentum $\mathbf{p} = \hbar\mathbf{k}$ in the conduction band is

$$W = \frac{2\pi}{\hbar}\left|\langle\psi_c|\mathbf{A}\cdot\nabla|\psi_c\rangle\right|^2 \frac{dN(E)}{dE},$$

where $\frac{dN(E)}{dE}$ is the density of states. Recall that we are dealing with a two color field so $\mathbf{A} = \mathbf{A}(\nu) + \mathbf{A}(2\nu)$. The resonant non-interfering contribution from the one-photon transition is,

$$W_{2\nu} \propto \frac{2\pi}{\hbar}|\mathbf{A}(2\nu)|^2\mathbf{p_{vc}}^2.$$

The two-photon transition is via an intermediate level, $|\psi_I\rangle$,

$$W_\nu \propto \frac{2\pi}{\hbar}\left[\frac{|\mathbf{A}(\nu)|^2 \mathbf{p_{vi}}^2}{\Gamma(\Delta)}\right] \times |\mathbf{A}(\nu)|^2 \mathbf{p_{ic}}^2.$$

Here, $\Gamma(\Delta)$ is a non-resonant denominator that is dependent on the detuning between the energy of the intermediate level[1] and the one-photon energy. The actual term of interest is the interfering term between the one- and two-photon transition pathways,

$$W_{2\nu,\nu} \propto \frac{2\pi}{\hbar}[\mathbf{A}(2\nu)^* \mathbf{p_{vc}}]\left\{\frac{[\mathbf{A}(\nu)\mathbf{p_{vi}}][\mathbf{A}(\nu)\mathbf{p_{ic}}]}{\Gamma(\Delta)}\right\} + c.c. \tag{6.4}$$

Neglecting photon momentum, $\mathbf{p_{cc}} = \hbar\mathbf{k}$. As a result eqn. 6.4 yields a transition rate,

$$W_{2\nu,\nu} \propto \frac{2\pi}{\hbar}\frac{\mathbf{p_{vc}}^2\,\mathbf{k}}{\Gamma(\Delta)}[|A_{2\nu}||A_\nu^2|sin(\Delta\phi)]. \tag{6.5}$$

As a consequence, two-color light interacting with GaAs yields a population transfer that is odd in $\mathbf{k}$. That means that there are two asymmetric electron populations created with opposite momentum, consequently yielding a current flow. To summarize, the interaction of coherently related two-color light results in a phase-dependent injected photo-current, $\mathbf{J}$,

$$\dot{\mathbf{J}}(\Delta\phi) \propto (A_\nu)^2 A_{2\nu}\, sin(\Delta\phi) - \mathbf{J}/\tau, \tag{6.6}$$

where τ is a phenomenological decay time (For a rigorous derivation and explanation of photocurrent injection in semiconductors see ref. [5].)

Quantum interference of photocurrents in a semiconductor, was first demonstrate by Haché *et al.*, who realized directional control over the injected photocurrent in bulk GaAs using the fundamental light from an optical parametric amplifier and its second harmonic [31]. The phase parameter between the one- and two-photon transitions, eqn. 6.1, was adjusted using a two-color interferometer and changing the relative phase between the fundamental and second harmonic light using a delay stage. In contrast,

[1] From more rigorous theory is turns out that the most probable dipole transition for the two-photon pathways is via an intermediate state that corresponds with the final state in the conduction band, that is $|\psi_i\rangle = |\psi_c\rangle$. The large detuning makes the cross term's transition rate weak as compared with those due diagonal elements.

for the experiments presented here, quantum interference control (QIC) in LT-GaAs is obtained by adjusting the overall phase of light pulses emitted by a Ti:S laser. This scheme allows for **single-pulse** control of the injected photocurrent in a semiconductor. This is possible, once again, since Kerr-lens modelocking of the longitudinal cavity modes transfers the phase information of the laser pulse train to the electric field of each comb element comprising the optical spectrum, $\mathbf{E}(\nu_n) = E_{\nu_n} exp[-i2\pi(nf_{rep} + f_0)t] = E_{\nu_n} exp\{-i[2\pi n f_{rep} t + \phi_{CE}(t)]\}$.

Control of the injected photocurrent generated in LT-GaAs requires coherently related light with frequencies ν and 2ν. Because the octave spanning Ti:S spectrum in Sect. 5.2 has insufficient power in the wings of the spectrum, the laser light is externally broadened in microstructure (MS) fiber [62]. Injected photocurrent in LT-GaAs is obtained by focusing the broadened light between two gold electrodes separated by 10 μm [see ref. [66]]. The generated photocurrent results in a space-charge effect that is measured as a voltage at the electrodes. Because of this effect, the faster recombination time of LT-GaAs is preferred over that of GaAs.

To facilitate signal detection and avoid noise at DC, we modulate the carrier-envelope phase of the laser pulse train by stabilizing the laser offset frequency to 2.2 kHz. Notwithstanding that ϕ_{CE} is common to both light at ν and 2ν, it results in a phase difference in the transition pathway, $\Delta\phi = \phi_{CE}(t) = 2\pi f_0 t + \phi_0$ [eqn. 6.1]. As a consequence we observe a QIC signal that varies sinusoidally at modulation frequency f_0, with a phase offset ϕ_0 [see. Fig. 6.1 b].

The creation of extra above gap carriers, not contributing to the interference signal, can in some instances reduce the detected photocurrent [32]. The loss in sensitivity that results, however, is dependent on several parameters that are difficult to determine exactly (e.g., pulse duration, pulse chirp and peak intensity). The production of incoherent carriers is of particular concern when using an extremely broadband source such as that generated from broadening in MS fiber. To ascertain the net affect these carriers

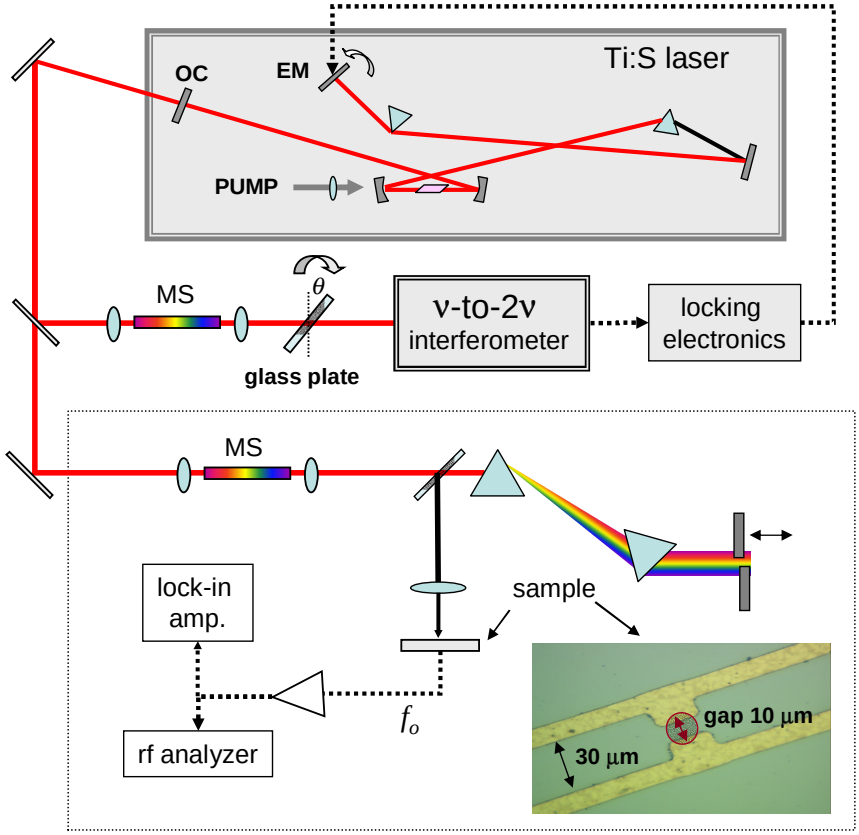

Figure 6.2: Experimental setup used for quantum interference control of injected photocurrents in LT-GaAs. The laser offset frequency is measured using a ν–to–2ν interferometer and stabilized via negative feedback to the laser. Microstructure fiber is used for external broadening of the Ti:S laser spectrum for stabilization and QIC characterization. Because of fiber dispersion a prism sequence for time delay compensation, and a split mirror after the second prism is used for spectral filtering. Light at ν and 2ν are p-polarized such that the electric field oscillates transversely along the axis between the two gold electrodes on the LT-GaAs sample (inset).

have on the photocurrent signal we use incident light that is both filtered and unfiltered. Figure 6.3 a) shows the spectrum of the photocurrent measured for the two different incident optical spectra [see Fig. 6.3 b]. As observed in Fig. 6.3, the use of above gap light ($>$ 874 nm) does not influence the observed SNR, which is 40 dBm at a 10Hz resolution bandwidth. The detected signal, measured using a lock-in amplifier, yields a maximum signal strength that is slightly greater than 1 mV for a pulse repetition rate of 93 MHz, with an average power (spot size) at ν and 2ν of 11.9 mW (10.2 $\pm$ 0.7

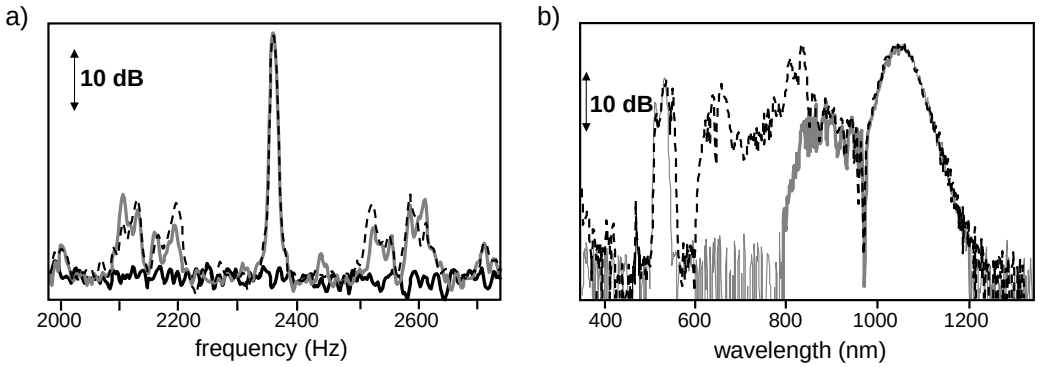

Figure 6.3: a) Spectrum of the measured QIC signal as detected with a resolution bandwidth of 10 Hz. The linewidth (resolution limited) of the measured QIC signal indicates the stability of the laser offset frequency/carrier-envelope phase. The dotted and solid lines indicate the QIC signal strengths corresponding to the optical spectra in b). The solid black line shows the sample electronic baseline. b) The dip at ~ 500 nm corresponds to unavoidable optical filtering due to the small gap between the split mirrors in Fig. 2.

μm) and 1.53 mW (11.5 $\pm$ 0.7 μm), respectively. Currently, the SNR is dominated by electronic pick-up from the sample, although distinct sidebands appear on the carrier due to light noise, which we believe to result from inadequate phase noise suppression in the stabilization feedback loop.

Next we use lock-in detection to demonstrate the sensitivity of quantum interference in the semiconductor system to small static shifts in the carrier-envelope phase, ϕ_0. Lock-in detection of a stable amplitude signal, due to the narrow detection bandwidth, is strongly affected by the coherence of the laser offset frequency. As a result, for lock-in detection of injected photocurrents, coherence in the carrier-envelope phase is a prerequisite. To change ϕ_0 we insert a 176.25 μm zinc borosilicate plate after the MS fiber, before the interferometer used to lock the laser offset frequency. The small phase difference due to dispersion of the glass plate facilitates fine tuning of ϕ_0. Rotation of the glass plate results in shifts in ϕ_{CE} that are measured by the ν–to–2ν interferometer [see Fig. 6.2]. The stabilization loop compensates for the ensuing error by adjusting ϕ_0 of the laser output that is then measured as an offset in the interference signal phase

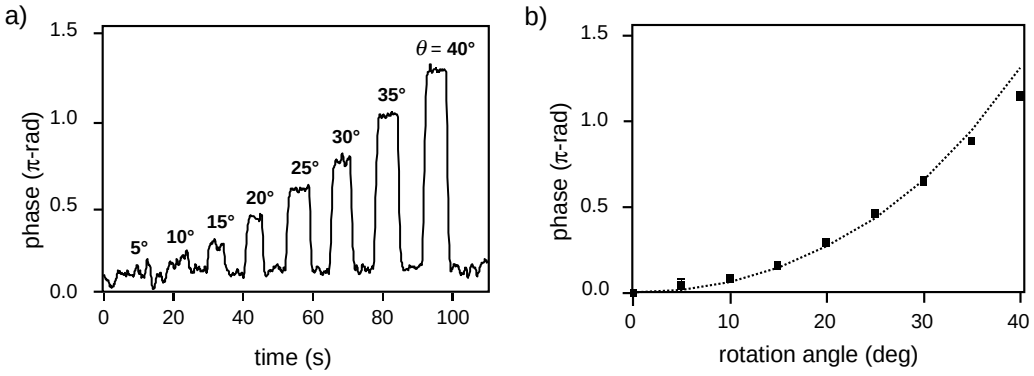

Figure 6.4: a) Phase of the QIC signal as measured relative to the reference used for laser stabilization. The time record of the QIC phase, measured with a time constant of 100 ms shows the phase jumps associated with rotations of the glass plate from 0 degrees to θ and back again, for eight different rotation angles. b) Comparison between the phase change measured in a) (squares) and the calculated carrier-envelope phase change (dashed line).

[Fig. 6.4 a]. The measured phase shifts in a) versus plate rotation are compared with those calculated knowing the dispersion and thickness of the glass plate [see Fig. 6.4 b]. The measured and calculated changes correspond well up until a plate rotation angle of 30^{o}, where the observed discrepancy may be the result of beam misalignment into the ν–to–2ν interferometer.

Quantum interference in the semiconductor system is advantageous over more common phase-sensitive schemes in that detection suffers only minimal phase offsets due to dispersion [46]. A significant improvement of the current SNR ($>$ 30 dB SNR in a 100 kHz resolution bandwidth) should be possible by better engineering the electrode geometry. With increased SNR of the QIC signal, injected photocurrents in semiconductors could be utilized for stabilization of the laser offset frequency. It is our hope that, in the near future, quantum interference of injected photocurrents will be used as a phase sensitive photodetector. Given the potential for chirp free octave spanning spectra, solid state detection of the CE could replace the optical ν–to–2ν interferometer, significantly reducing the complexity of the Ti:S stabilization loop [see Sect. 7].

6.2 Synchronization between a fiber laser and a stabilized Ti:sapphire laser: An absolute comb at 1.5 μm

With the technology available for absolute stabilization of modelocked lasers, a natural extension is to increase the bandwidth of an existing frequency comb by coherently stitching together spectra from separate oscillators, thus leading to a coherently synthesized pulse. The ultra broadband comb generated by synchronizing multiple modelocked laser sources can allow for extension of a frequency comb to access spectroscopic transitions in the far IR and the UV, and additionally for generation of single cycle pulses.

Even though the coherent synthesis of multiple CW lasers is the basis of the frequency chain, the first coherent synthesis of two modelocked lasers was demonstrated only in 2001 by Shelton *et al.* [70]. The lasers in question were two Ti:S lasers operating a different center wavelengths. Electronic referencing of the laser repetition rates and optical referencing of the offset frequencies resulted in the coherent addition of the two laser spectra. As a test of the coherence, an autocorrelation of synchronized pulse trains revealed a shorter duration pulse than could have been achieved from each laser separately [70].

Synchronization between two KLM Ti:S lasers has the advantage that the frequency combs of the lasers are known to be"well behaved", due to the strong modelocking mechanism provided by the formation of Kerr lens [Sect. 5.1.3.1]. The viability of using of other modelocked laser sources as optical comb references, relies strongly on the characteristics of the frequency combs produced by the lasers themselves. Questions arise as to the intrinsic stability available using lasers that rely on different modelocking mechanisms from the KLM Ti:S laser.

In this Section I will describe a well-behaved comb at 1.55 μm from a home-built erbium-doped fiber laser and systematic control of the fiber laser comb parameters.

This is achieved by synchronizing and frequency locking the fiber laser comb to that of a phase-stabilized Ti:S laser. This capability for a fiber laser presents the possibility of a wide bandwidth optical comb, located at telecommunications wavelengths.

Although Ti:S lasers are tremendously successful at producing optical frequency combs, they suffer from several drawbacks that limit their use outside of the laboratory. These includes critical alignment, size, pump laser requirements and expense. Thus it is desirable to examine other mode-locked lasers as possible sources of stable frequency combs. Mode-locked fiber lasers are particularly attractive, being direct diode-pumped, relatively compact and potentially much less expensive [55]. However, since fiber lasers use a different mode-locking mechanism than do Ti:S lasers, it is not a priori obvious that they will produce a clean frequency comb. Furthermore, fiber lasers present a different set of challenges for controlling the frequency comb, particularly the offset frequency.

The stretched-pulse mode-locked fiber laser here operates at a center wavelength of 1.54 μm and a bandwidth of 40 nm [55]. Mode-locking is achieved using nonlinear polarization rotation. The gain medium of the laser is provided by erbium doped fiber, which is pumped by a standard 980 nm diode. At the fiber laser's output, chirped pulses of 550 fs are observed with an average power of 45 mW at a 33.33 MHz repetition rate. The fiber laser is synchronized to the Ti:S laser described in Chap. 2. For these experiments, the Ti:S laser is operated at a center wavelength of 800 nm with an average power of 400 mW at a 100 MHz repetition rate. For ease of stabilization, the fiber laser is enclosed in a box to isolate it from air currents and acoustic noise.

Figure 6.5 depicts the all-electronic experimental setup used for synchronizing the two modelocked lasers and the optical scheme used to determine the quality of the synchronization. Determination of the fiber laser offset frequency is obtained via optical heterodyne against the Ti:S laser [33]. A stable beat signal, however, first requires tight synchronization between the laser repetition rates to maintain temporal overlap between

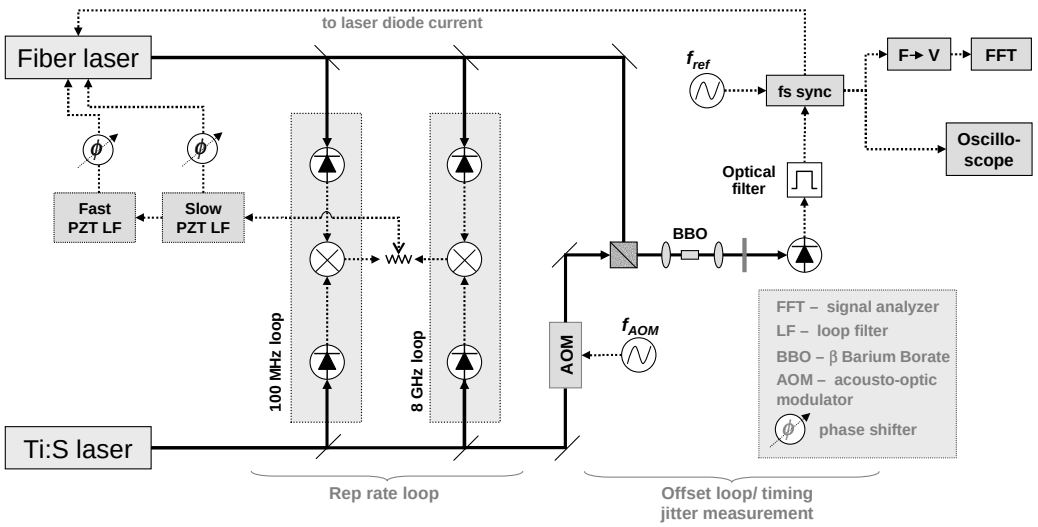

Figure 6.5: Schematic of the setup for synchronizing a fiber laser to a Ti:S. laser. Measurement of f_0 is obtained by angle tuning the BBO crystal such that it is phase matched for second harmonic generation at 1.55 μm. The optical filter used in the f_0 measurement is centered at 770 nm. Similarly, measurement of the timing jitter used the BBO crystal for sum frequency generation and an optical filter centered at ∼520 nm to detect the sum frequency mixing between the fiber and Ti:S laser pulses.

the laser pulses.

Synchronization of the two lasers uses an electronic scheme similar to that used previously to synchronize two Ti:S lasers [70]. The repetition rates of the two lasers are measured independently on fast photodetectors and are then compared using a doubly balanced mixer that provides a phase sensitive error signal to the feedback loop. The repetition rate servo loop to the fiber laser consists of two phase-locked loops. The first loop compares the third harmonic of the fiber laser repetition rate to the fundamental of the Ti:S laser at 100 MHz. Once phase lock is achieved with the 100 MHz loop, the phase lock is shifted to a second, higher phase sensitivity loop that compares higher harmonics of the repetition rates of the two lasers at 8 GHz. In this experiment, negative feedback to the repetition rate of the fiber laser is achieved by changing the cavity fiber length using two fiber-stretching stages. A slow stage (∼3 kHz) is used to correct for slow drifts in cavity length and a faster stage (∼ 6 kHz) is used to correct for the remaining

phase error. The slow stage consists of a low voltage, stacked piezo-electric transducer (PZT) with a range of 10 μm. A pre-tensioned section of fiber is glued to ends of this PZT. The fast stage is also constructed by fixing a fiber under tension to two shearing PZTs (with 1 μm travel), oriented in opposite directions.

Once the fiber and the Ti:S lasers are synchronized, a timing jitter measurement is performed to determine the quality. By using sum frequency generation (SFG) between the fiber and Ti:S laser pulses in a beta-Barium Borate (BBO) crystal an intensity cross-correlation may be obtained. Amplitude noise in the SFG signal results from timing/synchronization errors between the two lasers. To obtain the best sensitivity and linearity for the timing jitter measurement, the fiber and Ti:S lasers are offset in time by half a pulse width such that the SFG signal is generated at half of its peak value. From this cross-correlation a time record is recorded with an rms timing jitter of 12.4 fs (0.5 Hz - 2.5 kHz BW) is obtained [63]. The main limitations to the repetition rate synchronization are due to a relatively small servo bandwidth resulting from mechanical resonance in the fast fiber stretching stage at $\sim$ 6 kHz.

Once the laser repetition rates are locked, the fiber laser f_0 is obtained via optical heterodyne between the second harmonic of the fiber laser ($\sim$ 770nm) with the fundamental of the Ti:S laser. As seen in Fig. 6.5, the two laser beams are spatially overlapped at a dichroic beamsplitter before being passed through a BBO crystal. This employs the same setup as was used to measure the timing jitter, with the exception that the BBO crystal is tuned for phase matched frequency doubling at 1.55 μm. A 4 nm optical bandpass at $\sim$ 780 nm filters the optical signal before a fast photodetector measures the RF heterodyne signal with components at frequencies given by

$$\pm|(mf_{rep1} - 2nf_{rep2}) + (f_{01} + f_{02} + f_{AOM})|. \tag{6.7}$$

Here the indices 1 and 2 represent the Ti:sapph and fiber lasers respectively. For this experiment $f_{01} = 0$. From equation 6.7 it can be seen that timing jitter (first term)

in the repetition rates of the two lasers appears directly as sidebands on the offset frequency, indicating the importance the repetition rate synchronization. To stabilize the fiber laser offset frequency, the RF heterodyne signal at $mf_{rep1} = 2nf_{rep2}$ is detected and filtered. The signal is then referenced to the AOM drive frequency, f_{AOM}, using a digital phase detector. Negative feedback for the fiber laser f_0 lock is provided via amplitude modulation of the diode pump power. A frequency-to-voltage converter, in

cc

n

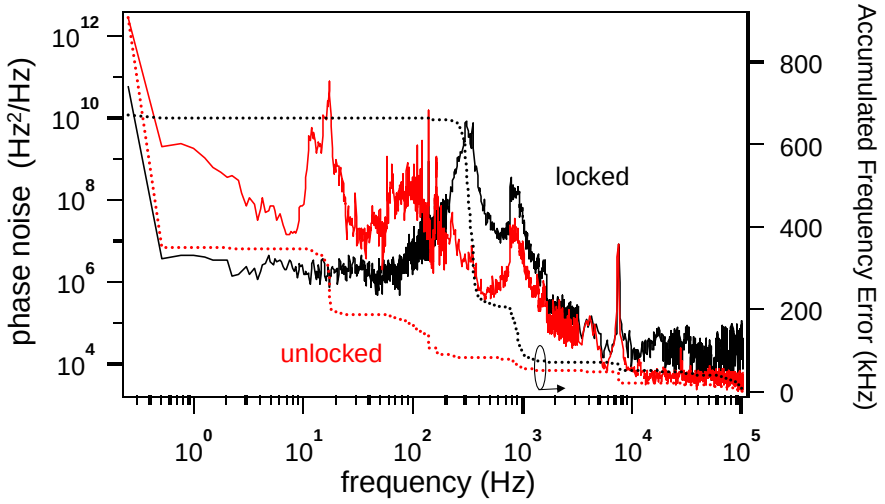

Figure 6.6: Fiber laser offset frequency noise PSD, $S_{f_o}(f)$ (solid lines, left axis) and integrated frequency noise (dotted lines, right axis) versus frequency offset from carrier. The grey (black) solid line is the PSD of the unlocked (locked) offset frequencies, respectively.

Figure 6.6 shows the in-loop measurement of the offset frequency for both the unlocked and locked cases. Integration of the locked frequency PSD in Fig. 6.6 yields a fiber laser f_0 linewidth of 355 kHz from 102 kHz to 0.5 Hz. Amplitude modulation of the pump diode suffers from a bandwidth-limiting steep roll-off beyond a few kHz, hence only a frequency lock of the offset frequency was achieved. Several physical mechanisms may underlie the limited bandwidth. We hypothesize that it is phase lag,

resulting from the lifetime of the Erbium doped fiber ($\sim$ 1 ms) that is the limiting factor in using pump amplitude modulation as an actuator. Improvement of the offset frequency lock will require investigation into the transfer function of the current servo loop and subsequent design of an electronic compensation system for the servo. Another possibility of circumventing this limiting factor may lie in the modulation of the fiber laser output by an AOM.

Servo limitations aside, the stretched-pulse mode-locked fiber laser produces a clean frequency comb that can be stabilized. A disadvantage of stabilizing the fiber laser by means of comparison against another laser is that instabilities in synchronization between the laser repetition rates results in a significant amount of noise on extra noise on the offset frequency. The repetition rate lock may be tightened by using the optical jitter measurement as the error signal instead of the high harmonic of the Ti:S f_{rep} signal. An even better possibility is to self-reference the fiber laser as a means to create an absolute comb at 1.5 μm [72], along much the same lines as that for the Ti:S laser. Broadening of the unamplified fiber laser output is achieved using MS fiber, designed to work at telecommunication wavelengths [20]. Self-referencing for the fiber laser has the definite advantage, over that for the Ti:S laser, in that the MS fiber used at 1.5 μm may be spliced directly to the fiber laser output, thus eliminating alignment difficulties.

There is still much research to be carried out to resolve which modelocked source will persist as the ultimate transfer oscillator for a primary optical standard. The choice of laser will no doubt be somewhat dependent on ease of use, long term stability and possibly on the choice of optical standard. In terms of simplicity, the broadband Ti:S laser that yields a direct measurement of the laser offset frequency without the use of MS fiber and the self-referenced fiber laser are both attractive candidates. The question that still needs to be addressed is the issue of stability. Both the Ti:S and fiber lasers

offer exceptional intrinsic stability of the comb parameters. Pump current control of the fiber laser offset frequency, necessary for this stabilization in the self-referencing scheme, nevertheless, still suffers from the steep servo roll off at low frequencies. However, a higher servo bandwidth for the fiber laser offset frequency may be obtain by inserting a set of glass wedges into the laser, and using dispersion as a means for controlling f_0.

Chapter 7

Conclusions and outlook

Stabilization of modelocked lasers via self-referencing heralds a new era for optical frequency metrology. The significant advances in phase stabilization of Ti:S lasers since 2000 allow for absolute optical frequency measurements to be performed using a single oscillator directly referenced to the primary Cs microwave standard. Additionally, stabilization of the optical spectrum of a Ti:S laser, which naturally leads to control of the optical carrier, now permits exploration into, and phase-determination of physical processes that are sensitive to the field of an ultrashort light pulse. Phase sensitive experiments of this type, however, are predicated on maintaining strong coherence in the pulse phase. High phase stability lasers, however, require good engineering and thorough characterization of the stabilization system, as demonstrated here. Notwithstanding the technical challenges, the stabilized modelocked laser serves a relatively simple and versatile tool for investigation of atomic, molecular and optical physics.

To summarize I would like to give a brief perspective from whence we have come to hopefully where we are going. Figure 7.1 depicts an example of a harmonic frequency chain used by the PTB (Physikalisch-Technischen Bundesanstalt) in Braunschweig, Germany used to perform an absolute optical measurement of Ca [67]. The details of the figure are not important. What fig. 7.1 is meant to indicate is the level of complexity (12 oscillators and 14 PLL's) involved in harmonic frequency synthesis, especially in comparison to Fig. 7.2 a), which shows the stabilized modelocked laser system that has

replaced it (1 oscillator and 2 PLL's).[1] Although a stabilized Ti:S laser represents a massive simplification over harmonic frequency chains, there is always room for further reduction in complexity. In particular, toward the application to all-optical clocks, a limiting factor in terms of the reproducibility and long term stability of the Ti:S laser is the use of miscrostructure fiber for measurement of the laser offset frequency. Aside from the issues of phase noise that we have been discussed here, complexities in coupling to MS fiber also can result in long-term loss in signal strength of f_0, which is not acceptable in a possible clockwork.

Thankfully, the use of broadband Ti:S lasers can circumvent issues of MS fiber altogether by generating sufficient bandwidth for direct measurement of f_0 using the unbroadened laser spectrum alone. Still, given the added simplification, there still exist the complexity of nonlinear interferometers used for detection of f_0. Phase drifts due to the optics and electronics are particularly problematic for maintaining long term CE phase coherence. A further reduction in complexity to the phase stabilization scheme may be obtained by using quantum interference in semiconductors as solid- state detection of the carrier-envelope phase [Sect. 6.1] instead of a ν–to–2ν interferometer. A shown in Fig. 7.2 b), this technique, used in tandem with a chirp compensated octave spanning laser spectrum, would allow for interferometer free optical phase detection on a chip. Solid state phase detection, via injected photocurrents, takes an optical input and produces a voltage, $V(t) \propto sin(2\pi\, f_0 t + \phi_0)$.[2] For $f_0 \neq 0$, the output signal is sensitive to the time evolution in the carrier-envelope phase, or in other words, measures the laser offset frequency. However, for $f_0 = 0$, the voltage signal directly yields the carrier-envelope phase [see Sect.4.1]. The quantum interference generated injected photocurrent alone provides an error-signal of the CE phase without the need for com-

[1] Typically optical frequency measurement uses higher repetition rate lasers that use only chirped mirrors for intracavity dispersion compensation because of the higher frequency mode spacing and greater power per optical mode.

[2] This is exactly the signal produced from a phase comparison using a double-balanced mixer, except operating at zero frequency.

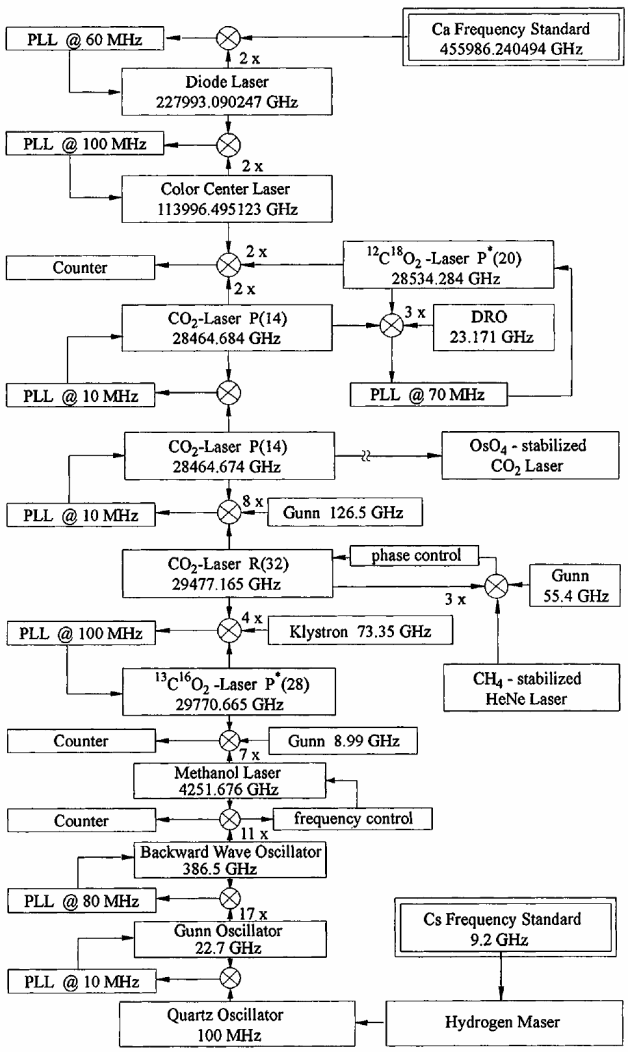

Figure 7.1: PTB harmonic frequency chain to the Ca intercombination line.

parison to an external reference. By including amplification and filtering directly on the same circuit as the semiconductor phase detector, one could condensed the entire ν–to–2ν interferometer and stabilization electronics onto a single chip. The final result would be a phase sensitive photodetector! It is our hope that solid state detection of the CE phase will allow for this realization of this amazingly simple stabilization scheme. Such a scheme would eliminate much of complexities due to drifts in optics and electronics and should allow for a more reproducible user friendly system.

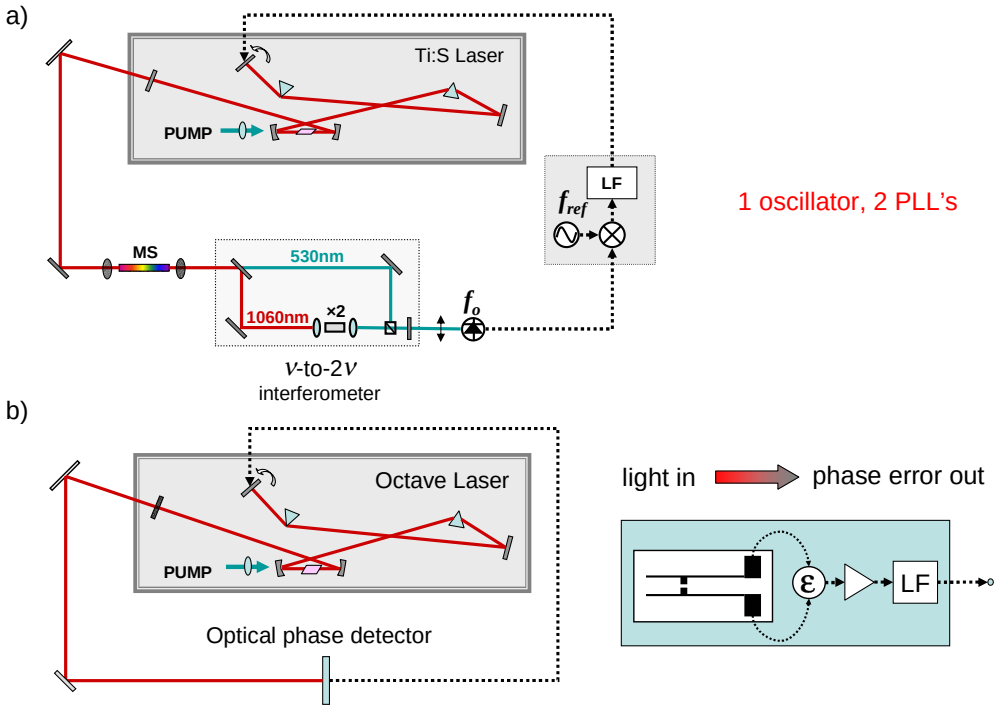

Figure 7.2: (a) Current experimental apparatus for stabilization of a Ti:S laser and (b) hopeful future experimental apparatus.

Bibliography

[1] J. N. Ames, S. Ghosh, R. S. Windeler, A. L. Gaeta, and S. T. Cundiff. Excess noise generation during spectral broadening in microstructure fiber. Appl. Phys. B, 77:279–284, 2003.

[2] D. Z. Anderson, N. B. Baranova, K. Green, Zel'dovich, and B. Ya. Interference of one- and two-photon processes in the ionization of atoms and molecules. Sov. Phys. JETP, 75(2):210–214, 1992.

[3] A. Apolonski, P. Dombi, G. G. Paulus, K. Torizuka, M. Kakehata, R. Holzwarth, Th. Udem, Ch. Lemell, J. Burgdörfer, T. W. Hänsch, and Krausz F. submitted, 2003.

[4] M. T. Asaki, C. P. Huang, D. Garvey, J. P. Zhou, H. C. Kapteyn, and M. M. Murnane. Generation of 11-fs pulses from a self-mode-locked ti-sapphire laser. Opt. Lett., 18(12):977–979, 1993.

[5] R. Atanasov, A. Haché, J. L. P. Hughes, H. M. van Driel, and J. E. Sipe. Coherent control of photocurrent generation in bulk semiconductors. Phys. Rev. Lett., 76(10):1703–1706, 1996.

[6] A. Baltuska, T. Udem, M. Uiberacker, M. Henschel, E. Gouliemakis, C. Gohle, R. Holzwarth, V. S. Yakovlev, i A. Scrinz, T.W. Hansch, and F. Krausz. Attosecond control of electronic processes by intense light fields. Nature, 421(6923):611–615, 2003.

[7] A. Bartels and H. Kurz. Generation of a broadband continuum by a ti : sapphire femtosecond oscillator with a 1-ghz repetition rate. Opt. Lett., 27(20):1839–1841, 2002.

[8] M. Bellini and T. W. H"ansch. Phase-locked white-light continuum pulses: toward a universal optical frequency-comb synthesizer. Opt. Lett., 25:1049–1051, 2000.

[9] P. Brumer and M. Shapiro. Chem. Phys. Lett., 126:541, 1986.

[10] S. T. Cundiff, W. H. Knox, E. P. Ippen, and H. A. Haus. Frequency-dependent mode size in broadband kerr-lens mode locking. Opt. Lett., 21(9):662–664, 1996.

[11] S. A. Diddams, D. J. Jones, J. Ye, T. Cundiff, J. L. Hall, J. K. Ranka, R. S. Windeler, R. Holzwarth, T. Udem, and T. W. Hansch. Direct link between microwave and optical frequencies with a 300 thz femtosecond laser comb. Phys. Rev. Lett., 84(22):5102–5105, 2000.

[12] S. A. Diddams, T. Udem, J. C. Bergquist, E. A. Curtis, R. E. Drullinger, L. Hollberg, W. M. Itano, W. D. Lee, C. W. Oates, K. R. Vogel, and D. J. Wineland. An optical clock based on a single trapped hg-199(+) ion. Science, 293(5531):825–828, 2001.

[13] P. Dietrich. Determining the absolute carrier phase of a few-cycle pulse. Opt. Lett., 25(1):16–18, 2000.

[14] V. A. Dzuba and V. V. Flambaum. Atomic optical clocks and search for variation of the fine- structure constant - art. no. 034502. Physical Review A, 6103(3):4502–+, 2000.

[15] V. A. Dzuba, V. V. Flambaum, and J. K. Webb. Calculations of the relativistic effects in many-electron atoms and space-time variation of fundamental constants. Phys. Rev. A, 59(1):230–237, 1999.

[16] J. N. Eckstein. Ph.d thesis. Stanford University, 1978.

[17] R. Ell, U. Morgner, F.X. Krtner, J. G. Fujimoto, E. P. Ippen, V. Scheuer, G. Angelow, T. Tschudi, M.J. Lederer, A. Boiko, and B. Luther-Davies. Generation of 5 fs pulses and octave-spanning spectra directly from a ti:sapphire laser. Opt. Lett., 26:373–375, 2001.

[18] K. M. Evanson, J. S. Wells, F. R. Petersen, B. L. Danielson, and G. W. Day. Accurate frequencies of molecular transitions used in stable laser stabilization: the 3.39 μm transition in ch_4 and the 9.33 and 10.18 μm transitions in co_2. Appl. Phys. Lett., 22(4):192–195, 1973.

[19] S.F. FELDMAN, D.A. WEINBERGER, and H.G. WINFUL. Polarization instability in a twisted birefringent optical fiber.

[20] X. Feng, T.M. Monro, P. Petropoulos, V. Finazzi, and Hewak D. Solid microstructured optical fiber. Opt. Exp., 11(18):2225–2230, 2003.

[21] A. I. Ferguson, J. N. Eckstein, and T. W. Hänsch. A subpicosecond dye laser directly pumped by a mode-locked argon laser. J. Appl. Phys., 49:5389, 1978.

[22] R. L. Fork, O. E. Martinez, and J. P. Gordon. Negative dispersion using pairs of prisms. Opt. Lett., 9(5):150–152, 1984.

[23] T. M. Fortier, S. T. Cundiff, and I. T. *et al.* Lima. Birefringence and nonlinear polarization rotation in microstructure fiber. (2), To be submitted.

[24] T. M. Fortier, Jones David. J., and Cundiff S. T. Octave spanning conventional geometry ti:sapphire laser. Opt. Lett., 18(28):2198–2200, 2003.

[25] T. M. Fortier, D. J. Jones, J. Ye, and S. T. Cundiff. Highly phase stable modelocked lasers. IEEE J. Quantum Electronics, 9(4):July/August, 2003.

[26] T. M. Fortier, D. J. Jones, J. Ye, S. T. Cundiff, and R. S. Windeler. Long-term carrier-envelope phase coherence. Opt. Lett., 27(16):1436–1438, 2002.

[27] T. M. Fortier, P. A. Roos, D. J. Jones, and S. T. Cundiff. submitted to PRL for publication, 2003.

[28] T. M. Fortier, J. Ye, S. T. Cundiff, and R. S. Windeler. Nonlinear phase noise generated in air-silica microstructure fiber and its effect on carrier-envelope phase. Opt. Lett., 27(6):445–447, 2002.

[29] P. Fritschel, G. Gonzalez, B. Lantz, P. Saha, and M. Zucker. High power interferometric phase measurement limited by quantum noise and application to detection of gravitational waves. Phys. Rev. Lett., 80(15):3181–3184, 1998.

[30] H. M. Golderberg, D. Kleppner, and N. F. Ramsey. Phys. Rev. Lett., 8:361, 1960.

[31] A. Haché, Y. Kostoulas, R. Atanasov, J. L. P. Hughes, J. E. Sipe, and H. M. van Driel. Observation of coherently controlled photocurrent in unbiased, bulk gaas. Phys. Rev. Lett., 78(2):306–309, 1997.

[32] A. Haché, J. E. Sipe, and H. M. van Driel. Quantum interference control of electrical currents in gaas. IEEE J. Quantum Electronics, 34(7):1144–1154, 1998.

[33] Lipphardt B. Stenger J. Telle H. R. Fallnich C. H. Hundertmark Haverkamp, N. Amplified femtosecond pulses from an er : fiber system: Nonlinear pulse shortening and self-referencing detection of the carrier-envelope phase evolution. Conference on Ultrafast Phenomena, Vancouver, BC,, pages p. ME31–31, 2002.

[34] F. W. Helbing, G. Steinmeyer, U. Keller, R. S. Windeler, J. Stenger, and H. R. Telle. Carrier-envelope offset dynamics of mode-locked lasers. Opt. Lett., 27(3):194–196, 2002.

[35] D. Hils and J. L. Hall. Improved kennedy-thorndike experiment to test special relativity. Phys. Rev. Lett., 64(15):1697–1700, 1990.

[36] L. O. Hocker, A. Javan, D. R. Rao, L. Frenkel, and T. Sullivan. Appl. Phys. Lett., 10:5, 1966.

[37] L. Hollberg and *et al.* Optical frequency standards and measurements. IEEE J. Quantum Electronics, 37(12):1502–1513, 2001.

[38] K. W. Holman, R. J. Jones, A. Marian, S. T. Cundiff, and J Ye. Intensity-related dynamics of femtosecond frequency combs. Opt. Lett., 28(10):851–853, 2003.

[39] K. W. Holman, R. J. Jones, A. Marian, S. T. Cundiff, and J. Ye. Intensity-related dynamics of femtosecond frequency combs. IEEE J. Quantum Electronics, 9(4):in press, 2003.

[40] R. Holzwarth, Zimmermann M., T. Udem, and T. W. Hänsch. Optical clockworks and the measurement of laser frequencies with a mode-locked frequency comb. IEEE J. Quantum Electronics, 32(12):1493–1501, 1999.

[41] T. Ikegami, S. Sudo, and Y. Sakai. Frequency stabilization of semiconductor laser diodes. Artech House, Norwood, 1995. Artech House, Norwood, 1995.

[42] K. Imai, M. Kourogi, and M. Ohtsu. 30-thz span optical frequency comb generation by self-phase modulation in optical fiber. IEEE J. Quantum Electronics, 34(1):54, 1998.

[43] Christov I.P. and V.D. Stoev. Kerr-lens mode-locked laser model: role of space-time effects. JOSA B, 15(7):1960–1966, 1998.

[44] D. A. Jennings, C. R. Pollock, F. R. Petersen, R. E. Drullinger, K. M. Evanson, J. S. Wells, J. L. Hall, and H. P. Layer. Direct frequency measurement of the i_2 stabilized he-ne 473 thz (633nm) laser. Opt. Lett., 8(3):136, 1983.

[45] D. J. Jones, S. A. Diddams, J. K. Ranka, A. Stentz, R. S. Windeler, J. L. Hall, and S. T. Cundiff. Carrier-envelope phase control of femtosecond mode-locked lasers and direct optical frequency synthesis. Science, 288(5466):635–639, 2000.

[46] D. J. Jones, T. M. Fortier, and S. T. Cundiff. submitted to JOSA B for publication, 2003.

[47] F. X. Kärtner, U. Morgner, R. Ell, T. Schibli, J. G. Fujimoto, E. P. Ippen, V. Scheuer, G. Angelow, and T. Tschudi. Ultrabroadband double-chirped mirror pairs for generation of octave spectra. JOSA B, 18(6):882–885, 2001.

[48] W. H. Knox, M. C. Downer, R. L. Fork, and C. V. Shank. Picosecond continuum generation by mode-locked lasers. Opt. Lett., 9:552–554, 1984.

[49] H. Kogelnik. Review of dye lasers. JOSA B, 61(11):1561–, 1971.

[50] M. Kourogi, K. Kakagawa, and M. Ohtsu. Wide-span optical frequency comb for accurate optical difference measurement. IEEE J. Quantum Electronics, 29:2693, 1993.

[51] H. Mabuchi, J. Ye, and H. J. Kimble. Full observation of single-atom dynamics in cavity qed. Appl. Phys. B, 68(6):1095–1108, 1999.

[52] E. J. Mayer, J. Mobius, A. Euteneuer, W. W. Ruhle, and R. Szipocs. Ultrabroadband chirped mirrors for femtosecond lasers. Opt. Lett., 22(8):528–530, 1997.

[53] T. M. Monro, D. J. Richardson, N. G. R. Broderick, and P. J. Bennett. Modelling large air fraction holey optical fibers. J. Lightwave Technology, 18(1):50–56, 2000.

[54] O. D. Mücke, T. Tritschler, M. Wegener, U. Morgner, and F. X. Kärtner. Determining the carrier-envelope offset frequency of 5-fs pulses with extreme nonlinear optics in zno. Opt. Lett., 27(23):2127–2129, 2002.

[55] L. E. Nelson, D. J. Jones, K. Tamura, H. A. Haus, and E. P. Ippen. Ultrashort-pulse fiber ring lasers. Appl. Phys. B, 65(2):277–294, 1997.

[56] N. R. Newbury, B. R. Washburn, K. L. Corwin, and R. S. Windeler. Noise amplification during supercontinuum generation in microstructure fiber. Opt. Lett., 28:944–946, 2003.

[57] C.W. Oates, E.A. Curtis, and L. Hollberg. Improved short-term stability of optical frequency standards: approaching 1 hz in 1 s with the ca standard at 657 nm. Opt. Lett., 25(21):1603–1605, 2000.

[58] G. G. Paulus, F. Grasbon, H. Walther, P. Villoresi, M. Nisoli, S. Stagira, E. Priori, and S. De Silvestri. Absolute-phase phenomena in photoionization with few-cycle laser pulses. Nature, 414(6860):182–184, 2001.

[59] A. Poppe, R. Holzwarth, A. Apolonski, G. Tempea, C. Spielmann, T. W. Hänsch, and F. Krausz. Few-cycle optical waveform synthesis. Appl. Phys. B, 72(8):977–977, 2001.

[60] J. D. Prestage, R. L. Tjoelker, and L. Maleki. Atomic clocks and variations of the fine-structure constant. Phys. Rev. Lett., 74(18):3511–3514, 1995.

[61] N. F. Ramsey. History of atomic clocks. NBS, 88(5):301–320, 1983.

[62] J. K. Ranka, R. S. Windeler, and A. J. Stentz. Visible continuum generation in air-silica microstructure optical fibers with anomalous dispersion at 800 nm. Opt. Lett., 25(1):25–27, 2000.

[63] J. Rauschenberger, T. M. Fortier, D. J. Jones, J. Ye, and S. T. Cundiff. Control of the frequency comb from a mode-locked erbium-doped fiber laser. Opt. Exp., 10(24):1404–1410, 2002.

[64] J. Reichert, R. Holzwarth, T. Udem, and T.W. Hänsch. Absolute optical frequency measurement of the cesium d-1 line with a mode-locked laser. Phys. Rev. Lett., 82(18):3568–3571, 1999.

[65] J. Reichert, R. Holzwarth, T. Udem, and T.W. Hänsch. Measuring the frequency of light with mode-locked lasers. Opt. Lett., 172(1-6):59–68, 1999.

[66] P. Roos, S. T. Bhat R. Quraishi, Q. Cundiff, and Sipe J. Characterization of quantum interference control of injected currents in lt-gaas for carrier-envelope phase measurements. Opt. Exp., 11(17):2081–2090, 2003.

[67] H. Schnatz, B. Lipphardt, J. Helmcke, F. Riehle, and G. Zinner. First phase-coherent frequency measurement of visible radiation. Phys. Rev. Lett., 76(1):18–21, 1996.

[68] C. Schwob, L. Jozefowski, B. de Beauvoir, L. Hilico, F. Nez, L. Julien, F. Biraben, O. Acef, and A. Clairon. Optical frequency measurement of the 2s-12d transitions in hydrogen and deuterium: Rydberg constant and lamb shift determinations. Phys. Rev. Lett., 82(25):4960–4963, 1999.

[69] M. Shapiro and P. Brumer. Adv. Atomic, Mol. and Opt. Phys., 42:287, 2000.

[70] R. K. Shelton, L. S. Ma, H. C. Kapteyn, M. M. Murnane, J. L. Hall, and J. Ye. Phase-coherent optical pulse synthesis from separate femtosecond lasers. Science, 293(5533):1286–1289, 2001.

[71] U. Tanaka, J.C. Bergquist, and S. *et al.* Bize. Optical frequency standards based on the hg-199(+) ion. IEEE T. Instrument Meas., 52(2):245–249, 2003.

[72] F. Tauser, A. Leitenstorfer, and W. Zinth. Amplified femtosecond pulses from an er : fiber system: Nonlinear pulse shortening and self-referencing detection of the carrier-envelope phase evolution. Opt. Exp., 11(6):594–600, 2003.

[73] H. R. Telle, D. Meschede, and T. W. Hänsch. Realization of a new concept for visible frequency division: phase locking of harmonic and sum frequencies. Opt. Lett., 15:532, 1990.

[74] H. R. Telle, G. Steinmeyer, A.E. Dunlop, J. Stenger, D.H. Sutter, and U. Keller. Carrier-envelope offset phase control: A novel concept for absolute optical frequency control and ultrashort pulse generation. Appl. Phys. B, 69:327–332, 1999. STC.

[75] T. Udem, A. Huber, B. Gross, J. Reichert, M. Prevedelli, M. Weitz, and T. W. Hänsch. Phase-coherent measurement of the hydrogen 1s-2s transition frequency with an optical frequency interval divider chain. Phys. Rev. Lett., 79(14):2646–2649, 1997.

[76] T. Udem, J. Reichert, R. Holzwarth, and T.W. Hänsch. Accurate measurement of large optical frequency differences with a mode-locked laser. Opt. Lett., 24(13):881–883, 1999.

[77] H. M. van Driel, J. E. Sipe, A. Haché, and R. Atanasov. Coherence control of photocurrents in semiconductors. Physica Status Solidi B-Basic Research, 204(1):3–8, 1997.

[78] D. J. Wineland, J. C. Berquist, W. M. Itano, F. Diedrich, and C. S. Weimer. The Hydrogen Atom, section "Frequency Standards in the Optical Spectrum". Editors, G. F. Bassani, M. Inguscio and T. W. Hänsch. Springer-Verlag, Berlin, 1989.

[79] X.Y. Xu, T.H. Loftus, and J.L. *et al.* Hall. Cooling and trapping of atomic strontium. J. Opt. Soc. Am. B, 20(5):968–976, 2003.

[80] J. Ye, L.-S. Ma, and J. L. Hall. Molecular iodine clock. Phys. Rev. Lett., 87(27):270801, 2001.

Appendix A

Phase stabilization of Ti:sapphire lasers: the details

In this Appendix I hope to fill in many of the design considerations and details for realization of a highly phase stable laser. Just as a reminder of the basic concept, we wish to directly measure and the two characteristic frequencies of the optical comb, the laser repetition rate, f_{rep} and the laser offset frequency, f_0. Recall that f_{rep} sets the comb spacing and is inversely proportional to the laser cavity length, and that f_0 decides the absolute comb position and is directly proportional to dispersion inside the laser cavity. Once these two rf frequencies are measured, they are electronically compared to reference frequencies, necessary for stabilization. Negative feedback to the laser is then used for error correction.

A.1 Frequency difference measurement of the optical comb

The most readily available method for measurement of light is using a photodiode (PD). However, because PD's are power law detectors they may only measure frequency differences obtained via comparison between two optical carriers. In the case of both the laser repetition rate and the laser offset frequency, optical comparison that yields a difference frequency proportional to f_{rep} and f_0 is provided within the comb itself via heterodyne between adjacent comb components. This will be explain in detail shortly.

First let us examine a more simple example of optical comparison for difference frequency measurement. Such a measurement may be obtained from the interference of

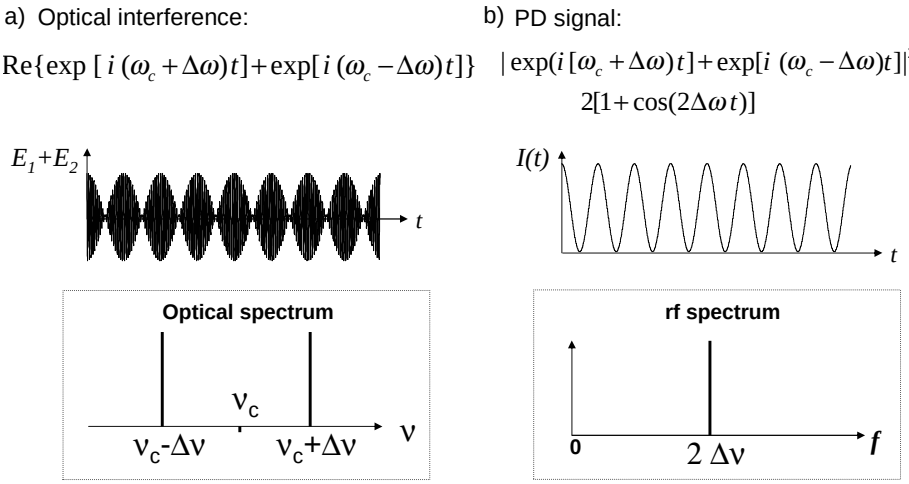

Figure A.1: (a) Optical interference between two electric fields separated in frequency by $\Delta\omega$. This results in sinusoidal modulation of the carrier-frequency, ω_c, at $2\Delta\omega$. (b) Radio frequency spectrum that results from the current signal produced from measurement of the optical signal using a photodiode.

two coherent light sources. Interference between two collinearly propagating light waves of different frequency, $\omega_c+\Delta\omega$ and $\omega_c-\Delta\omega$, will result in a modulation of the light at the difference frequency, $2\Delta\omega$, or in other words, in a time-dependent interference pattern [see Fig. A.1 a)]. If the two interfering wavelengths have a difference frequency within the bandwidth of the PD, the PD measures the change in strength of the light due to the travelling constructive and destructive interference pattern. Interference between two wavelengths of light is the simplest example of optical beating. The amplitude spectrum for this example is simply an rf spike at the difference frequency, $2\Delta\omega = 2\pi\Delta\nu$ [see Fig. A.1 b)].

A more complicated example of optical beating is the coherent addition of millions of frequencies, which leads to the synthesis of complicated waveforms. This is the physical mechanism behind pulse formation in the Ti:S laser [see Fig. A.2 a]. This is the ultimate in optical interference and permits easy measurement of the characteristic frequencies for the KLM Ti:S laser.

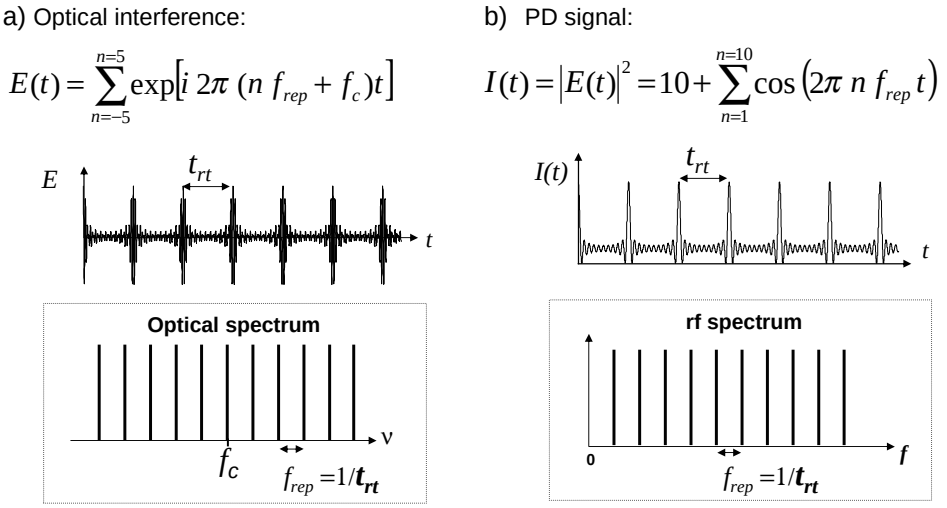

Figure A.2: a) Optical interference between multiple coherent optical fields separated in frequency by $\Delta\omega$, at a carrier frequency, ω_c. This results in severe AM modulation of the carrier-frequency, ω_c, whereby the net result is pulse formation b) The current signal produced by shining the light in a) on a photodetector (PD). The PD can only measure the intensity of the light which is phase (carrier) insensitive.

A.2 Measurement of the laser repetition rate

The intrinsic amplitude modulation of a pulse train of a modelocked laser can yield direct measurement of the the laser repetition rate, f_{rep}. The laser pulse train incident on a photodetector yields a series of amplitude spikes in time at $t_{rt} = 1/f_{rep}$. Therefore the signal out of the PD is the AM modulation of the pulse train, without the optical carrier, resulting in a current blip each time a pulse hits the detector at an interval, $t = t_{rt}$ [see Fig. A.2 a]. The Fourier transform of a voltage signal of delta function spikes in time is a *rf* frequency spectrum starting at zero Hz with frequency peaks at harmonics of $f_{rep} = 1/t_{rt}$ [see Fig. A.2 b]. (If the PD were sensitive to the optical carrier, the Fourier transform would yield the optical frequency spectrum of the laser, centered at the *optical* carrier frequency.)

Of course, given that we are using modelocked lasers, everything can be thought of both in the time and frequency domains (deciphering the frequency and time domain

aspects of the light field produced by the modelocked laser is the main fun offered in this field.) Generation of the rf spectrum can therefore also be explained by considering every harmonic in the rf spectrum as being generated by beating between successive components of the optical frequency comb, Fig. 2.3.

A.3 Measurement of the laser offset frequency, f_0

Measurement of f_0 relies on exactly the same principles of optical beating as does measurement of f_{rep}. However, to generate a beat signal sensitive to f_0 requires the use of a nonlinear interference. As described in Sect. 2.2, self-referenced measurement of the offset frequency is obtained using nonlinear comparison. Measurement of f_0 may also be determined using the classic optical frequency metrology technique of comparison against a secondary optical standard.

The offset frequency cannot be directly extracted from the pulse train in the way that f_{rep} may be. There are two ways to think of this. In the time domain, knowledge of f_0 is contained within the carrier-frequency. Because the PD is insensitive to the carrier it cannot provide direct measurement of f_0. In the frequency domain, generation of an rf spectrum is obtained by the beating harmonics of the optical comb, $|(m\, f_{rep} + f_0) - (n\, f_{rep} + f_0)|$, which results in perfect cancellation of f_0.

The nonlinear heterodyne that is utilized for measurement of f_0 is obtained using a ν–to–2ν interferometer that allows for optical comparison between the second harmonic of the low frequency comb components of an octave spectrum and the fundamental of the high frequency comb components of the spectrum. The comparison at the output of the interferometer may be thought of as interfering two pulse trains with a relative time dependent phase shift, $\phi(t) = 2\pi\ f_0\, t$. The two pulse trains are temporally overlapped so that interference is possible (interference occurs in free space, not only at the PD). If the two pulse trains were not shifted in frequency the PD would simply see the amplitude modulation of a single pulse train. The interference due to a shift in frequency between

the two pulse trains results in an additional, slightly slower AM modulation of the pulse train itself. The voltage signal out of the PD is then a series of delta function voltage spikes with an additional sinusoidal modulation envelope at f_0. The Fourier transform of this voltage signal is then the rf f_{rep} spectrum with AM sidebands at f_0 as in Fig. 2.4.

The bandwidth necessary for self-referencing of f_0 is an optical octave. Typically, the octave is obtained via external broadening of the Ti:S laser spectrum in MS fiber, although, as shown in Chap. 5, it is preferable to generate the necessary bandwidth within the oscillator directly.

A.4 Fun with microstructure fiber

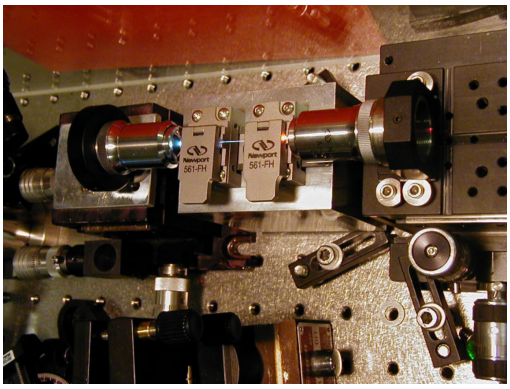

Figure A.3: High-stability mounting of MS fiber.

Microstructure fiber is, by far, the most difficult element to work with in the stabilization loop. The worst aspect of the fiber is that changes in the input coupling result in alterations in amplitude of the spectral output. Coupling problems of this sort can be minimized by using very high quality coupling stages. We use Thorlabs flexture stages (MDT616) each with differential micrometers for the x-, y- and z- translation axes [see Fig. A.3]. Also when clamping MS fiber it is best to minimize the amount excess fiber at the edge of the clamp. This will diminish pointing errors resulting from vibrations of the dangling fiber end. Additionally, I have found that it is useful to add

a thin piece of rubber sheet to secure the fiber in the clamp. All these precautions help to minimize AM-to-PM conversion in MS fiber [see Sect. 4.3.1] and cut down the effect of long term coupling problems.

To allow for fine tuning of the generated continuum we use a broadband polarizer and half-wave plate before the fiber. This allows us to control in the input polarization of the light pulses and the coupled power. The input polarization to the input of the fiber is crucial because the fiber is slightly birefringent. For MS fiber from Lucent Technologies, there exists a preferred axis which allows for maximum broadening as well as preservation of the input polarization [see Sect. 3.2].

A.5 Self-referencing: the interferometer

There are many different configurations that may be used for the ν–to–2ν interferometer. The main design specifications, however, are always the same. The point of the interferometer is to allow for generation of a self-referenced nonlinear optical interference signal of the optical frequency comb with itself. As explained above, interference is obtained by cross-referencing two pulse trains that differ in frequency by f_0. This requires temporal, spectral, polarization and spatial overlap of the beams of the interferometer.

A.5.1 The Mach-Zender interferometer

One design for the ν–to–2ν interferometer may be obtained using a nonlinear Mach-Zender interferometer. Light entering the interferometer is split into two arms using a harmonic beamsplitter at 1064/532 nm that reflects 1064 nm light and transmits 532 nm light, we use Newport 10QM20HB.12 high energy Nd:Yag laser harmonic beamplitter ($R_{1064} = 99.5\%, T_{532} = 80\%$). The choice of this beasmplitter satisfies the spectral (ν and 2ν) interference aspect and is also a readily available dichroic beamsplitter.

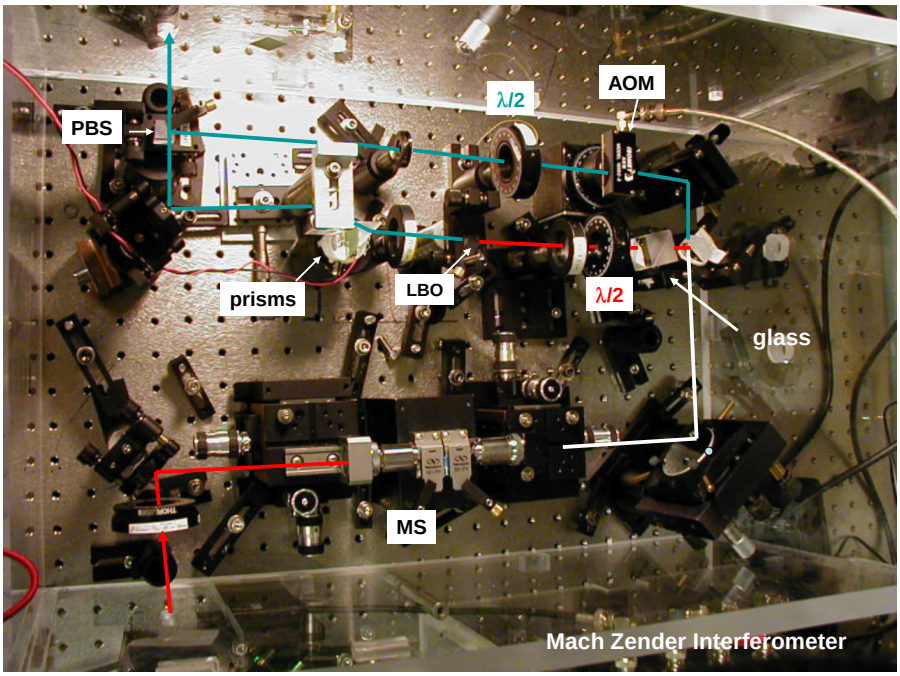

Figure A.4: The Mach-Zender ν–to–2ν interferometer. The optical filter, polarizer and photodetector are not shown in the figure. A big chunk of glass is used for fixed time delay in the 1060 nm arm.

A.5.1.1 Doubling crystal

Once the light is split at the dichroic beamsplitter, the 1064 nm arm is doubled in a nonlinear crystal. One has to consider, however, that one only has 10's of mW of power for doubling, and that the light is also chirped because of propagation through the MS fiber. As a result a longer crystal can be used to increase the nonlinear interaction length. Of course there are always trade-offs to be made. The longer the crystal, the narrower the phase matching bandwidth, and the smaller the acceptance angle. The latter may result in aperturing of the beam to a narrow line of second harmonic light, thereby decreasing the mode matching between the 2ν and ν light.

In the experiments here, we have used two nonlinear crystals, 4 mm BBO and 1 cm long LBO. Both crystals are cut for type I phase matching at 1064 nm and the input face should be anti-reflection coated at this wavelength. BBO has a higher nonlinear

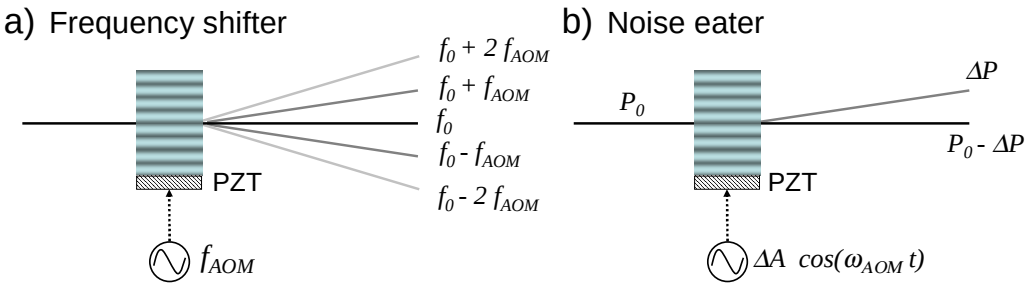

Figure A.5: a) Configuration for using an AOM as a phase sifter. The AOM is driven by a constant amplitude sinusoidal rf signal of frequency f_{AOM} that creates a pressure grating in the AOM material, which causes diffraction of the input light by harmonics of f_{AOM}. b) Configuration for using an AOM as a noise eater. Varying the amplitude of the driving signal proportionally changes the light power in the first diffracted order, thereby modulating the power on the undiffracted beam.

coefficient than LBO and thus can be shorter. However, using a longer crystal of LBO may allow for focussing of the beam within the acceptance angle, which better preserves the mode matching to the fundamental beam.

Because of the polarization rotation caused by doubling (there is a rotation of the second harmonic light by 90 deg with respect to the fundamental for type I phase matching), and also because of the random array of polarizations produced by the MS fiber (MS fiber is slightly birefringent, and is also susceptible to nonlinear polarization rotation [see Sect. 3.2], **half-wave plates** at 532 and 1064 nm are used to adjust the polarization in both arms of the interferometer.

A.5.1.2 The AOM

In the green arm of the interferometer an **AOM** is used to shift the frequency comb, of that arm only, by f_{AOM}. This is used so that the offset frequency may be locked to zero Hz. From the previous section, if the offset frequency is zero, there is no offset sideband on the harmonic spectrum of f_{rep}. To circumvent this, the AOM shifts the entire frequency spectrum of the green arm by f_{AOM}, such that when $f_0 = 0$, there

is still a sideband beat note at f_{AOM} [see Fig. A.5 a].

The AOM used here is from Isomet, model #1205C-2. The AOM uses high index (n $\sim$ 3) material to which a fast PZT is attached. By applying an amplified rf frequency (28 dBm , this requires a power amplifier) to the PZT, the pressure wave caused by the PZT results in the formation of an index grating transverse to the propagation direction of the light. Light diffracted off the grating is doppler shifted by $k\ f_{AOM}$, where k is the diffraction order. Therefore, to align the AOM requires that it is tuned such that the majority of the light is diffracted into the first order. If light is diffracted into $k = +1$, then the comb is shifted by $+f_{AOM}$. If light is diffracted into order $k = -1$, then the comb is shifted by $-f_{AOM}$.

A.5.1.3 Temporal, polarization, spectral and spatial overlap

Light from the two arms of the interferometer is re-combined at a polarizing beamsplitter (PBS). Such a beamsplitter transmits vertically polarized light and reflects horizontally polarized light. This is practical, since in general, light in the green arm is horizontally polarized, and that in the IR arm, because of the doubling crystal, is vertically polarized.

Good **spatial mode-matching** between the ν and 2ν beams is very important in obtaining a strong beat signal. This is because the interference results between the wavefronts of the doubled ν and fundamental 2ν beams. To optimize the interference requires that the mode size, wavefront curvature and propagation be same for both beams. Overlap between the beams can be ensured by verifying that the two beams remain overlapped over a large distance. This is done by checking the overlap just after the re-combining beamsplitter and then about 1 m away.

Before being recombined, however, the path lengths of the interferometer arms are balanced such that **temporal overlap** is obtained between the two pulse trains. This may be achieved by using a corner cube or by using glass and a wedge pair as

shown in Fig. A.4.

To satisfy the conditions for interference, a **polarizer** is used to ensure the polarizations of the 2ν and doubled ν light projected along the same axis. The polarizer is also a convenient means for selecting the relative power from the two arms to produce the strongest beat signal.

After the polarizer, we use a **spectral interference filter** to ensure both spectral overlap and purity. The interference filter should be chosen such that its bandwidth matches the phase matching bandwidth of the nonlinear crystal and has a center wavelength where there is best nonlinear spectral overlap. We use an interference filter centered at 530 nm with a 10 nm bandwidth.

Aside from ensuring spectral overlap, the interference filter is used to filter out any light not contributing to the interference signal, which would act to raise the detection noise floor. Filtering of the signal also minimizes saturation of the PD which can cause horrible oscillations in the PD amplifier circuit, or result in complete insensitivity to the measurement of f_0. The **photodetector** that is used uses a visible Si PIN photodiode that has a bandwidth of 1 GHz (S5973 - Hamamatsu). This diode is used in a low noise 2 GHz photodetector amplifier circuit (nearly all surface mount components) designed by Terry Brown.

A.5.2 The prism interferometer

A second interferometer design may be used that is much more simple that minimizes non-common mode mirrors is the prims interferometer. Its clever design was conceived by Henry Kapteyn. The interferometer uses a compressor prism pair, not for pulse compression but for spectral dispersion of the octave spectrum. The prisms are aligned such they diffract the input light to minimum deviation and chosen such that they give a high second order dispersion (SF10, SF18) for high spatial resolution for a short prism separation. At the exit of the second prism the light is horizontally

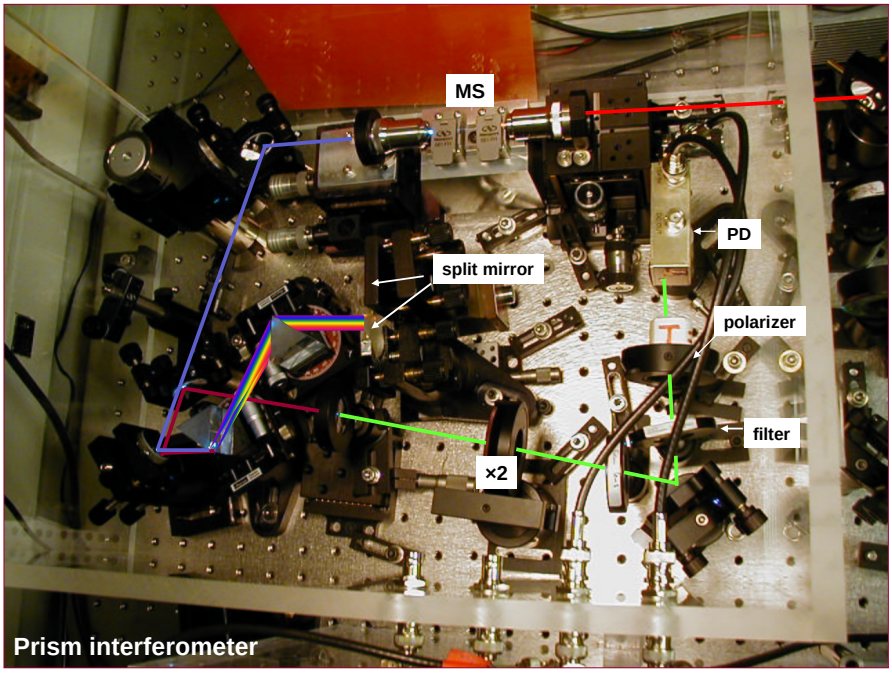

Figure A.6: The prism ν–to–2ν interferometer.

dispersed such that a split mirror after the second prism may be used for temporal overlap between the ν and 2ν portions of the octave spectrum. The position of the split mirror is chosen such that green light is reflected by one half of the mirror, and IR light is reflected by the other half. This serves two purposes. If one mirror is put on an x-z translation stage, the z-stage can be used to adjust the path length of the green with respect to the IR arm. The x-stage may be used to increase the mirror separation, for optical filtering. We use a SF10 prisms with a separation of ~ 5 cm. At this separation the distance difference between the split mirrors is ~ 1 mm, where the mirror reflecting the green light is pushed in further than that reflecting the IR.

Light is reflected from the two mirrors and sent back through the prism pair, but at a slight downward angle from the original beam. The return trip through the prism pair acts to re-combine the red and green portions of the light, which are then picked off and focused into a nonlinear crystal. The crystal is tuned for phase matching the IR light only. As in the Mach-Zender interferometer, a polarizer and optical filter are used

for filtering and a fast PD is used for detection of the offset beat signal.

Once the offset frequency beat signal and repetition rate are measured, the next job is to phase lock them to a reference frequency. This is done using a series of electronics that provide comparison to a reference and then negative feedback to the laser for error correction [see Fig. A.7].

A.6 The laser stabilization loop

In this section I will primarily discuss the feedback electronics and briefly discuss the feedback actuators for f_{rep} and f_0.

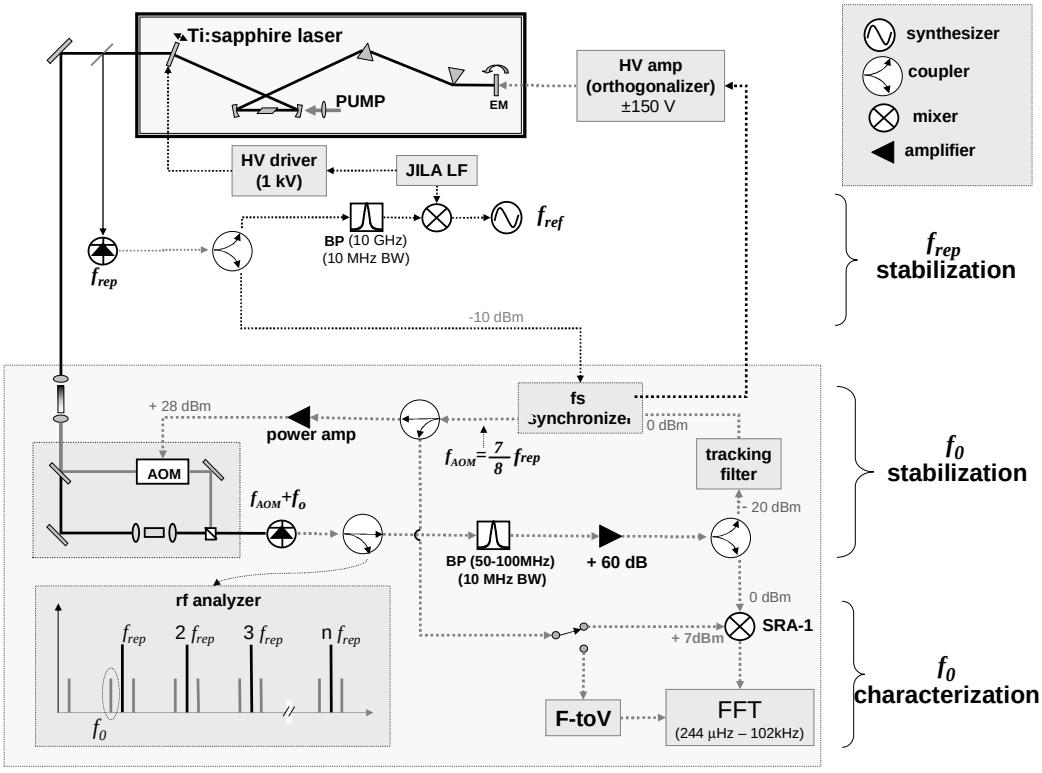

Figure A.7: The electronic diagram for phase lock of the offset frequency and the repetition rate. Details about the electronics may be found in the sections below. Note that in this schematic, the fs-synchronizer provides the reference frequency and provides the phase comparison (mixer in Fig. 2.7.)

A.6.1 Stabilization of the laser offset frequency

Once f_0 is measured using a ν–to–2ν interferometer, electronic filtering and comparison are necessary for feedback stabilization to the laser. The following section gives a break-down off the stabilization loop schematic in Fig. A.7. Before the f_0 beat signal is filtered and amplified, a small portion of the signal is split using a directional coupler. This allows for monitoring of the rf spectrum to ensure that the f_0 signal strength is maintained over time. The typical signal strength of the offset sidebands is $\sim$ -60 dBm with a SNR of 35-40 dB at a 100 kHz resolution bandwidth (res BW). Comparison of the f_0 signal to a reference frequency requires a signal strength of at least 0 dBm, achieved via amplification. However, before the signal is amplified, the rf spectrum is filtered such that only the one sideband that contains information about the f_0 alone [see Fig. A.7] is used for comparison. For filtering we use a simple 100 MHz low pass filter in series with a sharp bandpass filter. The filter we use is produced by K & L and yields a nearly perfect square bandpass, with a passband of $\sim$20 MHz and a 4 pole rejection roll off. [1]

Strong filtering of the beat note before amplification is necessary so that the amplifiers are not saturated by the other rf components of the spectrum. We use three Mini-circuits ZFL-500HLN amplifiers in series, each providing 24 dB gain. Once filtered and amplified the signal is split using a 3 dB coupler, whereby one half of the signal is used for locking [see below] and the other used for an in-loop measurement of the stability of f_0 [see Sect. A.7].

A.6.1.1 The fs-synchronizer: offset frequency phase-locked-loop

The phase-locked loop performs a comparison between a reference (master) signal and the signal to stabilized (slave). The action of the loop is to force the slave to take up

[1] n pole rejection indicates the slope of the roll off. 1 pole = 10 dB per decade, where one decade = 1 order of magnitude in frequency change.

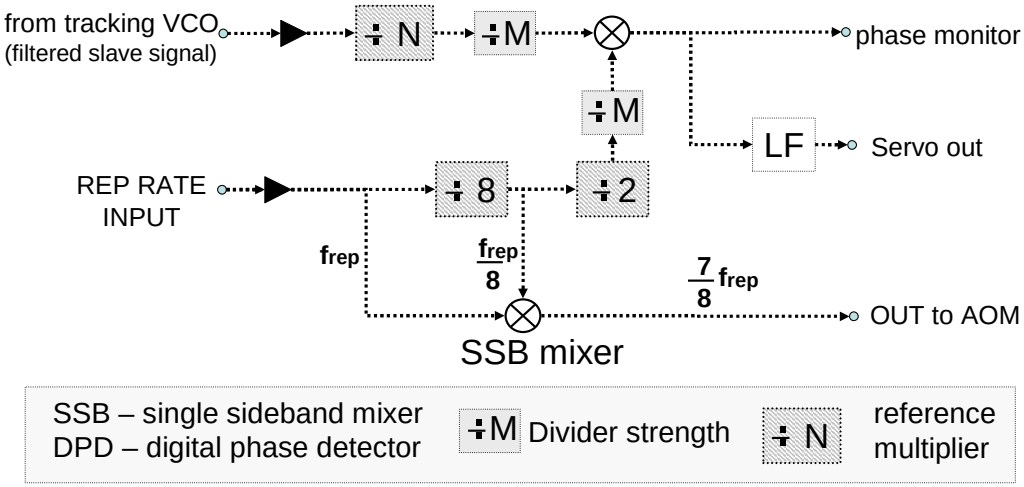

Figure A.8: Block diagram of the fs synchronizer. The reference "multiplier" allows for f_0 to be locked to 16 different reference frequencies, $f_{ref} = N(\frac{f_{rep}}{16})$. In reality division of the reference frequency by 16 and division of f_0 by N, performs the same task.

the frequency and phase information of the master through negative feedback actuated by a voltage-to-frequency converter (the laser) [see Fig. 2.7]. The stabilization circuit at the heart of the offset frequency stabilization loop is the"fs-synchronize" [see Fig. A.8]. The synchronizer is a wonderful device designed by John Hall. It serves several purposes: it 1) derives a reference frequency from an f_{rep} input, 2) produces a signal to drive the AOM to lock f_0 to zero, and 3) provides the phase comparison and error signal shaping.

The advantage of using the synchronizer over a mixer for stabilization of f_0 is that it utilizes a digital rather than analogue detector (double-balanced mixer) for comparison between the slave and master signal. The digital phase detector acts to produce an error signal proportional to the frequency difference between the master and slave, this allows for a frequency lock. Once the two signals differ only in phase, the digital phase detector (DPD) acts as a phase lock [see Fig. A.9]. The combination of frequency/phase lock allows for a larger capture range than a double balanced mixer, which can only produce an error signal if the master and slave are close in frequency. Therefore, if a perturbation knocks the laser out of lock, the DPD can recapture the slave and then

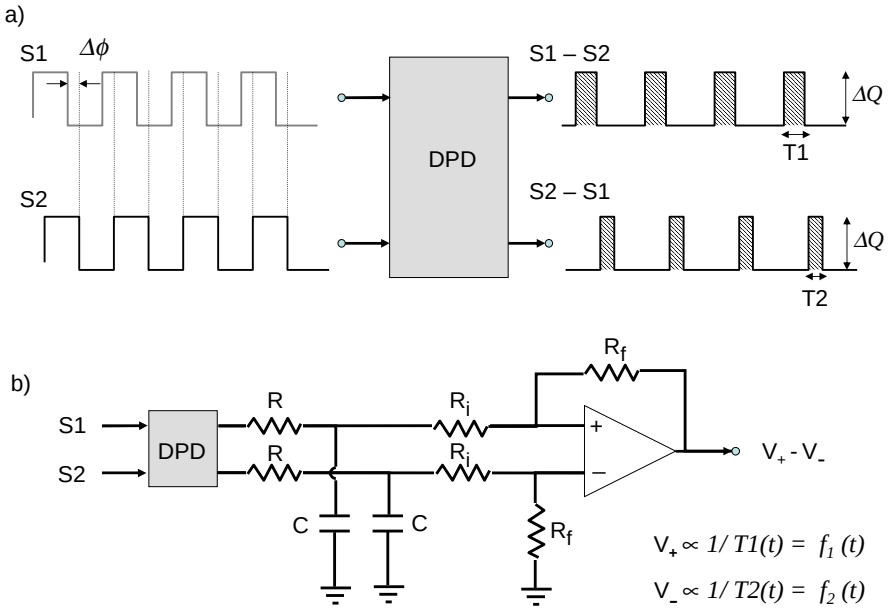

Figure A.9: a) Schematic of error detection using a digital phase detector (DPD). The DPD takes two input signals, $S1$ and $S2$ (50 % duty cycle produced from a flip flop that divides the original input frequency by 2), and produces two output signals, $S1-S2$ and $S2-S1$. Here $S1$ and $S2$ differ only by a constant phase offset. b) Schematic of how the digital phase detector is used for producing an error signal linearly proportional to the frequency difference between the square wave signals, $S1$ and $S2$. Given the two signals in a), the output of the differential amplifier would be a constant voltage proportional to the phase difference between $S1$ and $S2$. this scheme, however, produces a zero volt output if the phase difference is zero or 180 degrees. If the phase difference were time dependent, $\Delta\phi = 2\pi f(t)$, the output signal would evolve as $f(t)$.

re-phase lock it. The range of the DPD is determined by a divider stage. The larger the division, the larger the range and the looser the lock (the weaker the slope with frequency/phase). A drawback of using the DPD, however, is that it uses a comparator, which requires a SNR for the slave signal $>$ 30 dB (100 kHz res. BW) such that the comparator output is not dominated by zero crossings resulting from low SNR.

A.6.1.2 The tracking filter

If the f_0 beat signal exhibits low SNR or a strong amplitude modulation, a tracking filter is used to clean up and amplify the signal. Typically, a tracking filter is used in conjunction with the fs-synchronizer for low SNR f_0 beat signals. (A tracking filter is

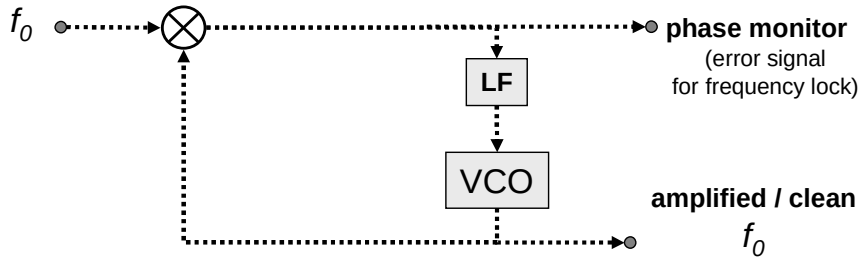

Figure A.10: Block diagram of the tracking filter used to produce an amplitude stable rf signal that tracks the phase information of the low SNR beat signal, f_0.

not typically necessary if a double balanced mixer is used instead of the fs-synchronizer.)

The tracking filter is a PLL that locks an rf voltage controlled oscillator (VCO) to a noisy rf signal. The VCO acts as a very narrow, dynamic filter that tracks the frequency and phase information of the input signal, but with a strong stable amplitude [see Fig. A.10]. Because the tracking filter is an electronic PLL its speed is limited only by that of the electronics. Typically, if the beat signal for f_0 is weak ($<$ 30 dB SNR in 100 kHz res BW), a tracking filter is used to increase the offset frequency's SNR for used with a DPD.

A.6.2 Negative feedback

Negative feedback to the laser for error correction of f_0 may be actuated either by tilting the laser end mirror or via modulation of the laser pump power. Of course, each different feedback mechanism requires a different driver to make the feedback error signal compatible with the actuator. In the case of the PZT, a high voltage driver must be used. The driver for the AOM is depicted in Fig. A.5 a.

A.6.2.1 Feedback using a PZT

Tilting of the laser end mirror is actuated using the PZT scheme in Fig. A.11. Tilting of the laser end mirror is achieved using two fast (100 kHz) PZT's driven in

opposition using the amplified error signal derived from the fs-synchronizer (maximum ± 150 V). Fast PZT's may be used in this configuration if the laser is passively stable. Our laser results in long time scale drifts in f_0 of around 1 MHz per minute. The range of the system is on the order of 50 MHz and the combined PZT + mirror system can yield a bandwidth up to 30 kHz if the mirror size is minimized.

A.6.2.2 Feedback using an AOM

Placing an AOM in the path of the pump beam allows for control of the offset frequency by inducing amplitude–to–phase modulation in the laser crystal. The AOM (IntraAction # ASM-803B47) is set up in a noise eater configuration [see Fig. A.11 b)]. This is different from the configuration used in the Mach-Zender interferometer that uses the AOM for frequency shifting the first order diffracted light. Here, in contrast, the first order diffracted light is used for low-level amplitude modulation of the zero order transmitted beam.

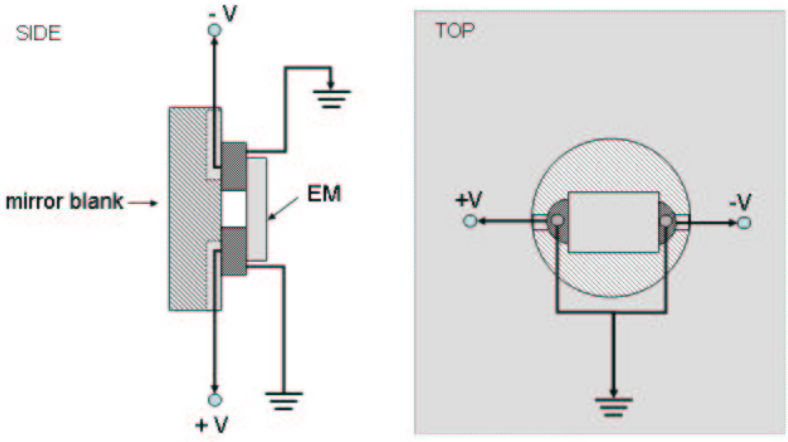

Figure A.11: The disc PZTs + mirror used for stabilization for fine tilting of the laser end mirror, EM. Two fast PZT's are attached to a blank mirror substrate using vacuum epoxy (Torr Seal) and the mirror is centered on the PZT's using sturdy wax for easy removal. Two small cuts are made in the mirror blank to allow room for contact wires. The mounted PZT system is held in a heavy copper mirror mount to minimize momentum transfer from the PZT to the mirror mount.

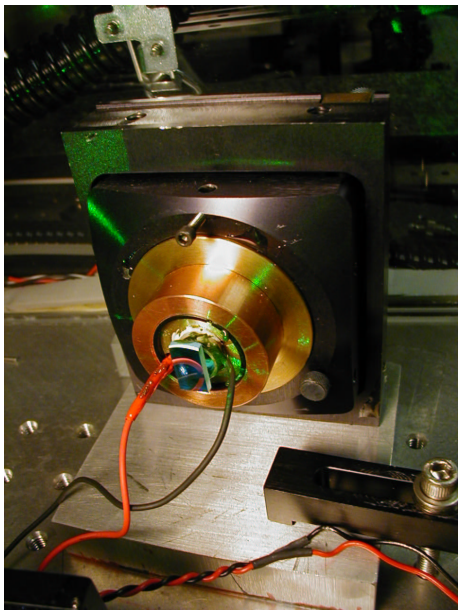

Figure A.12: The tube PZT + mirror used for stabilization of the laser cavity length. The PZT is attached to a blank mirror substrate using vacuum epoxy (Torr Seal) and the mirror is mounted on the PZT using sturdy wax for easy removal. The mounted PZT is held in a heavy copper mirror mount to minimize momentum transfer from the PZT to the mirror mount.

A.6.3 Stabilization of the laser repetition rate

Comparison of f_{rep} to a reference frequency is obtained using an SRA-1 double-balanced mixer. The mixer requires a signal strength of 0 dBm for the rf port, thus requiring filtering and amplification of the f_{rep} signal. The error signal generated via comparison to the synthesized reference is filtered and amplified using a loop filter. We use a JILA designed loop filter that allows for variable PI (proportional-integrator) corners to match the transfer functions of different feedback actuators. In the experiments here, only a slow tube PZT is used for cavity length correction [see Fig. A.12]. The large range required of the PZT results in a relatively low bandwidth ($\sim$ 1 kHz). More tight synchronization of f_{rep} requires using an additional fast PZT, and therefore splitting the error signal between a fast and slow feedback loop. Details about synchronization of f_{rep} may be found in [70].

A.7 Measurement of the offset frequency stability

In a typical PLL, the gain of the servo system drops with increasing frequency, whereby the rate of this drop is determined by the design of the servo loop (electronic response and the transfer function of the negative feedback actuator). As a result, the feedback loop has a much stronger ability to suppress noise at low frequency than at high frequency. Because of this characteristic, suppression of drift is by far the easiest task. Suppression of high frequency noise means hard work must be put into the design of the entire feedback system, at which point a limit is encountered. This limit is often determined by the point when accumulated phase shifts in the loop (electronic and actuator) result in positive feedback and hence oscillations in the loop. This point determines the unity gain of the servo or in other words the bandwidth of the feedback system.

Residual noise on f_0 due to imperfect stabilization is obtained in the frequency domain by analyzing f_0's linewidth. Remember, phase and frequency noise differentiate by only a time derivative, and thus may be considered one in the same. The noise spectrum of f_0's lineshape may be used to determine problem areas, and helps in identifying the causes of noise.

One important issue in measuring the noise spectrum of a signal is in distinguishing between amplitude and phase noise. In the Fourier domain, by naively looking at the linewidth of a signal on an rf analyzer, the sidebands on the carrier frequency are composed from contributions of both. Proper noise analysis, for determination of the linewidth of signal requires the separation of the two.

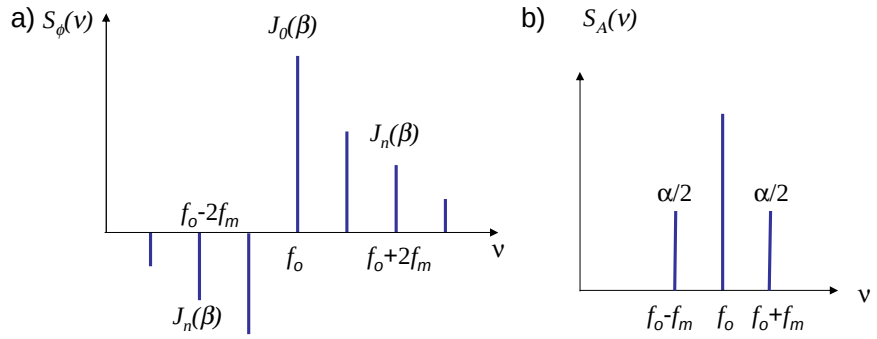

Figure A.13: a) Frequency spectrum of a carrier frequency, f_0 phase modulated at f_m with a modulation strength β. The conjugate sidebands on the carrier are shift in phase by π. b) Frequency spectrum of a carrier frequency, f_0 amplitude modulated at f_m with a modulation strength α.

A.7.1 Phase noise vs. amplitude noise

A.7.1.1 Amplitude Modulation

Amplitude modulation of a carrier frequency, ω_0, with amplitude modulation strength α and modulation frequency, ω_m is described by

$$V(t) = \delta A(t)\ cos(\omega_0\, t) = \left[cos(\omega_0 t) + \frac{1}{2}\ \alpha\right]\ \left\{cos\left[(\omega_m + \omega_0)\, t\right] + cos\left[(\omega_m - \omega_0)\, t\right]\right\}, \tag{A.1}$$

where $\delta A(t) = [1 + \alpha\ cos(\omega_m t)]$.

Given eqn. A.1, AM modulation results in the production of conjugate AM sidebands, where the height of each sideband is given by $\frac{\alpha}{2}$ [see Fig. A.13 a]. Because of this, pure AM noise, δA, on a carrier frequency is very easy to analyze. Integration of the power spectral density of the noise spectrum, $S_A(f)$, infinitely far from the carrier, to the carrier itself, will yield the total rms amplitude noise for the spectrum.

$$\Delta A_{rms} = \sqrt{2\int_{-\infty}^{0} S_A(f)df} \tag{A.2}$$

Here $S_A(f) = \left|\frac{F\{\delta A(t)\}}{\sqrt{\Delta f_{RB}}}\right|^2$, where Δf_{RB} is the resolution bandwidth and ν is the frequency relative to the carrier. Consequently, $S_A(\nu)$ is measured in V^2/Hz. The factor of two takes into account single sideband integration of the noise.

A.7.1.2 Phase modulation

Phase modulation of a carrier frequency, ω_0, with strength β and modulation frequency, ω_m is described as

$$V(t) = cos\left[\omega_0 t + \delta\phi(t)\right] = \sum_{n=0}^{\infty} J_n(\beta) cos\left[(\omega_0 + n\,\omega_m)t\right], \tag{A.3}$$

where $\delta\phi(t) = \beta\, cos(\omega_m t)$. As seen in eqn. A.3, phase noise is decomposed into harmonics of ω_m, whose strength is given by the Bessel function coefficients, $J_n(\beta)$ [see Fig. A.13].

Because of the nature of PM modulation, at strong modulation strengths ($\beta >> 1$), the contribution of the rms phase noise from several modulation frequencies cannot be determined directly from a phase noise spectrum. At weak modulation strength ($\beta << 1$), however, the first Bessel function sideband dominates the noise spectrum. In this limiting case, the strength of the $J_1(\beta)$ sideband is $\sim \frac{\beta}{2}$, thereby allowing for the straight forward noise analysis as used for AM modulation. In this limit eqn. 4.6 and 4.5 hold.

A.7.2 Measurement of the phase noise spectrum

Different devices may be used that allow for separation of phase and amplitude noise from a noisy signal. Both those presented in this section allow for a measurement of the single sideband spectrum of the noise on a carrier frequency. As in every device, the amplitude noise rejection is subject to study. Also, such devices may be prone to AM–to–PM conversion if the signal being measured exhibits strong AM noise.

A.7.2.1 The mixer

A double balanced mixer, SRA-1, may used for measuring the phase noise spectrum of a quiet signal. As a phase detector, the mixer allows for a phase comparison of two signals, with close carrier frequencies. The DC output of the mixer is a voltage

proportional to sinusoidal phase difference, $\delta\phi$, between the two signals. Because of this, the mixer output yields a linear relationship between phase and voltage only for small phase deviations ($\Delta\phi << 1$). In this limit the generated phase noise spectrum can be assumed to be dominated by the first order sidebands (see Sect. A.7.1).

The noise spectrum produced from a mixer is roughly calibrated by determining the peak-to-peak voltage due to a phase excursion, $\Delta\phi$, equal to π radians. An important consideration in using a mixer as a phase detector is that the phase offset between the two signals may make it such that, the mixer output is offset outside its linear range. This may result in clipping of the noise signal, thus giving a severe underestimation of the rms phase noise. To avoid this, a phase shifter[2] may be used and the mixer output

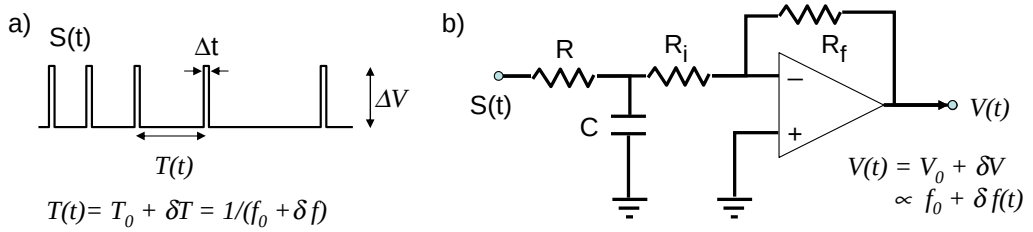

Figure A.14: a) Chirped square wave signal $S(t)$. b) Schematic of the basic operation of a frequency-to-voltage converter. b) Here the input signal exhibits a charge spikes separated in time by $T(t)$. This signal is low pass filtered (integrated) and then amplified using an operational amplifier. The output of the operational amplifier is a voltage $V_0 = R\frac{R_f}{R_i}\frac{C\,V\Delta t}{T_0} \propto f_0$. Frequency deviations, δf, away from f_0 appear as a change in voltage at the output of the amplifier, $\delta V = R(C\,V\,\Delta t)\frac{R_f}{R_i}\,\delta f$.

For phase noisy signals a frequency-to-voltage converter (F-to-V) may be used

[2] The simplest phase shifter is made by simply adding a length of cable to either the reference signal. This is much like adjusting the length of an interferometer. For standard 50 Ω BNC, 1 ft of cable = 1.5 ns time shift.

for an accurate determination of a noise spectrum. The F-to-V is an active electronic device that yields a voltage that is in proportion to the frequency of an electronic signal.

The basic operation of an F-to-V converter is shown in Fig. A.14. The input signal, with carrier frequency, f_0, and frequency noise, δf, is first converted to a square wave signal using a comparator with a period $T(t) = \frac{1}{(f_0+\delta f)}$. The amplitude of the square wave, ΔV, is a fixed and regulated thus removing amplitude noise from the carrier. On one half cycle, the square wave charges a capacitor, $Q = I\Delta t = CV$, and on the other half cycle, discharges it through a resistor, R. On the positive half cycle the charge on the capacitor results in a current, $V = IR$ input to an operational amplifier that is directly proportional to positive duration of the square pulse, $V = V_0 + \delta V = \frac{CV}{T} R = R\ (f_0 + \delta f\ ) CV$. Noise on the carrier frequency results in deviations in output voltage, δV, from V_0. The frequency spectrum of such a signal results in carrier-sidebands that are directly proportional to the strength of the frequency modulation, where $\frac{\delta V(\nu)}{V_0} = \frac{\delta f}{f_0}$. In essence, the F-to-V converter converts phase noise to amplitude noise thus removing the Bessel function sidebands intrinsic to phase modulation [see Sect. A.7.1]. The resulting noise spectrum produced by the F-to-V is straight forward to analyze using eqn. 4.6.